General Disclaimer

One or more of the Following Statements may affect this Document

- This document has been reproduced from the best copy furnished by the organizational source. It is being released in the interest of making available as much information as possible.

- This document may contain data, which exceeds the sheet parameters. It was furnished in this condition by the organizational source and is the best copy available.

- This document may contain tone-on-tone or color graphs, charts and/or pictures, which have been reproduced in black and white.

- This document is paginated as submitted by the original source.

- Portions of this document are not fully legible due to the historical nature of some of the material. However, it is the best reproduction available from the original submission.

Produced by the NASA Center for Aerospace Information (CASI)

CR 73496
AVAILABLE TO THE PUBLIC

N71-14613
(ACCESSION NUMBER)
116
(PAGES)
(NASA CR OR TMX OR AD NUMBER)
(THRU)
G3
(CODE)
01
(CATEGORY)
FACILITY FORM 602

RECEIVED
NASA STI FACILITY
INPUT BRANCH
JAN 1971

AEROPHYSICS RESEARCH CORPORATION
BELLEVUE, WASHINGTON

01

NASA CONTRACTOR
REPORT

NASA CR-73496

AVAILABLE TO THE PUBLIC

APPLICATION OF MULTIVARIABLE SEARCH TECHNIQUES TO THE DESIGN OF LOW SONIC BOOM OVERPRESSURE BODY SHAPES

By D. S. Hague and R. T. Jones

Distribution of this report is provided in the interest of information exchange. Responsibility for the contents of this report resides in the author or organization that prepared it.

Prepared under Contract NAS 2-4880
by

AEROPHYSICS RESEARCH CORPORATION
P. O. Box 187, Bellevue, Washington 98009

For

AMES RESEARCH CENTER, MOFFETT FIELD, CALIFORNIA
NATIONAL AERONAUTICS AND SPACE ADMINISTRATION

November 1970

PREFACE

This document reports the results of a study carried out by Aerophysics Research Corporation during the period October 1969 through July 1970. The work was carried out as part of an extension to Contract NAS 2-4880. The National Aeronautics and Space Administration Technical Monitor for this work was Mr. Raymond Hicks of Ames Research Center. Mr. D. S. Hague functioned as study Principal Investigator.

The aerodynamic subprogram employed in this study was supplied by NASA; the shock location subprogram was conceived and constructed by Aerophysics Research Corporation under the study effort. The optimization subprogram was originally constructed with NASA funding under contract NAS 2-4507; Mr. Richard H. Petersen of OART functioned as NASA Technical Monitor for that study.

Mrs. Jane Yonke and Mr. Rolf Reichel of Aerophysics Research Corporation assisted in the preparation of this report.

TABLE OF CONTENTS

Page

SUMMARY. 1

ANALYSIS 2
Mach Line Curvature. 2
Pressure Calculation and Shock Formation 4
Multivariable Search 9
Numerical Solution of Non-Linear Multivariable
Optimization Problems 12
One-Dimensional Search. 12
Multiple Extremals. 15
Sectioning Parallel to the Axes 19
Steepest-Descent Search 19
Steepest-Descent Weighting Matrices 22
Random Ray Search 25
Quadratic Search. 27
Davidon Method. 27
Pattern Search. 29
Adaptive Search 29
Magnification Search. 32
Summary of Multivariable Search Techniques. 34

MINIMUM OVERPRESSURE SINGLE POWER BODIES 35
Introduction of Slope Constraint 35
Solution with Base Area and Nose Length Fixed. 36
Solution with Volume and Length Fixed. 46
Two-Arc Bodies 52
Three-Arc Power Bodies 59
Solution Convergence and Numerical Accuracy 64
A Note on Variational Optimization. 66
Sensitivity Studies 67
Effect of Body Slope Limitation 68
Effect of Increasing Notch Width. 68
Bodies of Arbitrary Radius Distribution. 72

CONCLUSION 77

REFERENCES 79

APPENDIX A 81
MAIN Program and Program Structure 81
Data Input 85
NAMELIST Data Block "SELECT" 85
NAMELIST Data Block "SHOCKS" 85
NAMELIST Data Block "IAESOP" 89
AESOP Print Control. 89
AESOP Data Listing 99
Search Selection and Control. 99
Parameter Selection 99
Multiple Extremal Optimization. 100
Optimization Function Selection 100
Sectioning Search Data ($METHOP_i=1$). 101

Pattern Search Data ($METHOP_i$ = 2). 102
Magnification Search Data ($METHOP_i$ = 3). 102
Steepest-Descent Search Data ($METHOP_i$=4) 103
Adaptive Creepint Search Data ($METHOP_i$ = 5). . . .103
Quadratic Search Data ($METHOP_i$ = 6). 104
Davidon Search Data ($METHOP_i$ = 7). 105
Random Point Search ($METHOP_i$ = 8). 105
Random Ray Search ($METHOP_i$ = 9). 106
Subroutine Function 106
AESOP Function List for Shock Program 108

LIST OF FIGURES

Figure		Page
1	Straight and Approximate Curved Mach Lines	3
2	k As A Function of M	5
3	The Function h(z)	5
4a	"F" Function Model 4 of TN D-3106	6
4b	"F" Function Model 9 of TN D-3106	6
5	Pressure Wave from Power Body at Three Distances	7
6	Formation of Bow Shock	8
7	Formation of Rear Shock	8
8	Schematic of Shock Formations	10
9	Search Based on the Golden Section	11
10	Response Surface with Two Troughs	16
11	Search by Golden Section Fails to Detect Multiple Troughs on One-Dimensional Cut	17
12	Non-Convex Response Surface	18
13	Sectioning Parallel to the Axes	20
14	Perturbation Zones Corresponding to Three Weighting Matrices	23
15	Steepest-Descent Search	26
16a	Quadratic Search Behavior on a Near Second-Order Surface	28
16b	Quadratic Search on a Higher Order Surface	28
17	Pattern Search Following Sectioning Parallel to the Axes	30
18	Pattern Search Following Two Steepest-Descent Searches	31
19	Adaptive Search	31
20	Single Arc Power Bodies, Fixed Length, and Base Radius	37

LIST OF FIGURES (CONTINUED)

Figure		Page
21	Variation of Maximum Overpressure with Power Body Exponent, Constrained L and R	38
22	Selected Single-Arc Power Body Signatures	39
23	Length and Base Constrained Single Power Arc Solutions, Effect of Distance, M=1.414	41
24	Length and Base Constrained Single Power Arc Solutions, Effect of Distance, M=2.2	42
25	Length and Base Constrained Single Power Arc Solutions, Effect of Distance, M=2.7	43
26	Selected Signatures, Single Arc Power Bodies, Base and Length Constrained, M=1.414, h/ℓ = 10	44
27	Selected Signatures, Single Arc Power Bodies, Base and Length Constrained, M=1.414, h/ℓ =400	45
28	Variation of Optimum Exponent, N*, with Mach, h/ℓ, Base and Length Constrained	47
29	Variation of Maximum Overpressure with Distance, Single Arc Base Constrained Power Bodies	48
30	Variation of Maximum Overpressure with Power Body Exponent, Constrained V and L	49
31	Selected Single-Arc Power Body Signatures, V and L Constrained	50
32	Family of Bodies with Equal Nose Volume	51
33	Volume Constrained Single Power Arc Solutions, Effect of Distance, M=2.7, V_F=1.0	53
34	Volume Constrained Single Power Arc Solutions, Effect of Volume, M=2.7, h/ℓ=100	54
35	Effect of Mach Number on Single Power Arc Volume Constrained Bodies, V_F=1.0, h/ℓ=100	55

(LIST OF FIGURES (CONTINUED)

Figure		Page
36	Two-Arc Power Body	56
37a	Two-Arc Signatures	57
37b	Two-Arc Body Profiles	57
38a	Two-Arc Pressure Signature	58
38b	Two-Arc Body Shape Compared to That of a Three-Quarter Power Body	58
39	Optimal Two-Arc Body $M = 2.7$, $h/\ell = 30$	60
40	Typical Signatures, Two-Arc Solution $M = 2.7$, $h/\ell = 30$	60
41	Convergence Plot, Two-Arc Solution, $M = 2.7$, $h/\ell = 30$, Cone Nominal	61
42	Three-Arc Body Parameters	62
43	Optimal Three-Arc Body	63
44	Pressure Signature, Three-Arc Body	65
45	Trade Curves for Three-Arc Body	69
46	Effect of Maximum Body Slope Limitation	71
47	Wide Notch Solution - Body Shape	73
48	Wide Notch Solution - Pressure Signature	73
49	Solution Developing From Cusped Body	74
50	Solution Developing from Parabolic Body	75
51	Convergence of Two Test Problems	76
A1	Function of MAIN Program	82
A2	Typical Data Set-Up	83
A3	Subroutine Structure	84
A4	Schematic of Optimization Procedure	86

APPLICATION OF MULTIVARIABLE SEARCH TECHNIQUES TO THE DESIGN OF LOW SONIC BOOM OVERPRESSURE BODY SHAPES

By D. S. Hague and R. T. Jones

SUMMARY

The Whitham-Lighthill method for describing the flow about a supersonic body of revolution is outlined and a computational method for locating shocks within the field is described. An outline of multivariable search procedures is presented in some detail.

The method in which a series of body shaping problems are reduced to the multivariable optimization form is described. Several alternate multivariable optimization formats are employed including single and multiple-arc formulations. Each formulation is exercised, and a series of low boom shapes are defined. Several of the multiple-arc solutions arrive at sonic boom overpressure values well below previously reported single-arc variational solutions. The practicality of these lower boom shapes is discussed; it is recommended that some of the more promising low boom shapes be tested with the objective of confirming their predicted characteristics.

ANALYSIS

Mach Line Curvature

Sonic boom overpressure calculations for axisymmetric bodies or for equivalent bodies which incorporate the body lift distribution may be performed by the method of Whitham, reference 1, in conjunction with either the Lighthill aerodynamic technique, reference 2, or small perturbation theory, reference 3. Whitham's theory is based on the assumption that small perturbation theory provides a good first approximation throughout the flow provided that the value predicted for any physical quantity at a given distance from the axis on the straight downstream Mach line emanating from an element of body surface is taken as the value at that distance from the axis on the actual curved Mach line emanating from the body surface element.

On the straight Mach line it is readily seen, figure 1, that

$$Y = x - \beta r \qquad (1)$$

On the curved Mach line, figure 1, Whitham's theory predicts that

$$y = x - \beta r + k(M) \cdot F(y) \cdot r^{\frac{1}{2}} \qquad (2)$$

where k is a function of Mach number

$$k = \frac{(1+\gamma)M^4}{2^{1/2}\beta^{3/2}} \qquad (3)$$

This function, reference 2, is reproduced for convenience in figure 2. F(y) is a function of body shape given by

$$F(y) = \int_0^y \frac{f'(t)dt}{(y-t)^{\frac{1}{2}}} \qquad (4)$$

For smooth pointed bodies at zero lift

$$f(t) = S'(t)/2\pi \qquad (5)$$

where S(t) is the cross sectional area of the body. If the body carries a local axial distribution of lift per unit length of $\ell(t)$, then

$$f(t) = \frac{1}{2\pi}\left(S'(t) + \frac{\beta\ell(t)}{2q}\right) \qquad (6)$$

For bodies having slope discontinuities in area, $\Delta S'(t)$, an additional term, ΔF_i, must be added to F(y), equation (4), at each point of discontinuity, i. Thus for this class of bodies

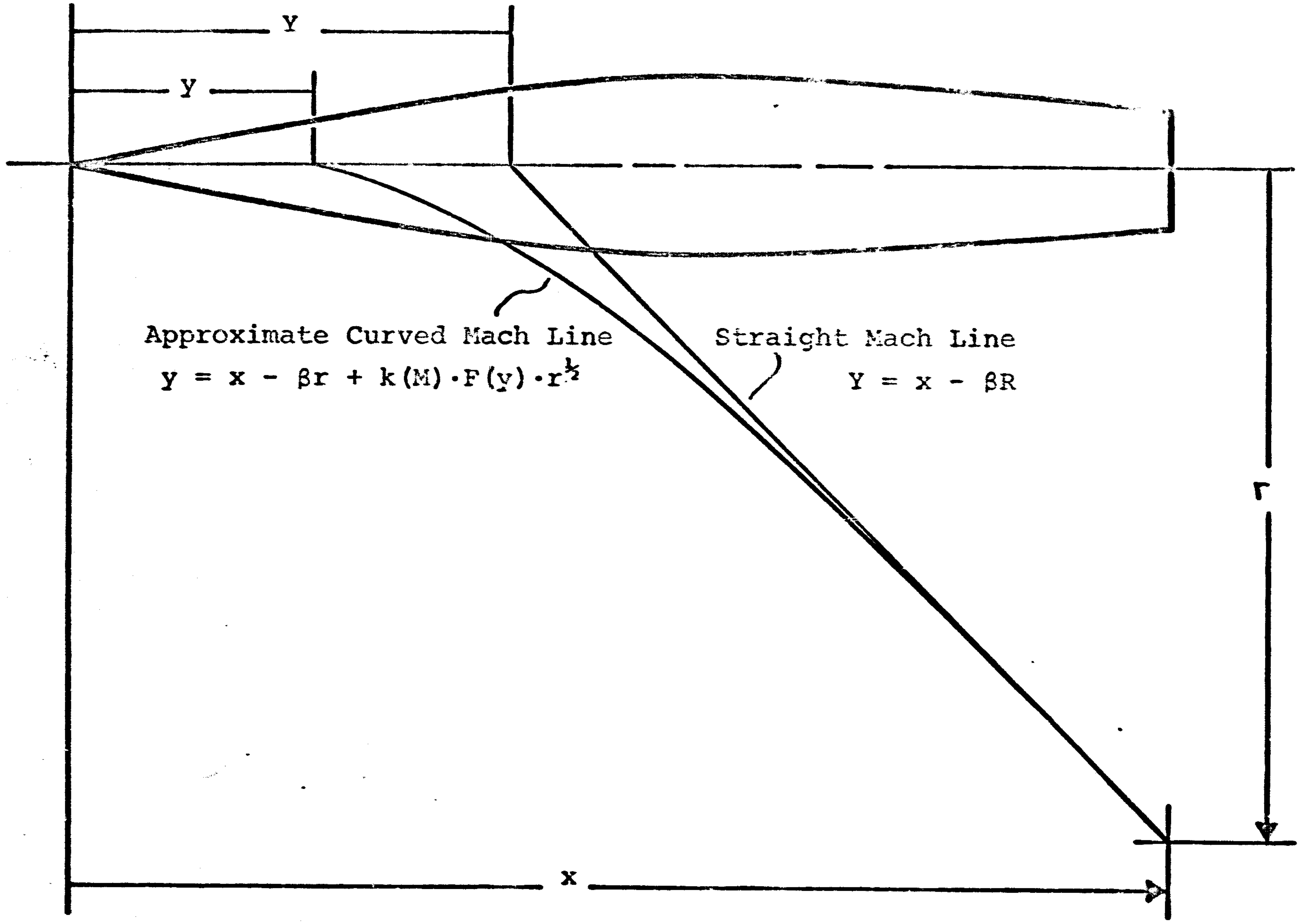

Figure 1.—Straight and Approximate Curved Mach Lines

$$F(y) = \left[\int_0^y \frac{f'(t)dt}{(y-t)^{\frac{1}{2}}} + \left(\frac{2}{\beta}\right)^{\frac{1}{2}} \sum_{i=1}^{N_i} \frac{h(z)\Delta S'(t_i)}{2\pi R_i}\right] \tag{7}$$

Here R_i is the body radius at the slope discontinuity occurring at $x = t_i$; $\Delta S'(t_i)$ is the slope discontinuity; N_i is the number of slope discontinuities up to and including the i^{th}, and $h(z)$ is the Lighthill function of reference 2, reproduced for convenience in figure 3. The argument z is given by

$$z = \frac{y-t_i}{\beta R_i} \tag{8}$$

It can be seen from equations (2) and (3) that a Mach line emanating from an element of body surface where F(y) is positive will advance ahead of the straight Mach line of equation (1) in proportion to both F(y) and $r^{\frac{1}{2}}$. Conversely, a Mach line emanating from a body surface element in a region where F(y) is negative will lag behind the straight Mach line in proportion to both the magnitude of F(y) and $r^{\frac{1}{2}}$. The F(y) or F functions corresponding to three bodies are presented in figure 4.

Pressure Calculation and Shock Formation

The Whitham theory predicts that the pressure perturbation at any point in a uniform field surrounding a body is directly proportional to F(y) and inversely proportional to the half-power of distance from the body

$$\frac{\Delta p}{p} = \frac{\gamma M^2 F(y)}{(2\beta r)^{\frac{1}{2}}} \tag{9}$$

It follows from the discussion in the preceding section that positive pressure perturbations will advance ahead of the straight Mach lines, and negative perturbations will lag the straight Mach lines. In either case the advance or lag is directly proportional to pressure magnitude at the originating surface. It follows that strong positive pressure perturbations will advance upon and ultimately overtake weaker positive or negative pressure perturbations and that strong negative pressure perturbations will lag and ultimately fall behind weaker negative or positive pressure perturbations. This behavior is illustrated in figure 5 where the pressure perturbations generated by a parabolic body of revolution, as predicted by equation (9), at three distances from the body are presented. It can be seen that the pressures predicted are multi-valued. Whitham, reference 1, reduces the multi-valued pressure signature to a single valued signature by introducing shocks into the flow field. The shock position can be determined by the Whitham area balancing technique, references 1 and 2.

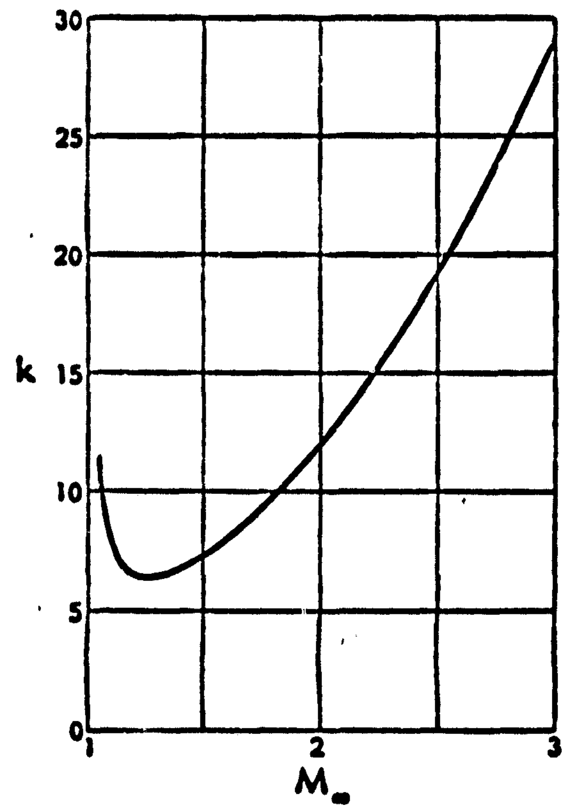

Figure 2.—k as a Function of M

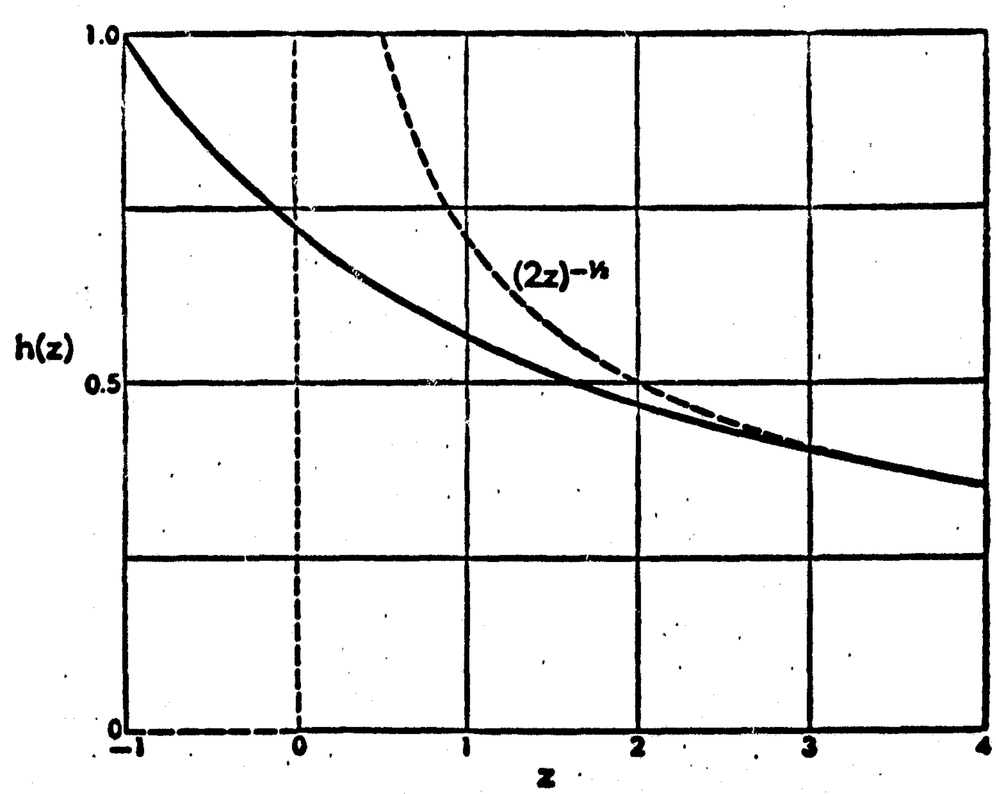

Figure 3.—The Function h(z)

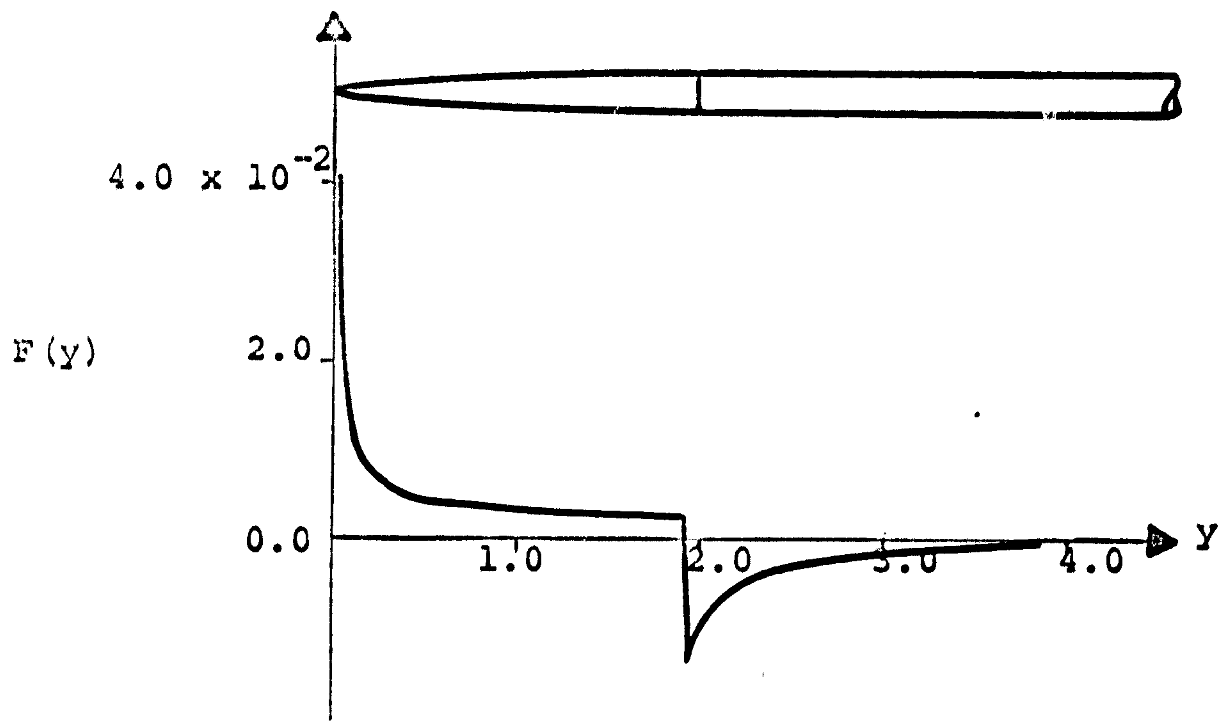

Figure 4a.—"F" Function, Model 4 of TN D-3106

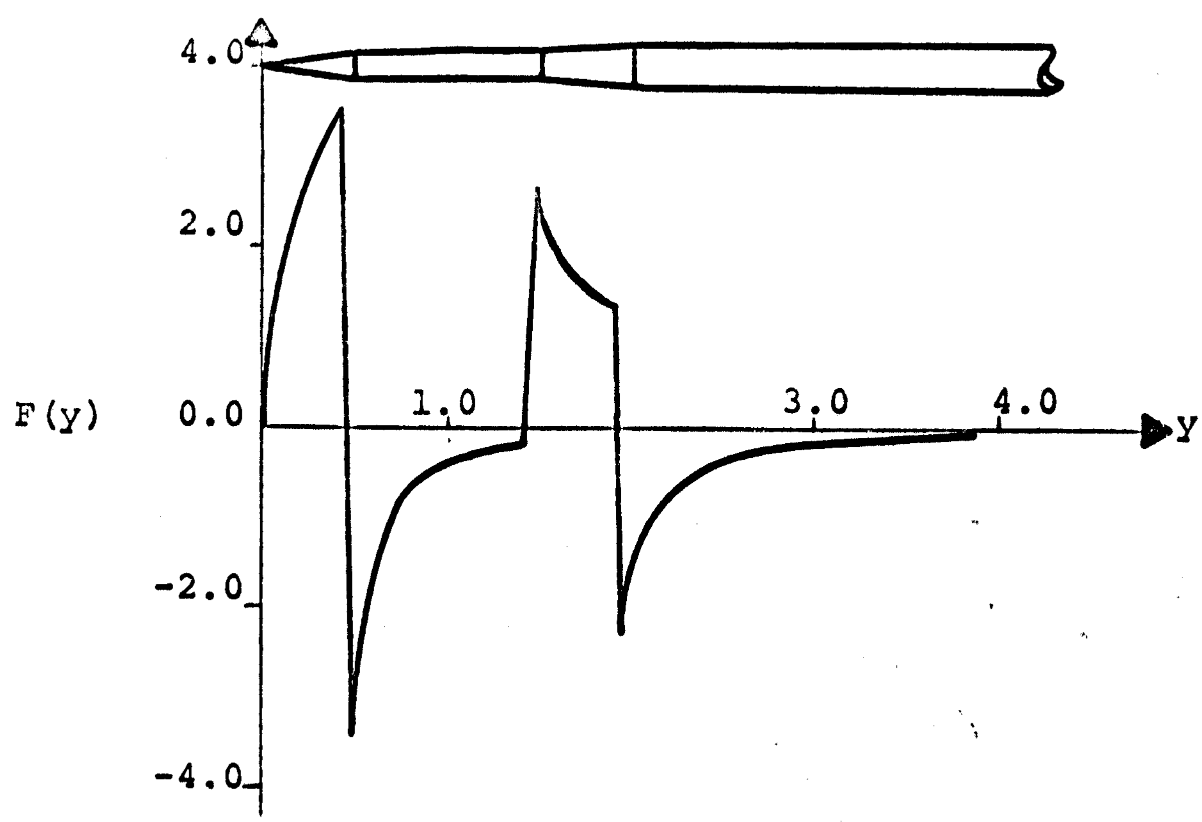

Figure 4b.—"F" Function, Model 9 of TN D-3106

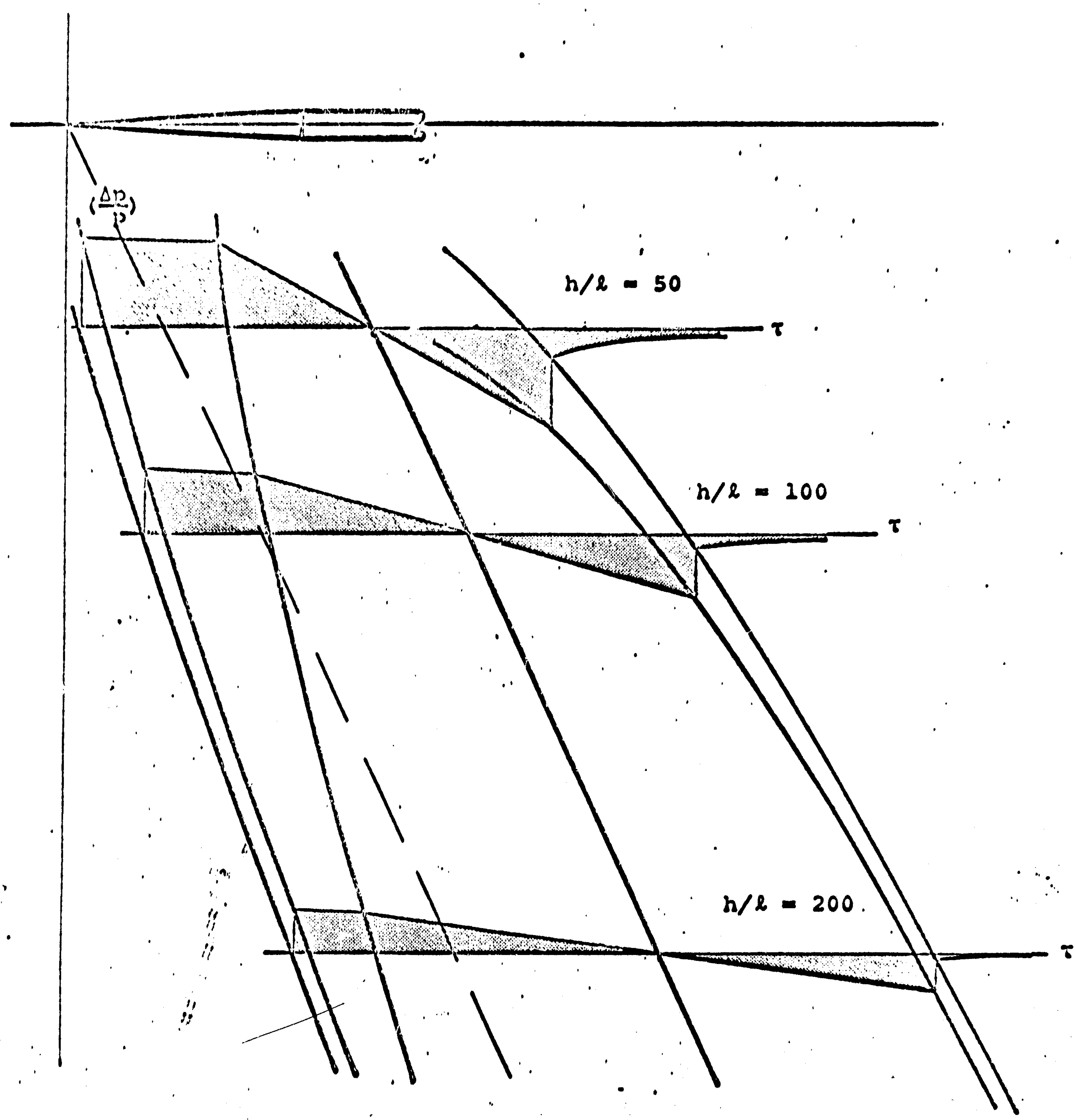

Figure 5.—Pressure Waves from Power Body at Three Distances

The area balancing technique of Whitham predicts that a shock will occur at points in the signature where a vertical line will eliminate equal amounts of positive and negative area. For example, in the case of bow shock, figure 6, the vertical line CE defines the shock location for

$$S(O:AC) = -S(D:EC) \tag{10}$$

and

$$S(AC:BD) = -S(BD:AC) \tag{11}$$

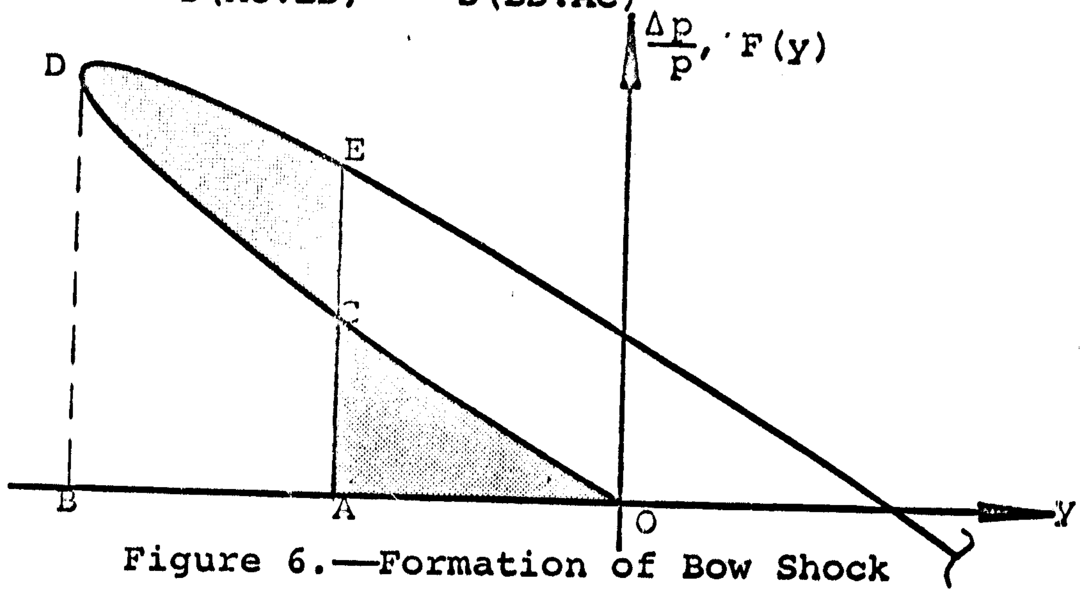

Figure 6.—Formation of Bow Shock

Here S(AC:BD) indicates that the area ACDB of the pressure signature generated as y passes from y = A to y = B, etc. Similarly, in figure 7 the rear shock is defined by

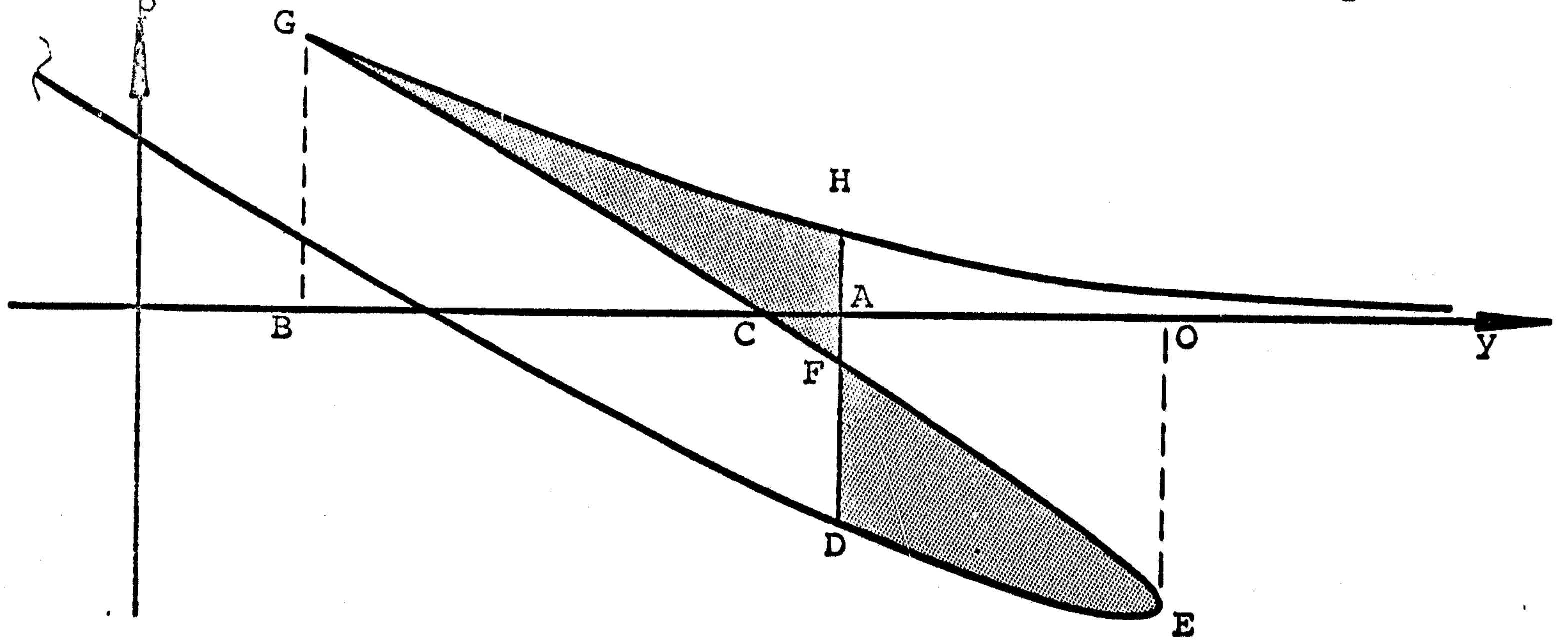

Figure 7.—Formation of Rear Shock

the line segment DEC for

$$S(E:DF) = -S(G:HF) \tag{12}$$

$$S(OE:AF) = -S(AF:OE) \tag{13}$$

$$S(C:BG) = -S(BG:C) \tag{14}$$

In general, a shock lies at a point A where

$$\oint_{BA} F(y)dy = \oint_{AO} F(y)dy \tag{15}$$

where the integrals are the total integral as y performs both the left and right sweep(s) in the interval $\overline{OB}$. The process of shock insertion defined by equation (15) must be continued until a single valued signature other than at shock locations has been created.

A systematic method for determining shock location lies in the definition of the upper bound or "hull" of the integral of F(y). Defining

$$I(y) = \oint_{-\infty}^{y} F(t)dt \tag{16}$$

shocks will occur at all multi-valued points on the upper boundary of this function; for any such point A, figure 8, formed by the intersection of two distinct arcs of the function I(y) defines a point at which

$$\oint_{AOBA} F(y)dy = 0 \tag{17}$$

Multivariable Search

The general non-linear multivariable optimization problem is concerned with the maximization or minimization of a pay-off or performance function of the form

$$\phi = \phi(\alpha_i), \quad i = 1,2,\ldots, N \tag{18}$$

Subject to an array of constraints

$$C_j = C_j(\alpha_i) = 0, \quad j = 1,2,\ldots, P \tag{19}$$

The α_i are the independent variables whose values are to be determined so as to maximize or minimize equation (18) subject to the constraints of equation (19). They may be looked upon as the components of a control vector, α, in a space R^N of dimension N. Since maximization of a function is equivalent to minimization with a change of sign, it suffices to discuss the case in which the performance function is to be minimized.

Multivariable optimization problems involving inequality constraints may also be encountered. If the constraints are applied directly to the independent variables

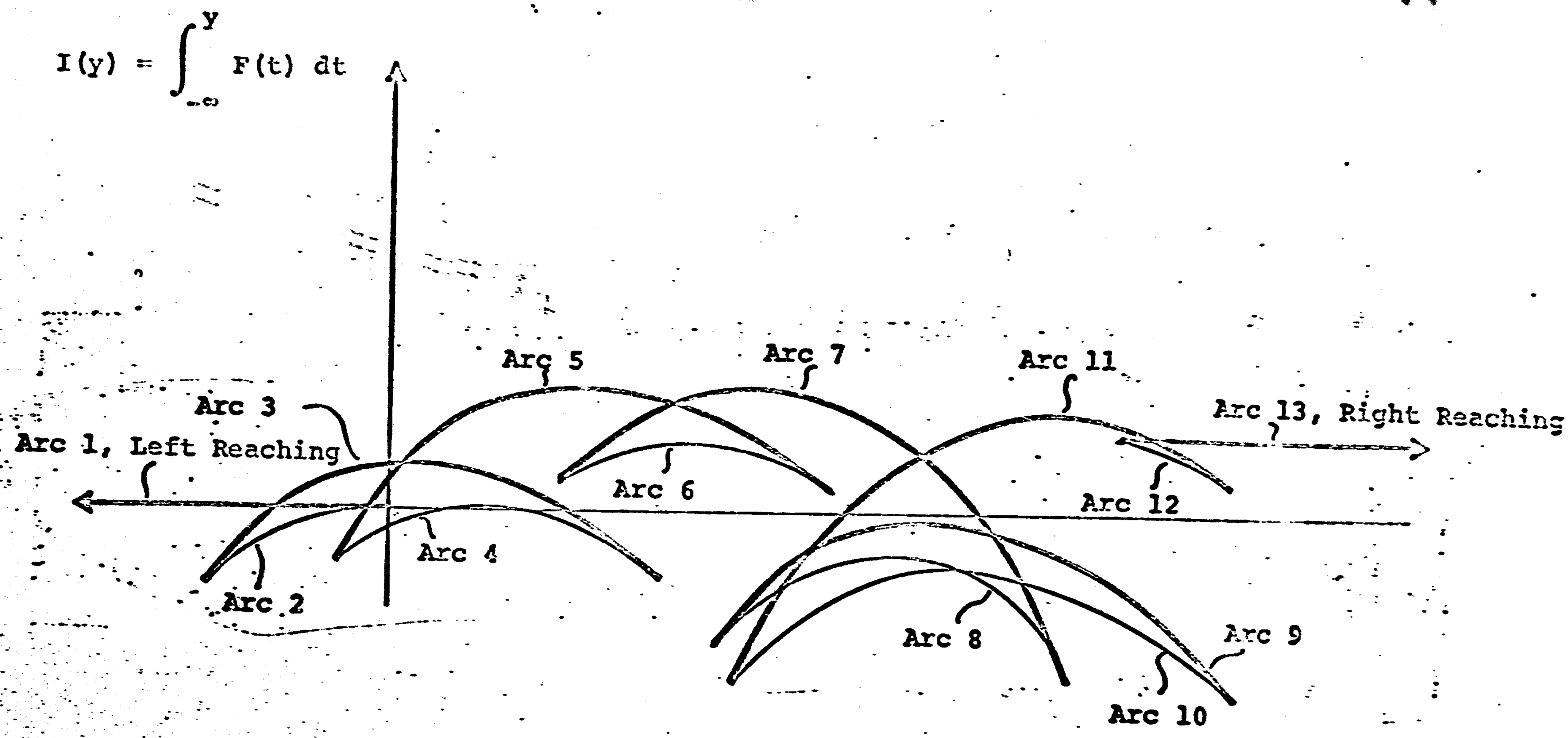

Figure 8.—Schematic of Shock Formations

$$\alpha_i^L \le \alpha_i \le \alpha_i^H \tag{20}$$

Constraints of this type define a region of the control space R^N within which the solution must lie. Inequality constraints on functions of the independent variables similarly restrict the region in which the optimal solution is to be obtained. In this case

$$E_k^L(\alpha_i) \le E_k(\alpha_i) \le E_k^H(\alpha_i) \tag{21}$$

Inequality constraints can be used to restrict the search region directly, or, alternatively, they may be applied in an indirect fashion by a transformation to equality constraints. Several transformations may be used for this purpose. For example, let an equality constraint, C_k, be defined by the transformation

$$C_k = \begin{cases} (E_k^L - E_k)^2, & E_k < E_k^L \\ 0 \qquad\qquad , & E_k^L \le E_k \le E_k^H \\ (E_k^H - E_k)^2, & E_k^H < E_k \end{cases} \tag{22}$$

Constraining C_k to zero will result in the constraint, equation (21), being satisfied.

Problems involving equality constraints can be treated as unconstrained problems by replacing the actual performance function, equation (18), by an augmented performance function ϕ^* by writing

$$\phi^* = \phi + \sum_{j=1}^{p} U_j \cdot C_j^2 \tag{23}$$

It can be shown that provided the positive weighting constants U_j are sufficiently large in magnitude, minimization of equation (18) subject to the constraints, equation (19), is equivalent to minimization of the unconstrained penalized performance function defined by equation (23). This approach permits search techniques for finding unconstrained minima to be applied in the solution of constrained minima problems at the cost of some increased complexity in the behavior of the performance function.

Alternatives to this approach are available, notably Bryson's approach to the steepest-descent search, reference 4. This method has been exploited in connection with the numerical solution of variational problems encountered in the optimization of aerospace vehicle flight paths, references 5, 6, and 7.

Numerical Solution of Non-Linear Multivariable Optimization Problems

A wide variety of search algorithms have been devised for the solution of multivariable optimization problems, many of which are restricted to the solution of linear or quadratic problems. Algorithms of this type will not be discussed further, for engineering problems in general tend to lead to non-linear formulation with the possibility of discontinuities in both the performance function and its derivative. Most of the searches which prove effective in these problems are based on the reduction of the direct search through the N dimensional control space to a succession of steadily improving one-dimensional searches. The direction of each of the one-dimensional searches is specified by a particular search algorithm, for example, the steepest-descent method. Distance traversed through the control space in the selected direction is determined by a step-size, or perturbation parameter, DP. The object of the one-dimensional search is to determine the value of DP which minimizes the performance function along the chosen ray and to establish the corresponding control vector.

In practice, the diverse nature of non-linear multivariable optimization problems leads to the conclusion that no one search algorithm can be uniquely described as being the "best" in all the situations which may be encountered. Rather, a combination of searches, some of which may be of a quite elementary nature is best calculated to provide reliable and reasonably economical convergence to the optimal solution.

One-dimensional search.—Multivariable search problems are reduced to one-dimensional problems whenever a search algorithm is used to establish a one-to-one correspondence between the control vector and a single scalar perturbation parameter, (DP). In such a situation

$$\alpha_i = \alpha_i(DP), \; i = 1,2 \; . \; . \; ., N \qquad (24)$$

so that equation (18) becomes

$$\phi = \phi(\alpha_i) = \phi(DP) \qquad (25)$$

Similarly, the right hand sides of equations (19) and (23) become functions of the scalar perturbation parameter.

The relationship, equation (24), specifies a ray through the control space. The objective of the one-dimensional search along this ray is to locate the value of DP which provides the minimum performance function value.

Numerical search for the one-dimensional minima can be carried out in a local fashion, by steepest-descent search, for example, or by a global search of the ray throughout the feasible region. The localized approach is appropriate to the terminal convergence phase in a problem solution when some knowledge of the extremal's position has been accumulated by the preceding portion of the search. The global search can be used to advantage in the opening moves of a search. In the early phase of a search the object is to isolate the location of the minimum performance function value as rapidly as possible, often with little or no foreknowledge of the performance function behavior. One measure of the effectiveness of a search algorithm in such a situation is the number of evaluations required to locate the minimum point to some prespecified accuracy. It can be shown that the most effective method of locating the minimum point of a unimodal function is a Fibonacci search, reference 8. In this method the accuracy to which the minimum is to be located along the perturbation parameter axis must be selected prior to the commencement of the search. Since the accuracy required is highly dependent on the behavior of the performance function, this quantity is difficult to prespecify. Prespecification of the accuracy to which the extremal's position is to be located can be avoided for little loss in search efficiency by use of an alternative search based on the so-called golden section, reference 8.

Search by the golden section commences with the evaluation of the performance function at each end of the search interval and at $G = 2/(1 + \sqrt{5})$ of the interval from both of these bounding points. This is illustrated in Figure 9.

The boundary point furthest from the lowest resulting performance function value is discarded. The three remaining points are retained,and the search continues in a region which is diminished in size by G. The internal point at which the performance function is known in the reduced interval will be at a distance G of the reduced interval from the remaining bounding point of the original interval for $(1-G) = G^2$. The search can, therefore, be continued in the reduced interval with a single additional evaluation of the performance function. It follows after Q evaluations of the performance function the position of the extremal point will be known to within R of the original search region where

$$R = G^{(Q-3)} \tag{26}$$

To reduce the interval of uncertainty to .00001 of the original search interval, about 27 evaluations of the performance function are required. For a reasonable number of evaluations of the performance function this type of search is almost as efficient as a Fibonacci search.

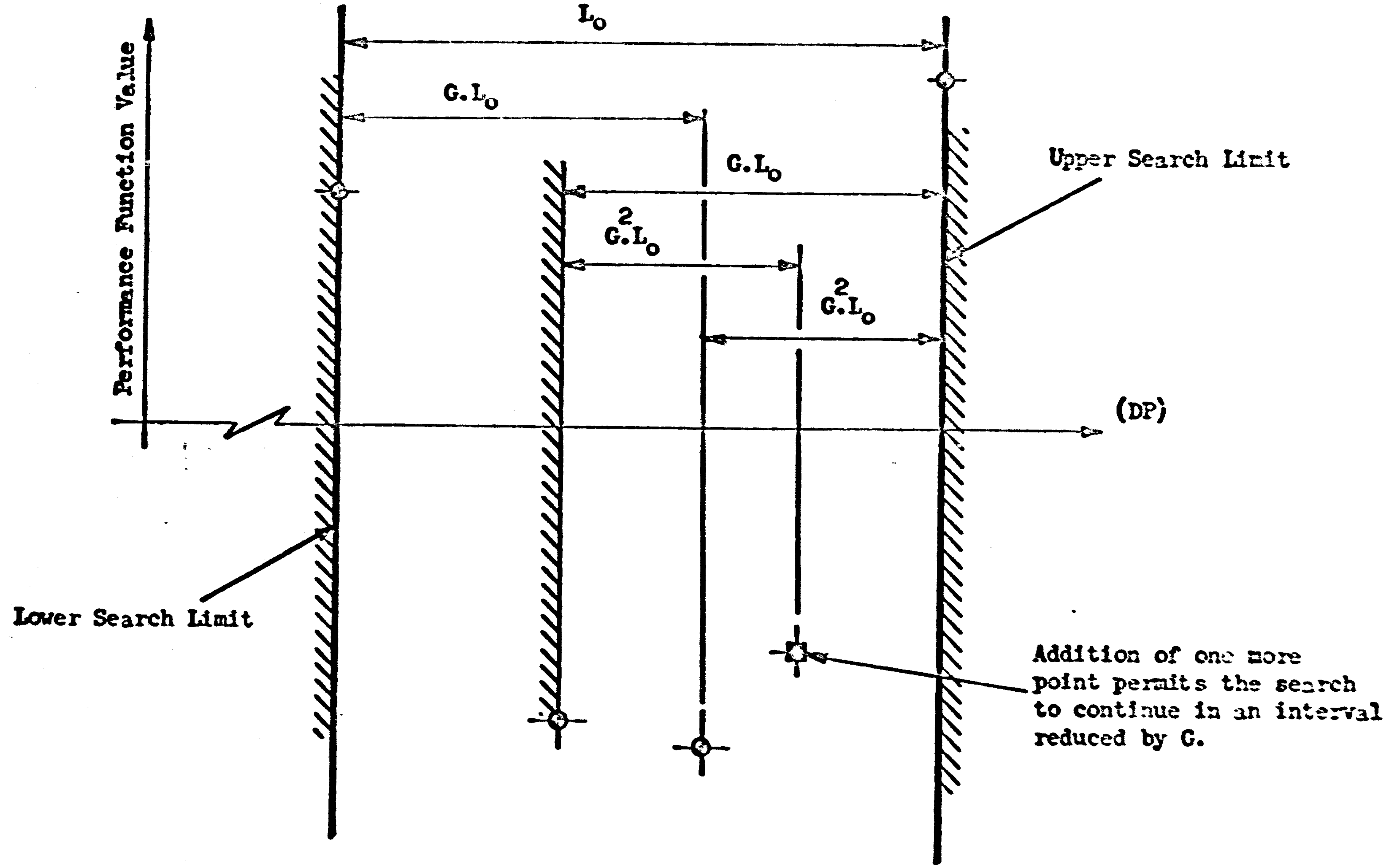

FIGURE 9. SEARCH BASED ON THE GOLDEN SECTION

It should be noted that search by the golden section proceeds under the assumption of unimodality; hence, it will often fail to detect the presence of more than one minimum when the performance function is multimodal. If more than one minimum does exist, the one located depends on performance function behavior within the original search interval.

Multiple Extremals.— The one-dimensional section search described above is unable to distinguish one local extremal from another; it will merely find one local extremal. This difficulty can be largely eliminated by the addition of some logic to the search, at least for moderately well behaved performance functions; that is, for functions having a limited number of extremals in the control space region of interest. An effective method for detecting multiple extremals is to combine the one-dimensional search with a random one-dimensional search on the same ray through the control space. This is illustrated in figures 10 and 11. In figure 10 the response contours of a performance function having two minima are illustrated together with some of the initial points at which a global one-dimensional search by the method of the preceding section would use for performance function evaluation. The behavior of the function at these points is shown in figure 11. The left hand minimum is not apparent from these points. If a single random point is added in the interval L_o, the probability of this point revealing the presence of the second minimum is

$$P_1 = L_1/L_o \tag{27}$$

for any point in the interval AB indicates the presence of a local minimum somewhere in the interval AB, and any point in the interval BC indicates the presence of a local maximum somewhere in the interval BC. In this latter case, there must be a minimum of the function both to the left and to the right of the newly introduced point.

If R random uniformly distributed points are added in the interval L_o, the probability of locating the presence of the second minimum becomes

$$P_N = 1.0 - (1.0 - L_1/L_o)^R \tag{28}$$

The function (L_1/L_o) is a measure of the performance function behavior. For a given value of this behavior function the number of random points which must be added to the one-dimensional search to provide a given probability of locating a second minimum can be determined.

The presence of multiple minima on a one-dimensional cut through an N-dimensional space does not necessarily indicate that the performance function possesses more than one minimum in a multi-dimensional sense. It may be that the performance function is merely non-convex. This is illustrated by figure 12. The performance function behavior on the one-dimensional search in figures 10 and 12 is identical. In figure 10 this indicates the presence of two local extremals; in figure 12, a non-convex performance function.

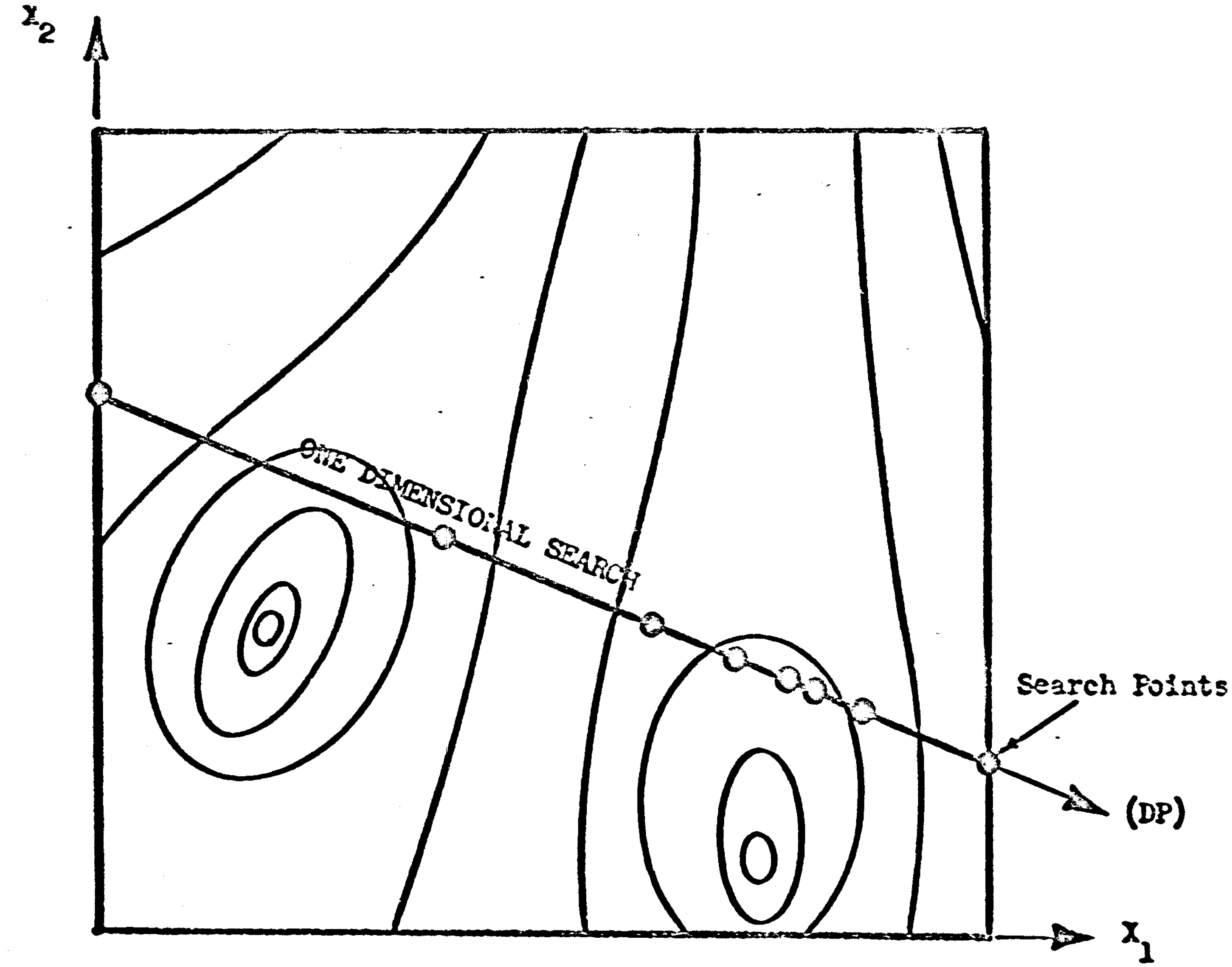

FIGURE 10. RESPONSE SURFACE WITH TWO TROUGHS

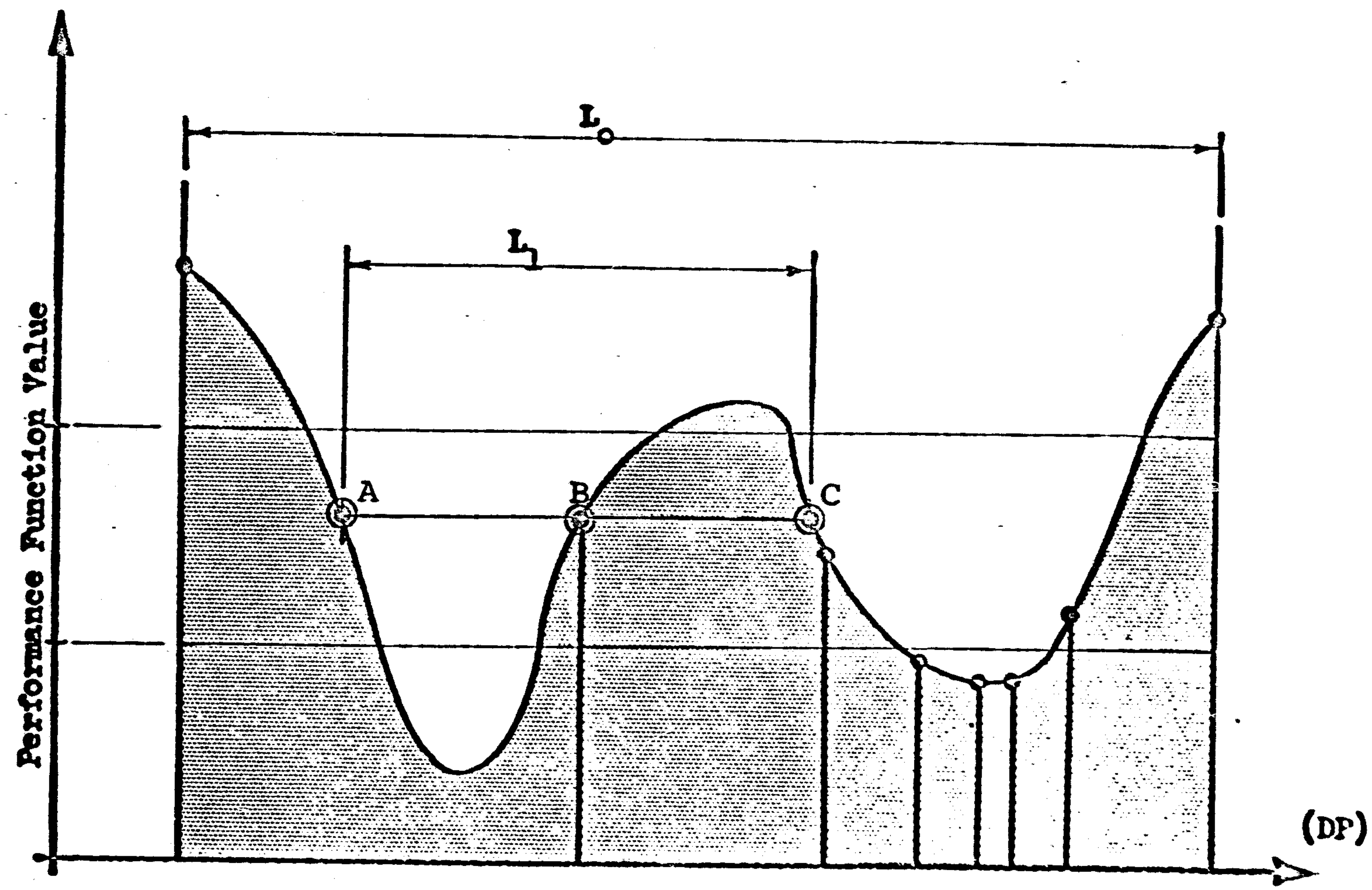

FIGURE 11. SEARCH BY GOLDEN SECTION FAILS TO DETECT MULTIPLE TROUGHS ON ONE DIMENSIONAL CUT

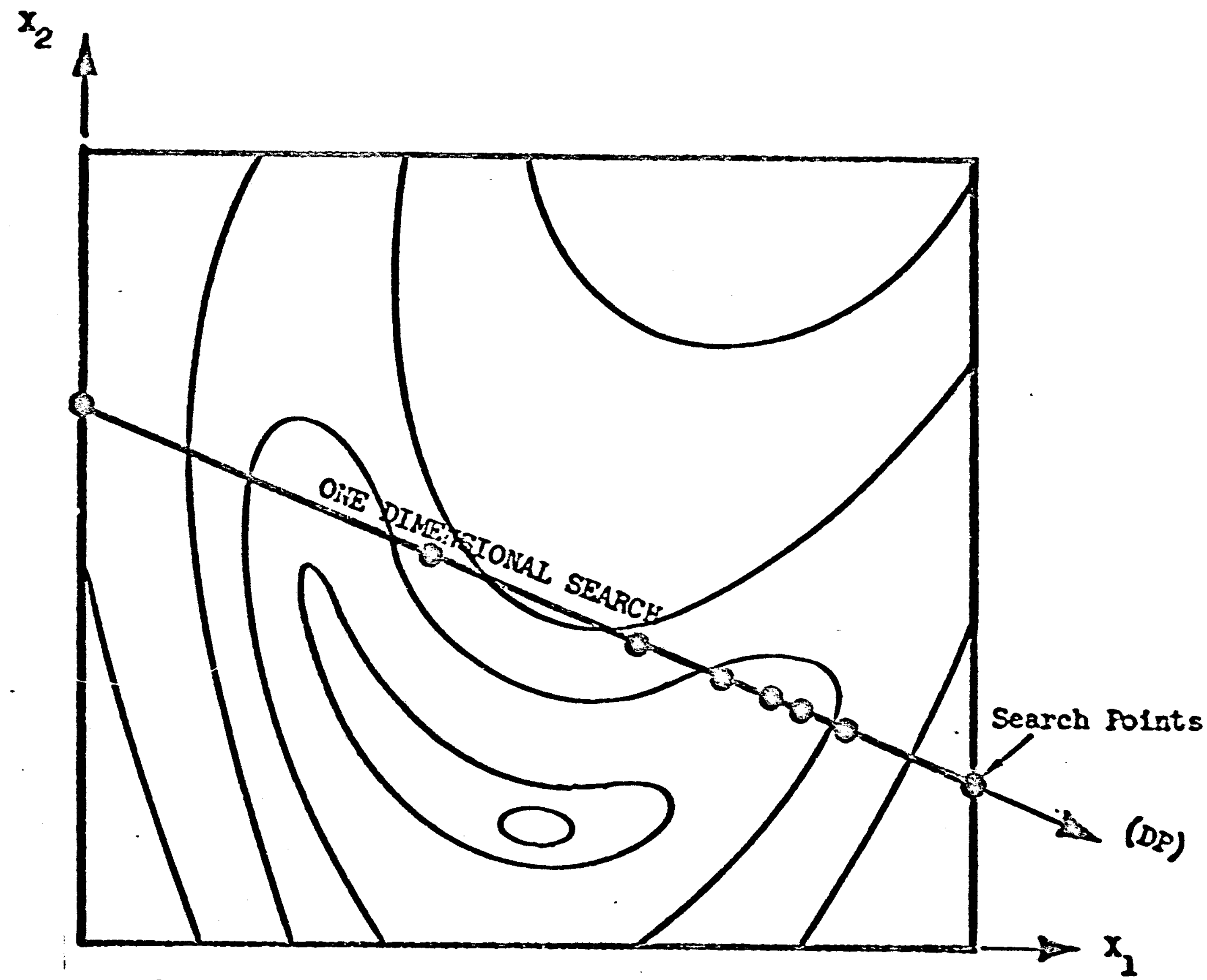

FIGURE 12-NON-CONVEX RESPONSE SURFACE

When a one-dimensional search detects the presence of multiple extremals in the local sense above, a decision must be made as to which of the apparent extremals is to be pursued during the remainder of the search. Here, without foreknowledge of the performance function behavior, logic must suffice. Typically, the left or right hand extremal, the extremal which results in the best performance, or even a random choice may be made.

The remainder of this section is devoted to the presentation of a selection of search algorithms for the solution of non-linear multivariable optimization problems.

Sectioning Parallel to the Axes.—The independent variable perturbation algorithm in the sectioning search is

$$\begin{aligned} \Delta\alpha_i &= 0, \quad i \neq r \\ &= DP, \; i = r \qquad r = 1,2,\ldots, N \end{aligned} \tag{29}$$

This is simply the parametric search approach. All but one of the independent variables are held constant while a one-dimensional search parallel to the R^{th} variable axis determines the best value of the remaining variable, α_r. The variable α_r is then set to this value, and the process is repeated with one of the remaining independent variables. When all N independent variables have been perturbed in this way, a sectioning search cycle has been completed.

The N-dimensional search can then be continued with another cycle of sectioning or by one of the other search techniques described below. In practice, it has been found advantageous to perturb the independent variables in a random order within each sectioning cycle. The method can be used in conjunction with either a local or a global search as outlined in the two preceding sections. The behavior of this search in the solution of a straightforward two-variable optimization problem is illustrated in figure 13.

Steepest-Descent Search.—The steepest-descent search algorithm is

$$\begin{aligned} \{\Delta\alpha\} = &-[W]^{-1}\left\{\left\{\frac{\partial\phi}{\partial X}\right\} - \left[\frac{\partial C}{\partial X}\right]^T[K_3]^{-1}\{K_2\}\right\} \\ &\times \sqrt{\frac{(DP)^2 - \lfloor DC \rfloor [K_2]^{-1}\{DC\}}{K_1 - \lfloor K_2 \rfloor [K_3]^{-1}\{K_2\}}} \\ &-[W]^{-1}\left[\frac{\partial C}{\partial X}\right]^T[K_3]^{-1}\{DC\} \end{aligned} \tag{30}$$

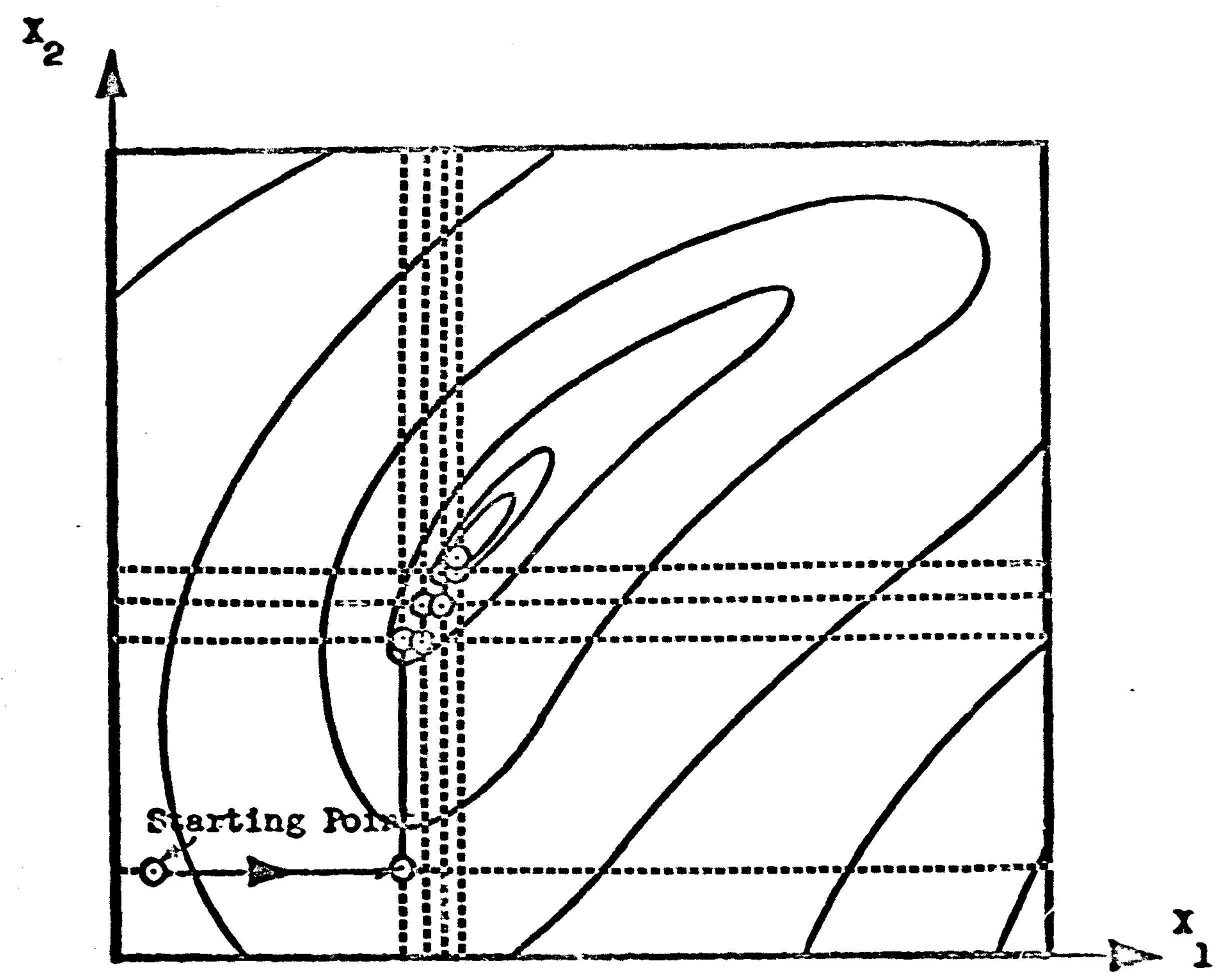

FIGURE 13. SECTIONING PARALLEL TO THE AXES

Here the matrix W is the metric tensor of the control space and serves to define a generalized measure for the magnitude of a control vector perturbation. The K matrices are defined as

$$K_1 = \left\lfloor\frac{\partial\phi}{\partial X}\right\rfloor [W]^{-1}\left\{\frac{\partial\phi}{\partial X}\right\} \tag{31}$$

$$\{K_2\} = \left[\frac{\partial C}{\partial X}\right][W]^{-1}\left\{\frac{\partial\phi}{\partial X}\right\} \tag{32}$$

$$[K_3] = \left[\frac{\partial C}{\partial X}\right][W]^{-1}\left[\frac{\partial C}{\partial X}\right]^T \tag{33}$$

and the perturbation parameter, (DP), is defined by

$$(DP)^2 = \lfloor\Delta\alpha\rfloor[W]\{\Delta\alpha\} \tag{34}$$

The vector $\overline{DC}$ is the desired change in the constraint functions. For an unconstrained problem, (30) reduces to

$$\{\Delta\alpha\} = -[W]^{-1}\left\{\frac{\partial\phi}{\partial X}\right\}\sqrt{\frac{(DP)^2}{K_1}} \tag{35}$$

The performance function change associated with the perturbation of equation (30) is

$$D\phi = -\left(K_1 - \lfloor K_2\rfloor[K_3]^{-1}\{K_2\}\right)^{.5}\left((DP)^2 - \lfloor DC\rfloor[K_3]^{-1}\{DC\}\right)^{.5} + \lfloor K_2\rfloor[K_3]^{-1}\{DC\} \tag{36}$$

Equation (30) does not specify a one-dimensional search directly since the perturbation parameter (DP) and each component of the constraint vector change $\overline{DC}$ can be independently specified. This difficulty is conveniently eliminated if the components of $\overline{DC}$ are expressed in terms of the perturbation parameter. Let (DP) and $\overline{DC}$ be arbitrarily assigned, say (DP_0) and $\overline{DC}_0$, respectively. Now consider the one parameter set of values for $\overline{DC}$ defined by

$$\overline{DC} = \frac{(DP)}{(DP_0)} \cdot \overline{DC}_0 \tag{37}$$

It follows from equations (30) and (36) that (37) specifies a one parameter family of perturbations in which the performance and constraint functions vary linearly with (DP), to first order.

Equations (30) to (36) are valid for small perturbations in the independent variables provided the derivatives involved are continuous in the region of the control space defined by equation (34). In practice when this condition is not satisfied, the steepest-descent algorithm can be used to locate a promising direction for a one-dimensional search provided the derivatives are computed numerically. In this case, however, equation (36) ceases to provide an accurate indication of the performance function behavior along the specified ray.

When dealing with performance and constraint functions having continuous first derivatives the perturbation parameter value to be used in equation (30) can be determined from a second order Taylor's expansion of the performance function behavior in terms of DP. The coefficients in this series expansion can be readily obtained from the conditions of zero change for DP=0, linear slope for DP=0, and from the actual value of the performance function at a point in the neighborhood of the point at DP=0. This method for determining the best perturbation parameter value is discussed in some detail in references 5 and 6. When dealing with less regular functions the one-dimensional search of the preceding section can be used to determine the perturbation parameter value. This is the technique employed in the optimization program, AESOP, references 9 through 11.

Steepest-Descent Weighting Matrices.—The weighting matrix introduced in equations (30) and (34) must be positive definite to assure a positive distance between any two non-coincident points in the control space. Apart from this imposed restriction, the choice of weighting matrix is arbitrary. Inspection of equation (30) reveals that any descending direction is a steepest-descent path for some choice of the weighting matrix W. This can be simply illustrated when only two independent variables are involved. Figure 14 depicts a small region of the control space R^2. The performance function response contours appear as a series of parallel lines on this microscopic region of the control space. The perturbation zones corresponding to three weighting matrix choices are shown. The first zone corresponds to the choice of a unit matrix for W. It follows from equation (34) that for a given value of $(DP)^2$ the search zone is a circle of radius (DP). The steepest-descent direction is that in which the performance improvement is the greatest. This is the direction of a line from the origin of the circular search zone to that point on its circumference which provides the smallest value of the performance function $\phi(\bar{\alpha})$. With this choice of weighting matrix the steepest-descent direction is perpendicular to the response contours. Paths of this type are illustrated in figure 15 by the solid lines emanating from points A and B. From the nominal point A, search perpendicular to the performance response contours is very efficient. From point B, however, this type of search results in the meandering path illustrated. It is assumed here that once a steepest-descent direction is located an exhaustive

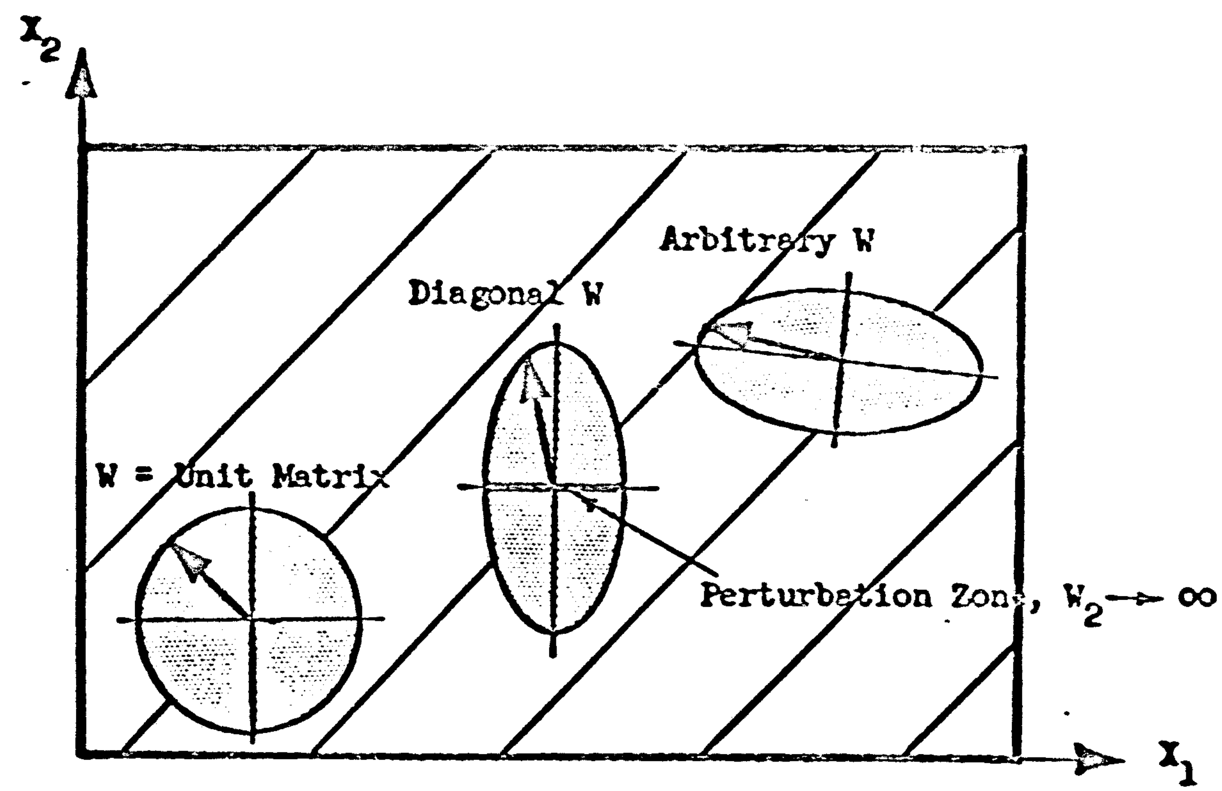

FIGURE 14.-PERTURBATION ZONES CORRESPONDING TO THREE WEIGHTING MATRICES

search for the minimum in that direction will be undertaken in view of the high cost of recomputing the derivatives in many problems. Even if this were not the case, search normal to the response contours can often be improved upon. For example, it is obvious that even in the straightforward two dimensional problem of figure 15 the dashed search direction is superior. This direction requires a priori knowledge of the extremal's position, information not normally available.

Returning to figure 14, the second search zone depicted corresponds to the choice of a diagonal matrix for W. The positive-definite constraint on W requires that all diagonal elements of the weighting matrix be positive. In this case the search zone becomes elliptical with the major and minor axes of the ellipse being parallel to the coordinate axes. It may be noted that as either of the diagonal elements of W becomes large in relation to the remaining element, the corresponding element in W inverse together with the predicted change in the associated independent variable becomes small. In the limit this reduces the search to a one-dimensional search in the remaining coordinate. The perturbation zone then becomes a slit parallel to that coordinate axis of length 2 · (DP), as illustrated. In this case, the steepest-descent path is in the descending α_1 direction.

Finally, the search zone corresponding to the choice of an arbitrary positive-definite weighting matrix is shown. From equation (34) and the positive-definite constraint on W, the search zone remains elliptical, but the principle axes may now have an arbitrary orientation to the axes of α_1 and α_2. It follows that since the elliptic search zone can have any orientation and eccentricity, any direction in the control space is a possible steepest-descent path; for in all cases, the path of steepest-descent lies in the direction of a line joining the search zone origin to the lower point of tangency between the boundary of the search zone and the performance function response contours. The discussion above may readily be extended to control spaces of higher dimensionality.

When attempting the solution of optimization problems by the steepest-descent method, the analyst is constantly faced with the problem of choosing a satisfactory weighting matrix for the search continuation. The problem is compounded by the fact that the slopes of the performance function with respect to the independent variables can, and frequently do, vary by many orders of magnitude. The arbitrary choice of a unit matrix in such situations can lead to distressingly slow convergence of the numerical search; for it is in the nature of many problems that in those directions in which the slopes are greatest, the response surface is highly non-linear.

Only small perturbations will be successful in the direction of these strong variables. In those directions in which the slopes are small, the contours are often relatively linear, and large perturbations may be required in these weak variables.

In such situations the local steepest-descent direction for $[W] = [I]$ is quite misleading; for contrary to the resulting steepest-descent direction which, by equation (35), results in independent variable perturbations which are in proportion to the response surface partial derivatives, the best direction in which to proceed may well involve large perturbations in the weak variables of small slope. This behavior is illustrated for a two-dimensional case in figure 15 by the dashed line emanating from B.

The problem of choosing a satisfactory weighting matrix also arises when the steepest-descent search is applied in its variational form, reference 5, and when a combination of continuous control variables and parameters are encountered as in the optimization of multiple-arc problems in flight path optimization problems, reference 6. In these references it is suggested that the weighting matrices be based on the first derivatives of the unconstrained performance function with respect to the control. This approach can be used in the solution of multivariable optimization problems also, by writing

$$W_{ij}^{-1} = A_i + B_i \cdot \left|\frac{\partial \phi}{\partial X_j}\right|, i = j$$

$$= 0, \; i \neq j \qquad (38)$$

In practice, alternate use of equation (38) and the unit matrix for W tends to provide a reasonable convergence rate at points well removed from the extremal.

Random Ray Search.—The difficulty of defining a suitable control variable metric tensor together with the fact that any descending path is a steepest-descent direction for some choice of metric tensor suggests the possibility of searching along a random ray through the control space. The algorithm for random ray search is

$$\Delta\alpha_i = R_i \cdot (\pm DP), \; i = 1,2,\ldots, N \qquad (39)$$

where the R_i, the direction cosines of the ray, are uniformly distributed random numbers satisfying

$$-1.0 \leq R_i \leq +1.0, \; i = 1,2,\ldots N$$

The positive sign in equation (39) is taken if $\frac{d\phi}{d(DP)}$ is negative ; the negative sign is taken when this derivative is positive.

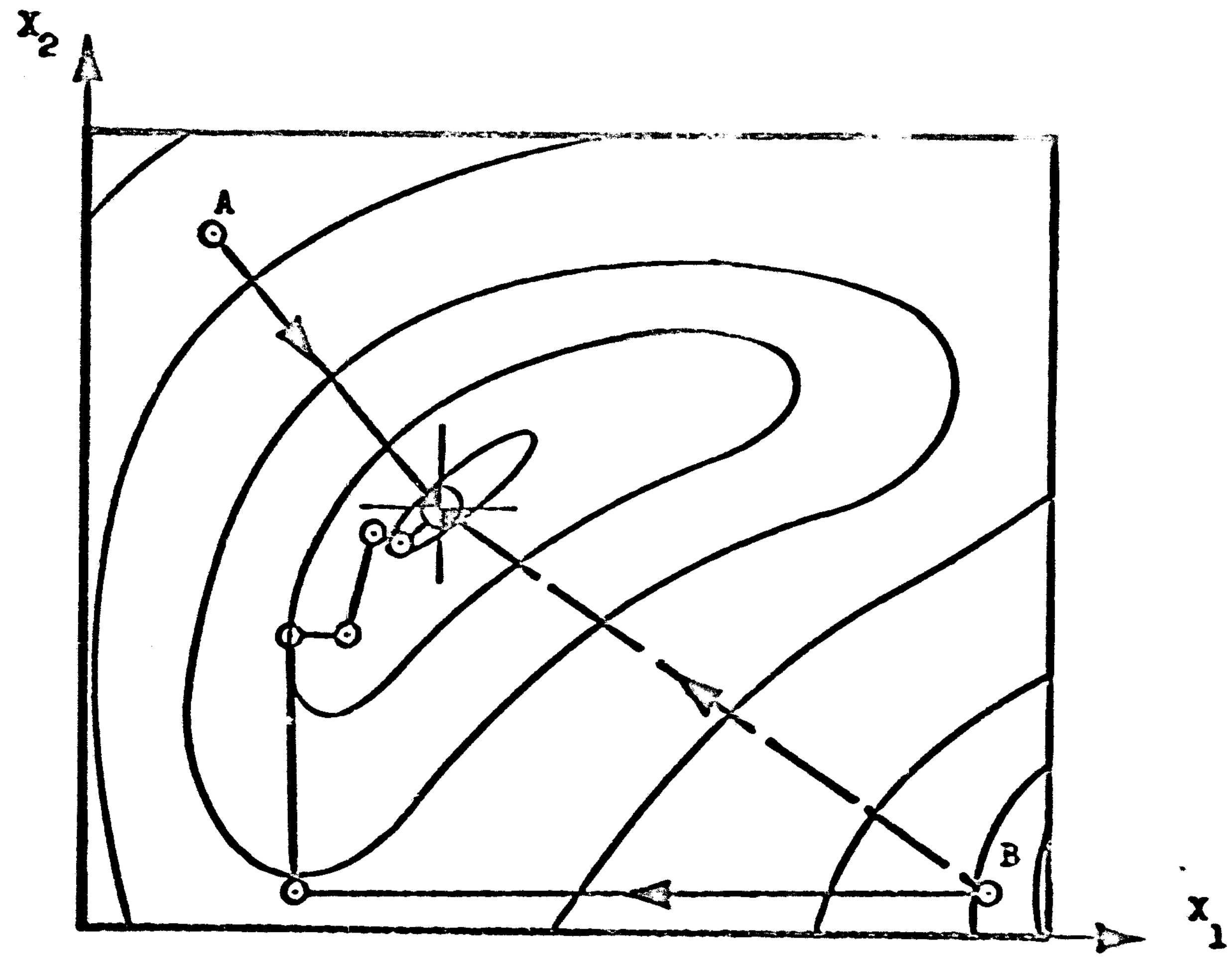

FIGURE 15.-STEEPEST-DESCENT SEARCH

The utility of this type of search tends to be in proportion to the complexity of the performance function response contours. On a well-behaved problem there is little to recommend this type of search; on a problem involving unexpected behavior on the part of the performance function, a random ray search has a certain appeal. The method is, of course, equivalent to a steepest-descent search using a randomly generated metric tensor.

Quadratic search.—An alternative approach to the definition of an arbitrary or empirical weighting matrix is provided by second order or quadratic method. It can be shown, for example, in reference 9 that on an elliptic second order response surface the weighting matrix

$$W_{ij} = \left(\frac{\partial^2 \phi}{\partial \alpha_i \partial \alpha_j}\right)_0 \tag{40}$$

will immediately define the extremal point

$$\{\alpha^*\} = \{\alpha_0\} + \{\delta\alpha\} \tag{41}$$

where $\{\delta\alpha\}$ is computed from equation (35) with $(DP)^2 = .5K_1$. On a more general non-linear response surface, equation (41) merely defines a direction for subsequent search in the manner of the steepest-descent technique. This is illustrated in figure 16. Here the approximating elliptical contours computed at point 0 define an approximate extremal location at P through equations (40) and (41). Subsequent search along the ray OP results in the definition of a one-dimensional extremal. This point is then used to fit another approximating elliptic contour, and the process is repeated until the extremal point at Q is located.

The quadratic search procedure can be quite rapid in control spaces of low dimensionality. In high order spaces the approach is usually impractical as a result of the requirement to establish the second order weighting matrix of equation (40). In many practical engineering problems these derivatives cannot be obtained in closed form; in such cases the derivatives must be obtained numerically, for example, reference 9. Computation of these derivatives requires at least $(N+1)(N+2)/2$ evaluations of ϕ at each point where an approximating quadratic is employed. Clearly, for large N this computation may become impractical.

Davidon's Method.—Davidon's method is a hybrid first order/second order technique. The objective of Davidon's method is to arrive at a reasonable approximation to the second order weighting matrix of equation (40) without the use of $(N+1)(N+2)/2$ evaluations of ϕ. It can be shown that on a quadratic (second order) response surface M steepest-descent searches performed in the manner described previously

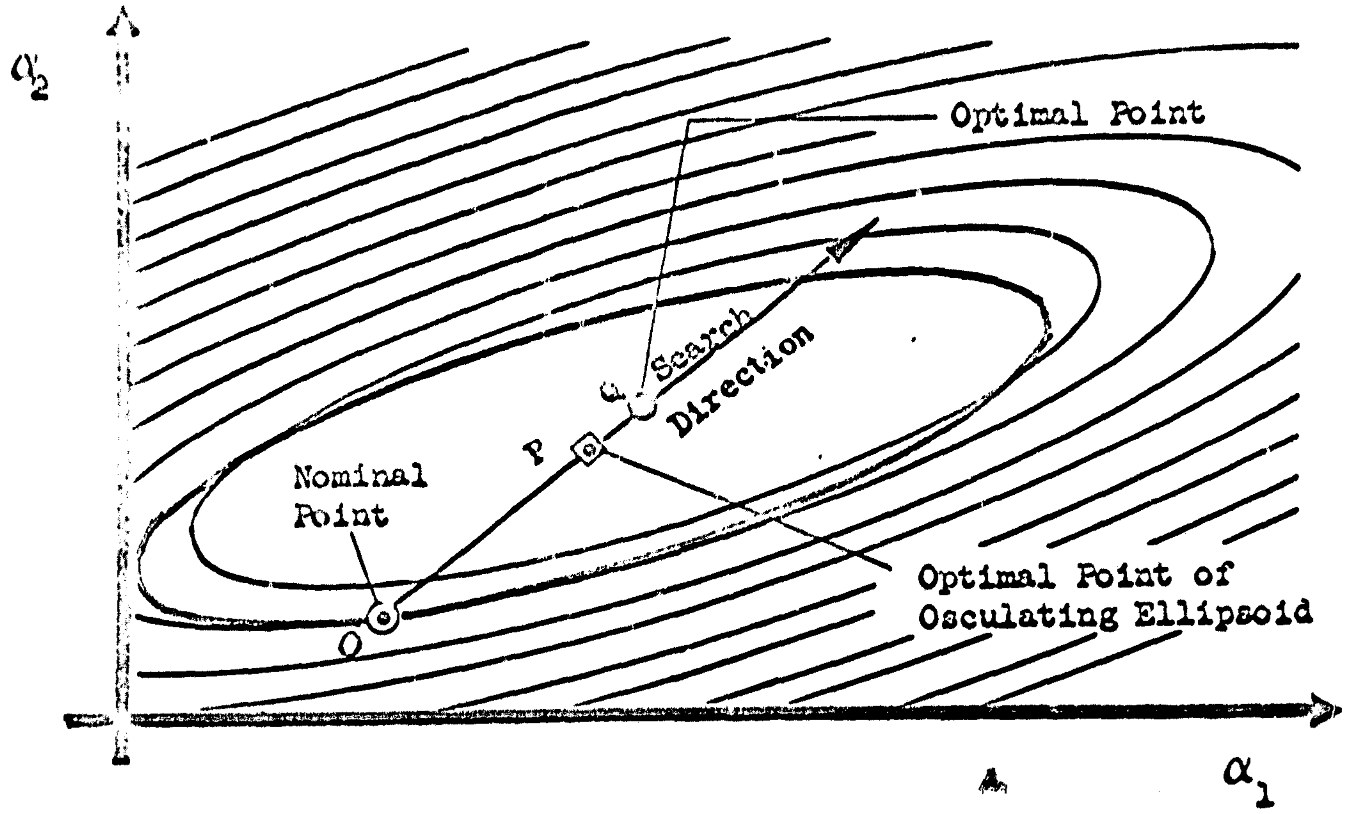

FIG. 16a - QUADRATIC SEARCH BEHAVIOR ON A NEAR SECOND-ORDER SURFACE

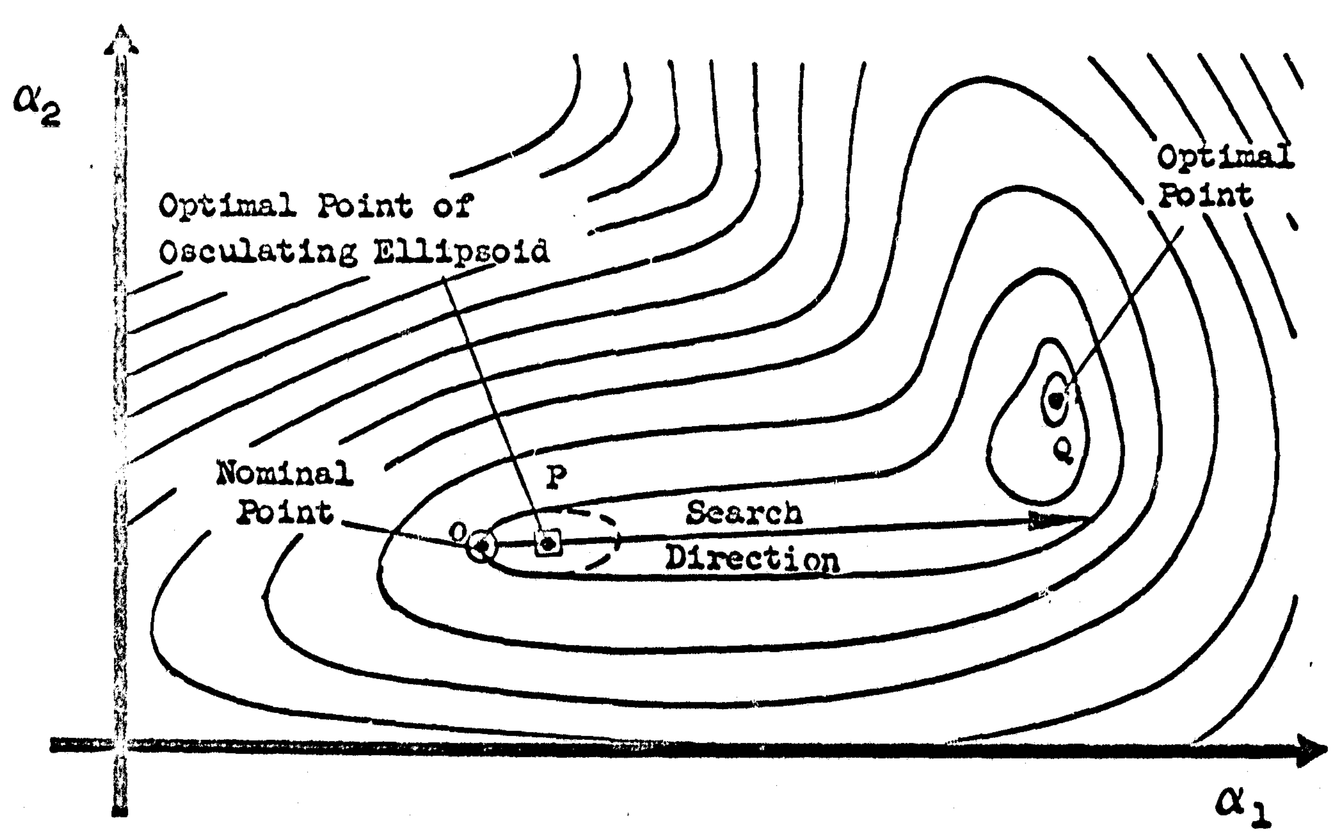

FIG. 16b - QUADRATIC SEARCH ON A HIGHER ORDER SURFACE will lead to definition of the weighting matrix of equation (40) if the following recursion formula is employed:

$$[W]^{-1}_{i+1} = [W]^{-1}_{i} + [A]_i + [B]_i \tag{42}$$

where

$$[A]_i = \frac{\{\Delta\alpha\}_i \lfloor\Delta\alpha\rfloor_i}{\lfloor\Delta\alpha\rfloor_i \{\Delta\cdot\frac{\partial\phi}{\partial\alpha_i}\}} \tag{43}$$

$$[B]_i = -\frac{[W]^{-1}_i \{\Delta\cdot\frac{\partial\phi}{\partial\alpha}\}_i \left\lfloor\Delta\cdot\frac{\partial\phi}{\partial\alpha}\right\rfloor_i [W]^{-1}_i}{\left\lfloor\Delta\cdot\frac{\partial\phi}{\partial\alpha}\right\rfloor_i [W]^{-1}_i \{\Delta\cdot\frac{\partial\phi}{\partial\alpha}\}_i} \tag{44}$$

$$[W]^{-1}_1 = [I] \tag{45}$$

Here, $\lfloor\Delta\alpha\rfloor_i$ is the change in position during the i^{th} one-dimensional search and

$$\left\lfloor\Delta\cdot\frac{\partial\phi}{\partial\alpha}\right\rfloor_i$$

is the change in gradient vector between the beginning and end of the i^{th} one-dimensional search. On a numerically well-behaved function this technique works well. When appreciable numerical noise is present in the calculation, the method may produce erratic convergence to the extremal point or convergence failure.

Pattern Search.—In the present report pattern search refers to a search which exploits a gross direction revealed by one of the other searches. The search algorithm is

$$\Delta\alpha_i = (\alpha_i^2 - \alpha_i^1)\cdot(DP),\ i = 1,2,\ldots,N \tag{46}$$

where α_i^2 and α_i^1 are the components of the control vector before and after the use of a preceding search technique. This type of search is illustrated in figure 17 following a section search. The combination of a section search and a pattern search in the problem illustrated leads directly to the neighborhood of the extremal. Repeated sectioning, on the other hand, would be a very slowly converging process due to the orientation of the contours with respect to the axes of the independent variables. It may be noted that a simple rotation of the independent variable axes by 45° results in sectioning alone becoming a rapidly converging process in this example. The pattern search can also be used to accelerate the steepest-descent process provided it follows two successive descents as in figure 18.

Adaptive Search.— Adaptive search is a form of small scale sectioning; however, instead of locating the position of the one-

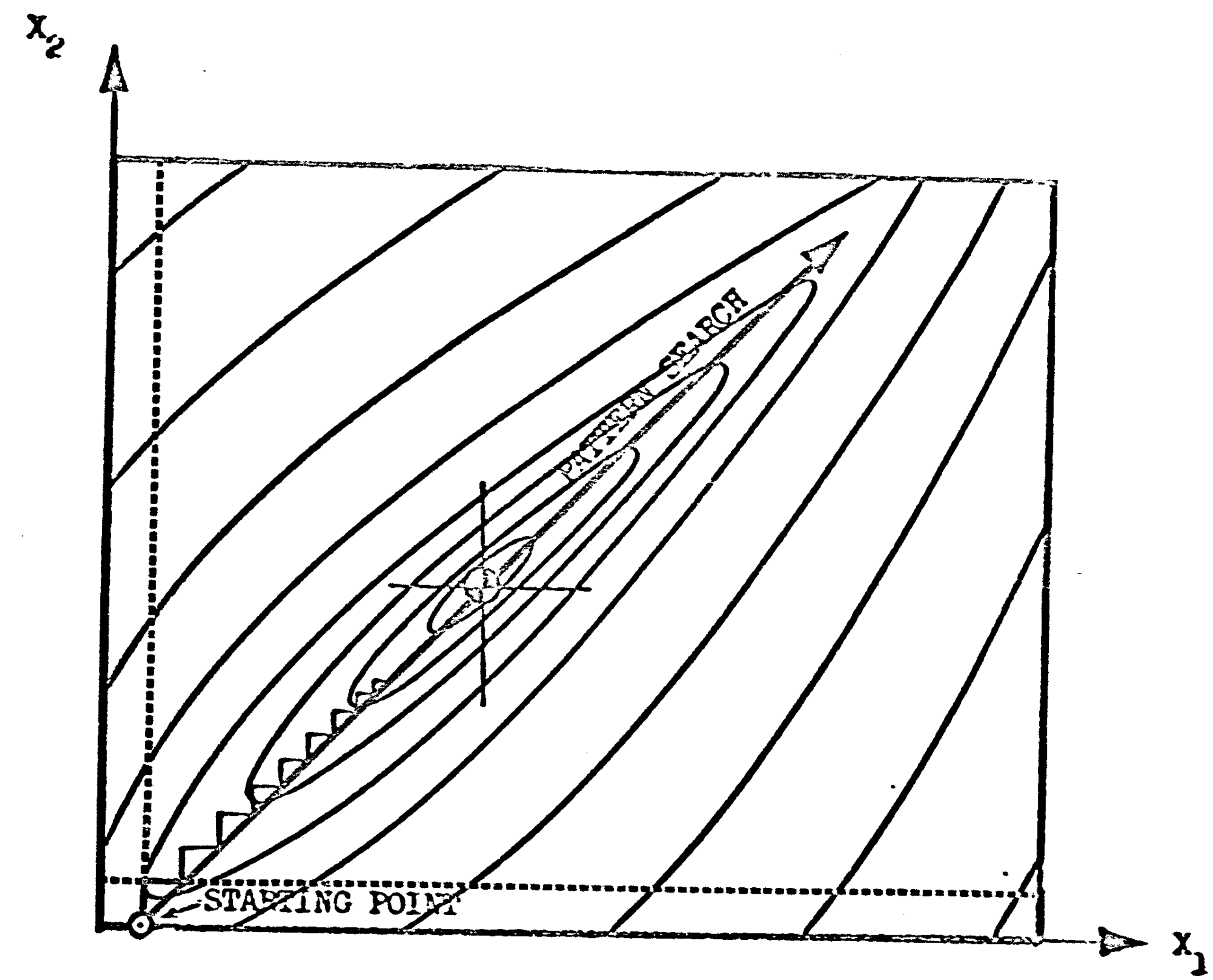

FIGURE 17. PATTERN SEARCH FOLLOWING SECTIONING PARALLEL TO THE AXES

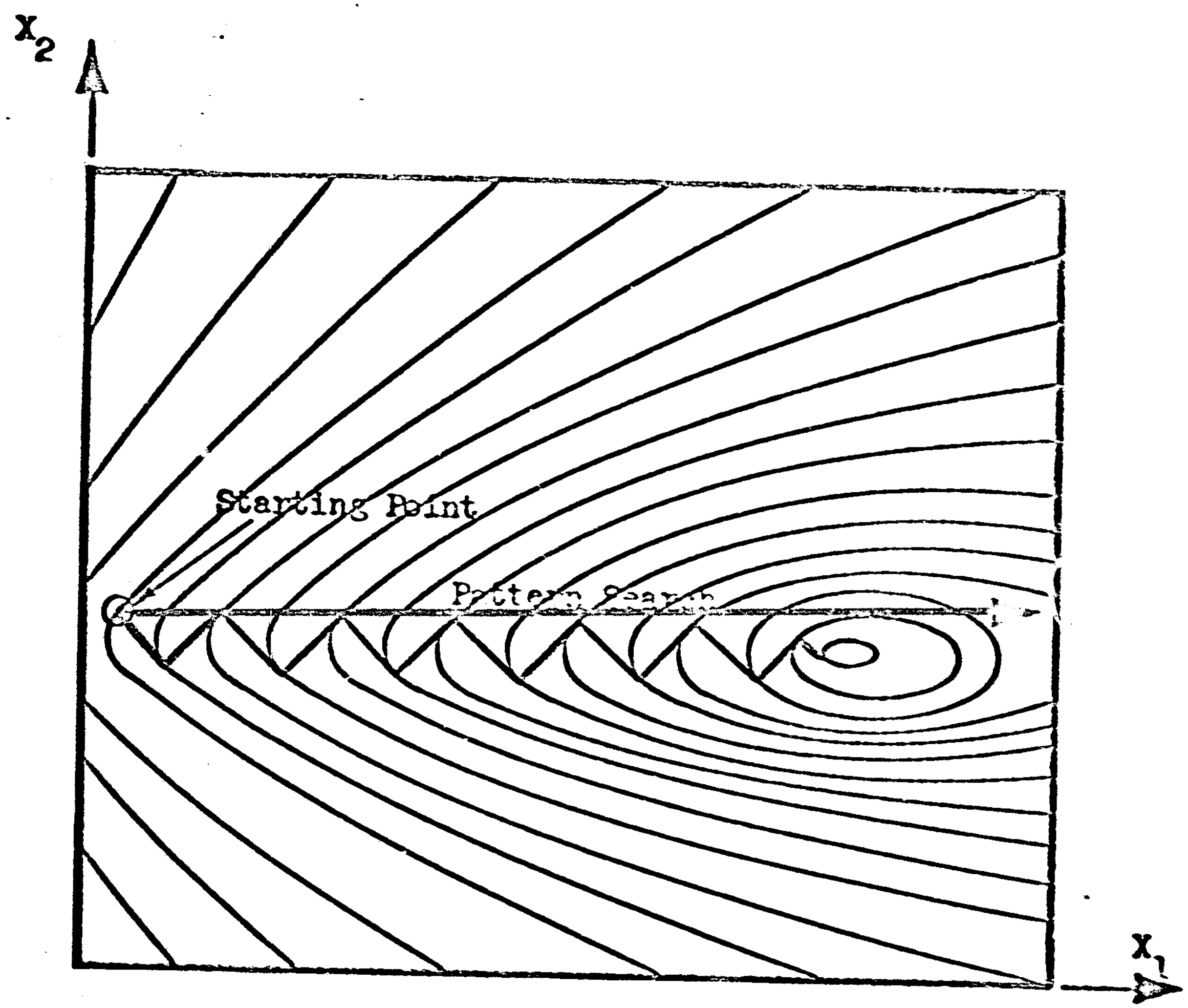

FIGURE 18.-PATTERN SEARCH FOLLOWING TWO STEEPEST-DESCENT SEARCHES

dimensional extremal on each section parallel to a coordinate axis, the coordinate is merely perturbed by a small amount, $\Delta\alpha_r$, in the descending direction.

The search commences with a small perturbation in one of the independent variables, α_r; the perturbation is first made to the left;if this fails to produce a performance improvement, the variable is perturbed to the right. If neither of the perturbations produces an improved performance value, the variable retains its nominal value, and $\Delta\alpha_r$ is halved. If a favorable perturbation is found, the variable α_r is set to this value, and $\Delta\alpha_r$ is doubled. The process is repeated for each independent variable in turn, the order in which the variables are perturbed being chosen randomly. At this point an adaptive search cycle is complete, and the cycle is then repeated. A two-dimensional illustration of this search is presented in figure 19. In the particular problem illustrated the method converges rapidly reaching the neighborhood of the extremal within six evaluations.

The search algorithm can be written in the form

$$\Delta\alpha_r = 2.0^{(S_r - T_r)} \cdot (DP), \tag{47}$$

where S_r is the number of cycles in which the search has successfully perturbed the r^{th} independent variable, and T_r is the number of cycles in which a perturbation of the r^{th} variable has proved unsuccessful. While this search can be looked upon as a one-dimensional approach, this viewpoint is somewhat artificial. Here, the scalar quantity (DP) merely defines an initial perturbation for each independent variable. Once started the search proceeds inevitably to its conclusion, the perturbation in each independent variable being adaptively determined according to equation (47) on the basis of the performance function response contour behavior encountered during the particular problem solution.

Magnification.—When studying discrete models of continuous systems of the type encountered in aerodynamic shaping problems there is a tendency on the part of some search algorithms to achieve a favorable shape before satisfying the desired constraint levels. In such cases a simple magnification search can lead to rapid convergence to the desired solution. The magnification algorithm is

$$\Delta\alpha_i = \alpha_i \cdot (DP), \ i = 1,2,. . .N \tag{48}$$

Here (DP) is positive and all components of the control vector are to be simultaneously perturbed. Generally, when the unconstrained extremal point corresponds to the null vector, this method may prove efficient.

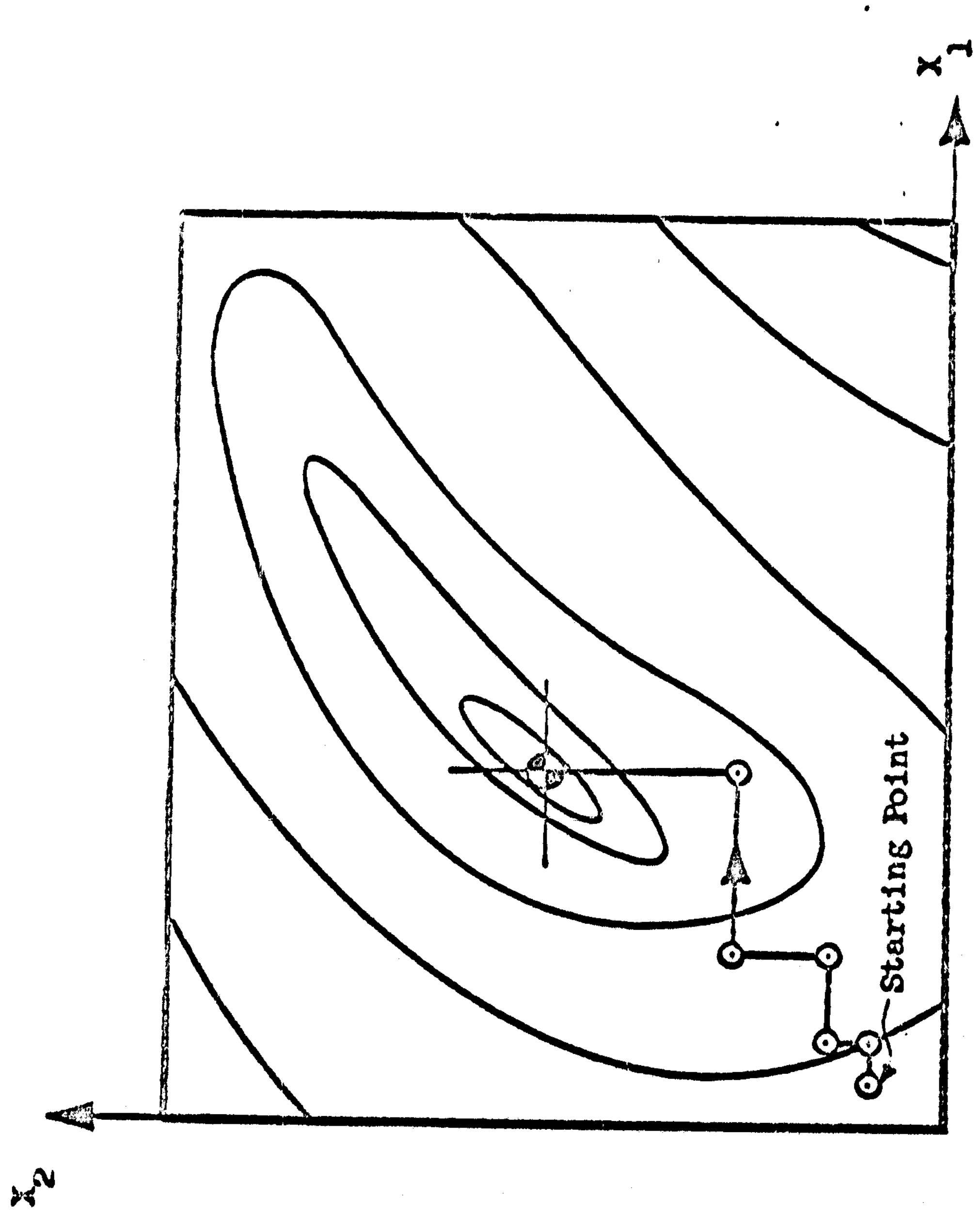

FIGURE 19.—ADAPTIVE SEARCH

Summary of Multivariable Search Techniques.—The searches described above have proved adequate for the solution of a wide range of practical engineering optimization problems. They are not a comprehensive collection of all the multi-dimensional search procedures which have been proposed to-date. In view of the diverse behavior exhibited by the multivariable performance function response surfaces, there is a strong likelihood that a combination of searches will prove superior to any single search procedure whenever an extensive array of optimization problems are to be studied. With this point in mind the suggested searches have been combined into a single generalized multivariable optimization computer program, AESOP, references 9 through 11. The program construction allows the equations of a particular problem to be introduced as a subroutine or main program to the optimizer. The major requirement of the subroutine or main program is that on receipt of a control vector it computes unique performance and constraint function values. By perturbing the control vector according to the algorithms described above, the optimizer traces a sequence of improving paths through the control space and thus ultimately arrives at a point within the neighborhood of the extremal.

Past applications of program AESOP have been fairly widely reported; for example, references 11 through 13. In this report the program is applied to the definition of certain restricted classes of minimum sonic boom overpressure (for axi-symmetric or equivalent body) shapes. The remainder of the report describes these applications in detail.

MINIMUM OVERPRESSURE SINGLE POWER BODIES

Single power body shapes are defined as those body shapes described by a radius distribution, $r(x)$ of the form

$$r(x) = Cx^N \qquad (49)$$

They are, thus, a two parameter family of body shapes. Generally, one of these parameters, the constant C, will be specified by a geometric constraint imposed on the body; thus, if the body radius at the point $x = L$ is to be constrained

$$C = \frac{r(L)}{L^N} \qquad (50)$$

Again, if the body volume between the nose and the point $x = L$ is to be constrained

$$C = \left[\frac{(2N+1)V_N}{\pi L^{(2N+1)}}\right]^{1/2} \qquad (51)$$

for the nose volume V_N is given by

$$V_N = \pi \int_0^L (Cx^N)^2 dx$$

$$= \pi C^2 \cdot \frac{L^{2N+1}}{2N+1} \qquad (52)$$

In either case, equation (50) or (51), imposition of the geometric constraint reduces the number of parameters defining the family of bodies to one. Since the constraint of equation (50) or (51) reduces the family of permissible body shapes, equation (49), to dependence on the single parameter N, determination of the minimum overpressure body shape has been reduced to a one parameter optimization problem. Such problems are readily solved by the sectioning technique described in the preceding section. The remainder of the section discusses results obtained in this manner when the constraints of equation (50) and (51) are applied. The effect of varying h/ℓ, Mach number, and, to a limited degree, the body fineness ratio are discussed in detail. Prior to this discussion a modification to the body shape of equation (49) which limits the maximum body slope, dr/dx, is discussed.

Introduction of Slope Constraint

When the body shape generated by equation (49) represents a physical body and not an equivalent body which includes an equivalent area component, equation (6), it may be desirable to limit the body slope, dr/dx, to be less than some prescribed value, M. In the calculations of this section, this is achieved by imposing the constraint

$$r(x+\delta x) = r(x) + M \cdot \delta x \tag{53}$$

whenever

$$C(x+\delta x)^N > Cx^N + M \cdot \delta x \tag{54}$$

Some typical body shapes generated by equations (49) and (50) with and without the constraint of equation (53) are presented in figure 20. It should be noted that in all numerical solutions in this section, $L = 4.0$.; for $x > 4.0$, the body assumes a cylindrical form with $r(x) = r(L)$; $x \geq 4.0$.

Solution with Base Area and Nose Length Fixed

With base area and nose length fixed the body radius distribution becomes

$$r(x) = \frac{R_B}{L^N} x^N \tag{55}$$

subject to the overriding constraint of equation (53). For the more blunt bodies (small values of N) this constraint will introduce a conical forebody with a consequent expansion fan at its intersection with the smooth unmodified power body. The objective of the solutions studied in this section is to determine, for given Mach number and altitude, the power N which minimizes the maximum overpressure of the bow shock. For the more blunt bodies, it is clear that the conical forebody may introduce an expansion fan which dominates the bow shock. For the more slender bodies, the conical forebody and its slope of area discontinuity will be absent.

A typical result illustrating the variation of the bow shock overpressure with the exponent N is given in figure 21. Some associated pressure signatures obtained by the methods of the preceding section are presented in figure 22. Figures 21 and 22 pertain to solutions obtained at $M = 2.2$, $h/\ell=100$. A total of 100 points were used in the body definition. These points were stationed at intervals of .1 along the body length and thus extend well aft of the juncture between the power law forebody and the cylindrical body shank.

Points used by the sectioning multivariable search algorithm to arrive at the optimal exponent, $N^* = .79$, are illustrated in figure 21. The corresponding signatures, figure 22, clearly reveal the variation in pressure signature form

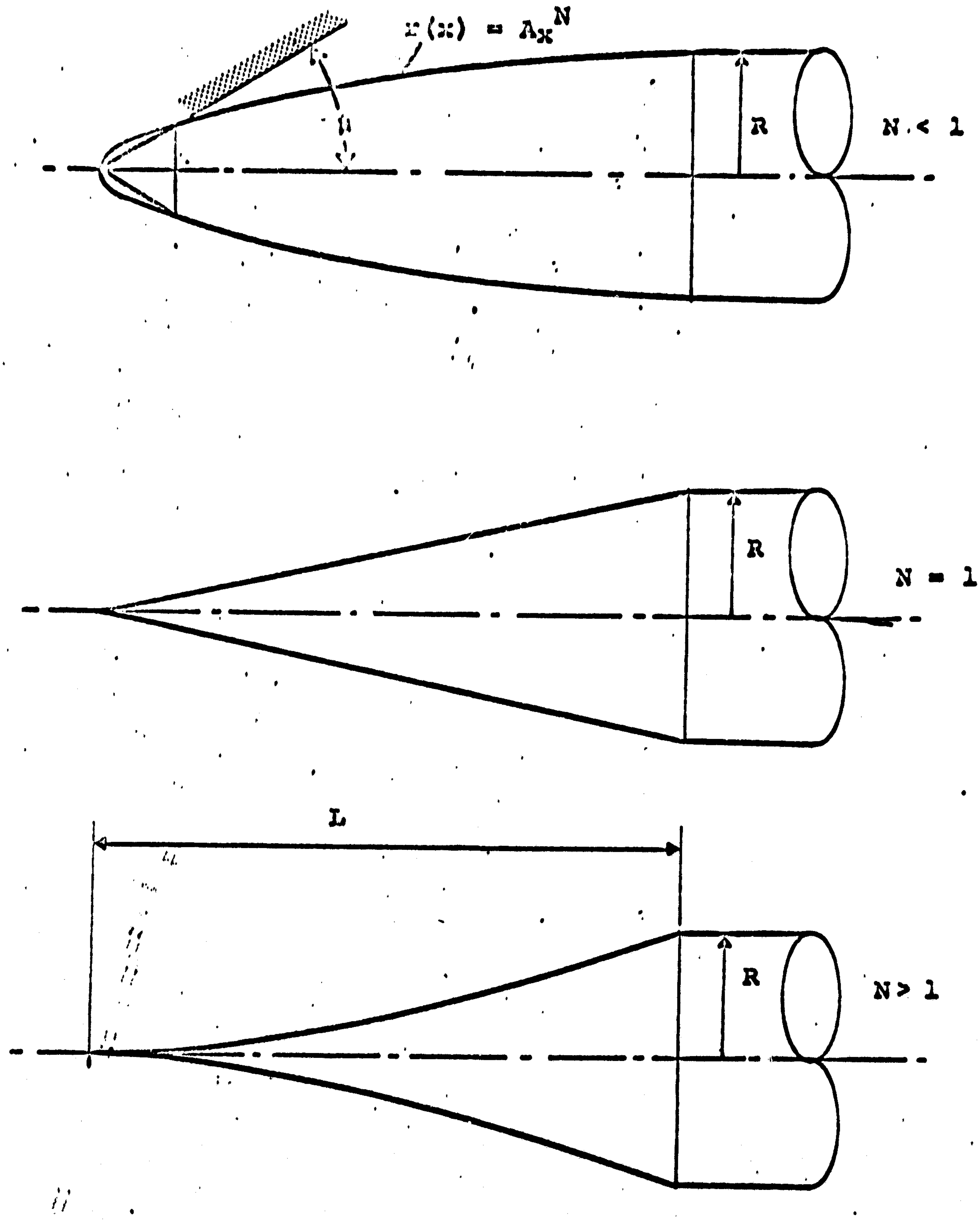

FIGURE 20.—SINGLE ARC POWER BODIES, FIXED LENGTH AND BASE RADIUS

FIGURE 21 —VARIATION OF MAXIMUM OVERPRESSURE WITH POWER BODY EXPONENT, CONSTRAINED L AND R

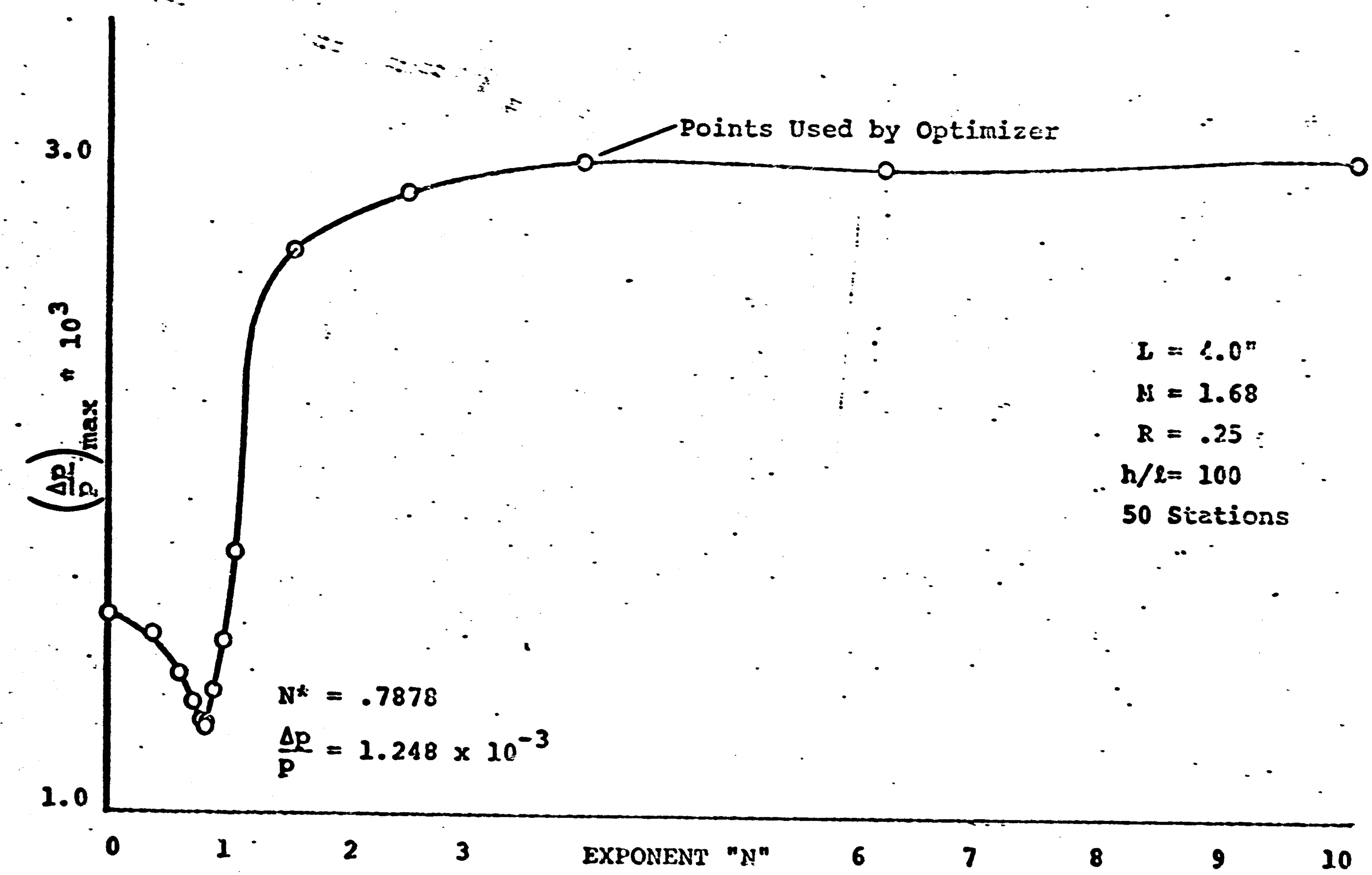

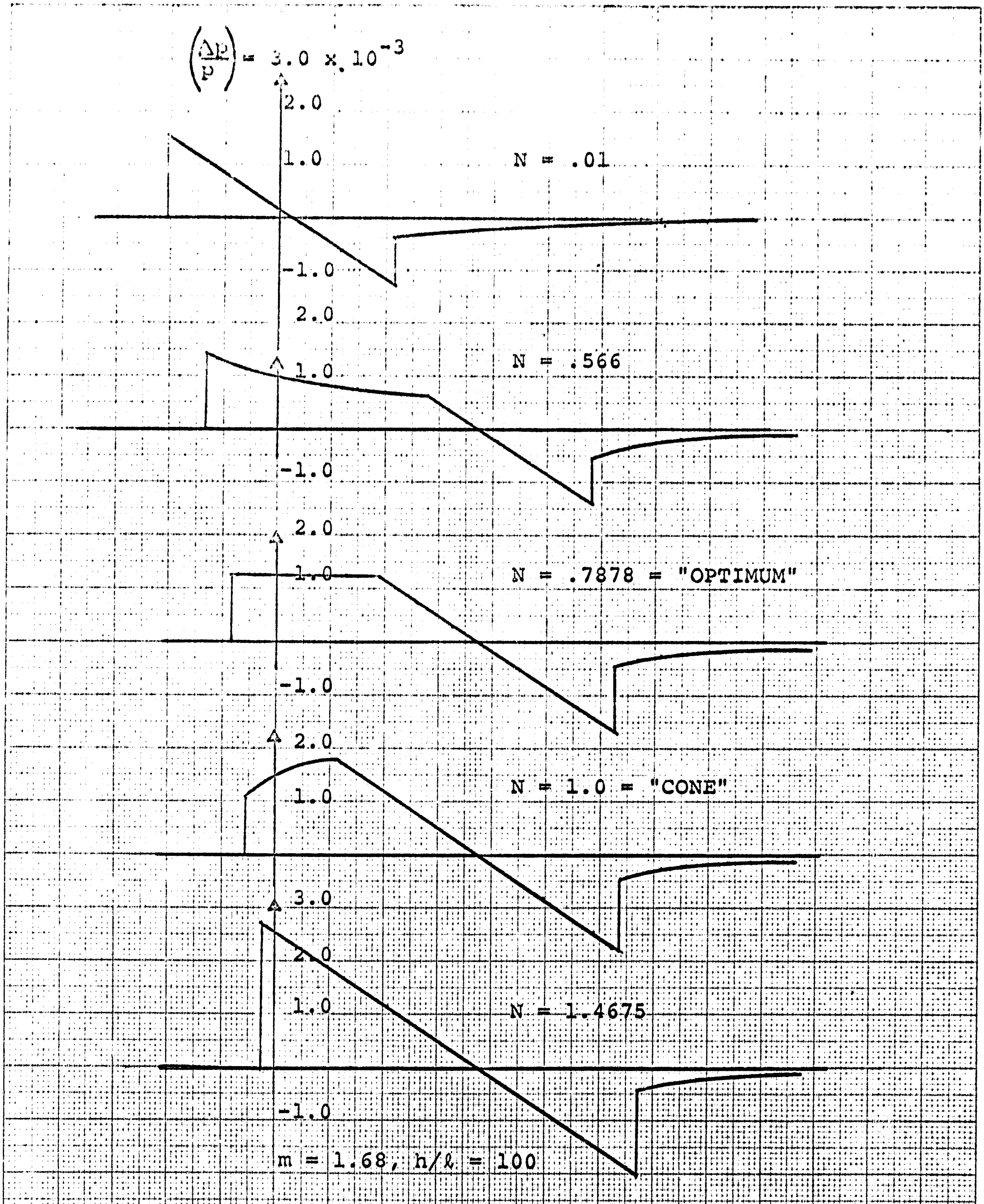

FIGURE 22—SELECTED SINGLE-ARC POWER BODY SIGNATURES

with the exponent N. It can be seen that a well developed "N" wave is obtained at both low and high values of the body power law exponent. For low powers the zero pressure point of the N wave occurs close to the straight Mach line originating from the body nose indicating the dominance of the conical forebody. For higher values of power law exponent, the N wave zero pressure point moves aft close to the straight Mach line originating from the juncture of the power law portion of the body and the cylindrical shank. For intermediate values of the power law exponent a flat top or almost flat top signature is found. It should be noted that in the present calculations based on the Lighthill method the flat top signature does not provide the minimum overpressure; a lower exponent than that which gives the flat top signature, $\approx .75$, is found to produce the lower overpressure. The difference between the flat top and minimum overpressure is small--approximately 1/2 per cent--and could conceivably be the result of small numerical errors in the calculation.

Figures 23, 24, and 25 present the results of a sequence of optimization calculations performed at Mach numbers of 1.414, 2.2, and 2.7, respectively, for a range of h/ℓ ratios between 10 and 700. At the smaller h/ℓ values it can be seen that the minimum overpressure occurs at a discontinuity of slope, $\partial(\Delta p/p)/\partial N$. At the higher h/ℓ values the minimum overpressure occurs smoothly with $\partial(\Delta p/p)/\partial N = 0$. The occurrence of minimum overpressure at a point of slope discontinuity is more pronounced at the lowest Mach number, $M = 1.414$. Some typical signatures associated with the results for $M = 1.414$ are presented in figure 26.

Figure 26 reveals a wide variety of signature types generated by the straightforward body shape of equation (49). A well developed N wave is obtained for the lowest power body. This wave is dominated by the slope constrained forebody as can be seen from the zero pressure point. At the optimum exponent, $N^* = .79$, a flat top signature is found while intermediate to these two signatures a declining pressure, almost flat top, signature is found. As the exponent increases beyond N^*, the almost flat top signature is maintained at first (not shown) but with increasing pressure. Ultimately, as the magnitude of the front shock diminishes, a finite rise signature is encountered, $N = 1.24$. At still higher exponents, $N = 2.0$, an initial finite rise signature develops into a delayed, relatively well developed, N wave.

At the larger values of h/ℓ a similar variety of signature is found, figure 27. However, the flat top portion of the signature is of smaller extent; the finite rise time signature is not encountered, at least not at the points employed by the sectioning search algorithm. The minimum overpressure signature occurs at a value of N less than that which provides a flat top signature.

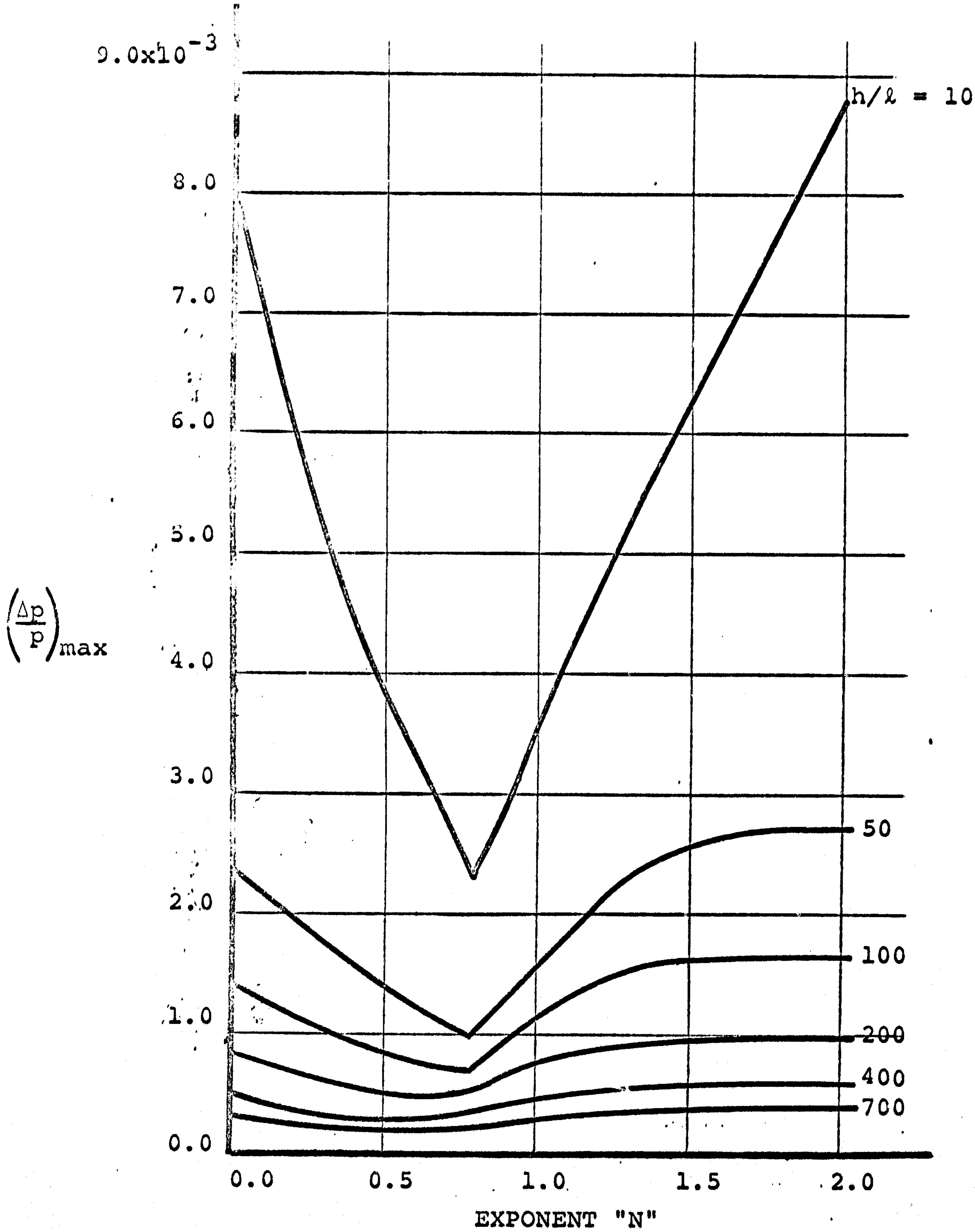

Figure 23.—Length and Base Constrained Single Power Arc Solutions, Effect of Distance, M = 1.414

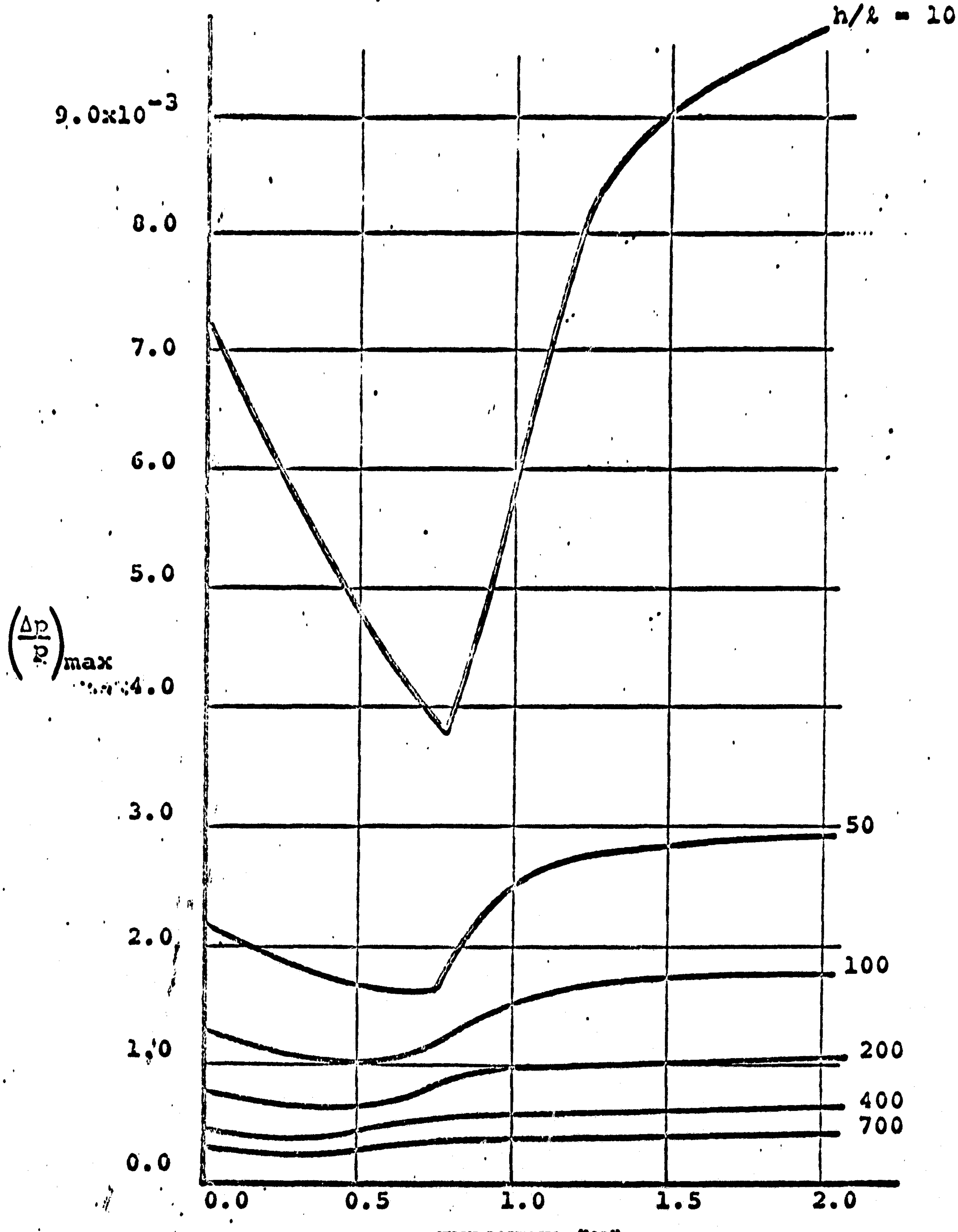

Figure 24.—Length and Base Constrained Single Power Arc Solutions, Effect of Distance, M = 2.2

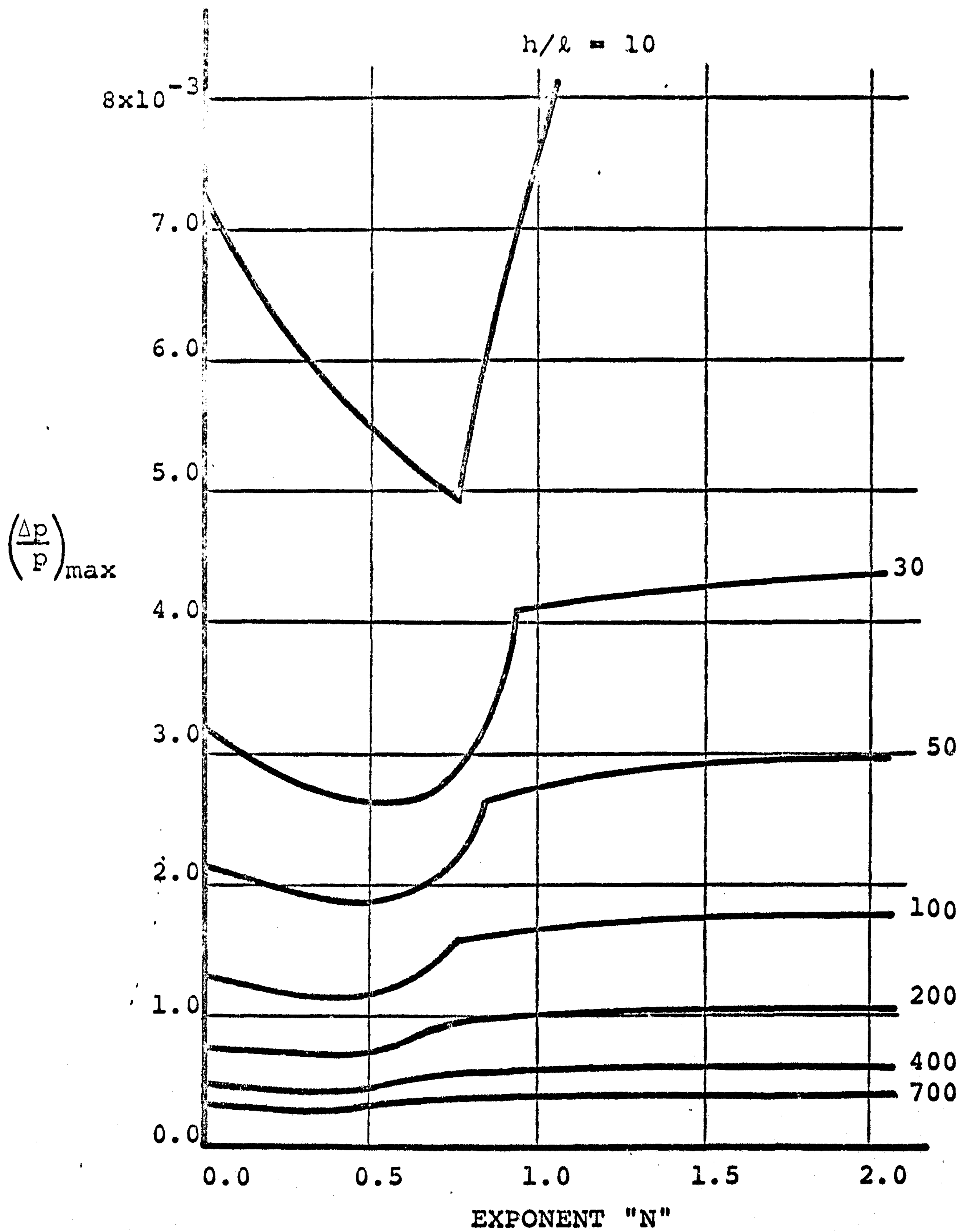

Figure 25.—Length and Base Constrained Single Power Arc Solutions, Effect of Distance, M = 2.7

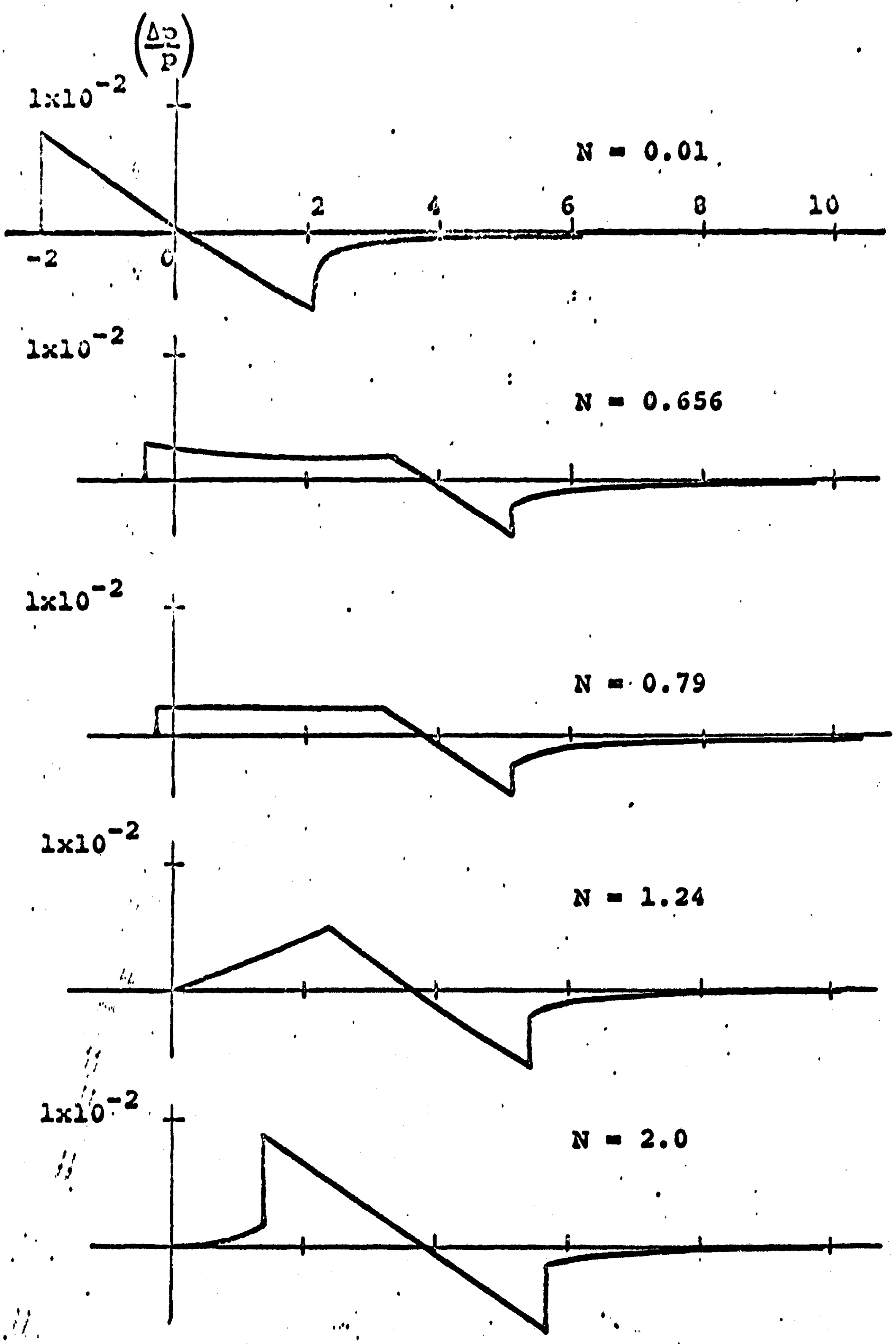

Figure 26.—Selected Signatures, Single Arc Power Bodies, Base and Length Constrained, M = 1.414, h/ℓ = 10

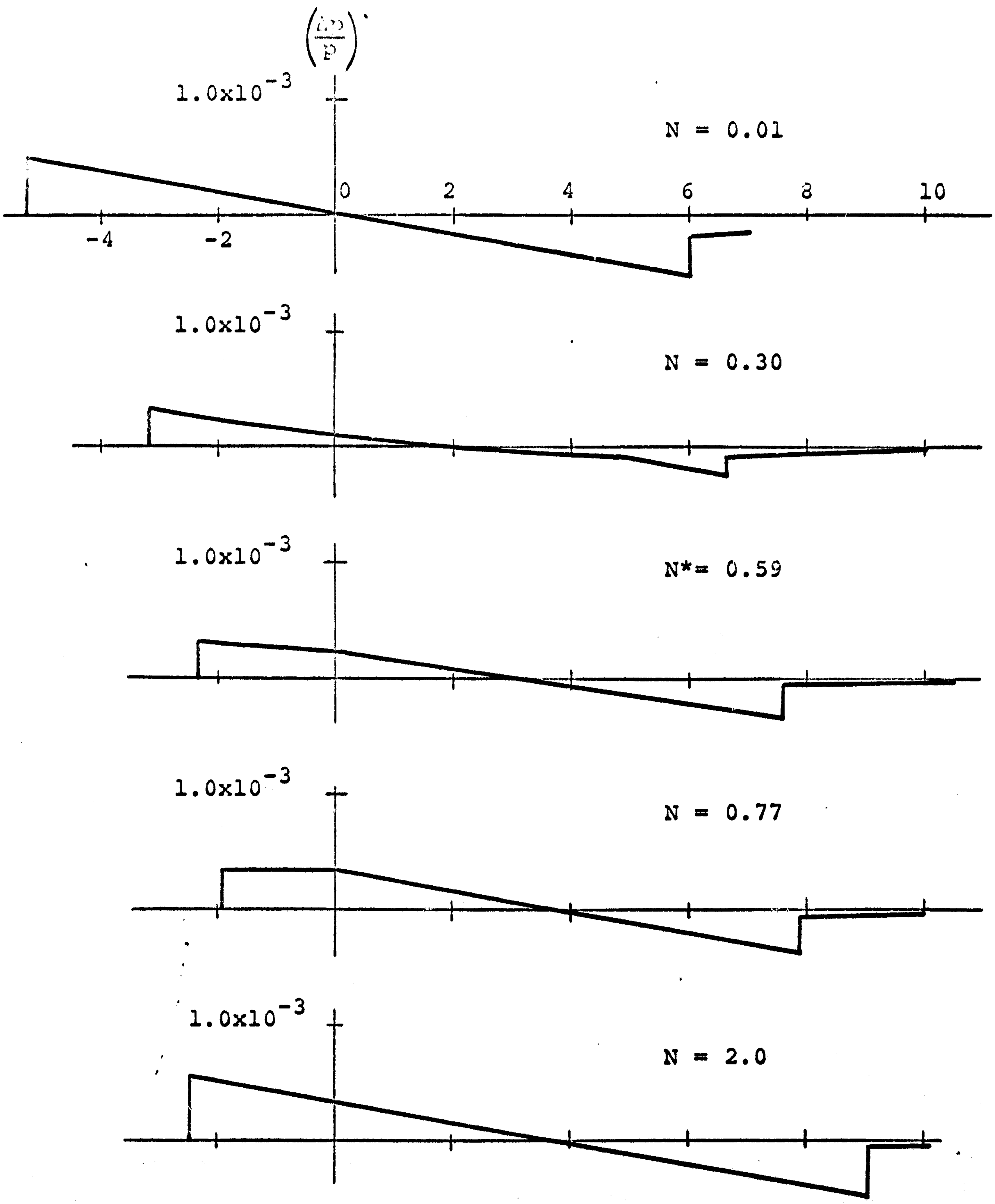

Figure 27.—Selected Signatures, Single Arc Power Bodies, Base and Length Constrained, $M = 1.414$, $h/\ell = 400$

A summary chart presenting the variation of optimal exponent N^* with Mach number and h/ℓ is given in figure 28. Regions of rapid change of N^* with h/ℓ are found. However, on comparison of the figure with the charts of figures 23 to 25, it is apparent that the rapid change in exponent occurs at points where the variation of overpressure with N is slight. Thus, the rapid change in optimum exponent with h/ℓ has little effect on variation of maximum overpressure with h/ℓ, presented in figure 29.

Solution with Volume and Length Fixed

With nose volume and length fixed the body radius distribution becomes

$$r(x) = \left[\frac{(2N+1)V_N}{\pi L^{(2N+1)}}\right]^{\frac{1}{2}} x^N \tag{56}$$

subject to the overriding constraint of equation (54). The bodies defined by equation (56) have a base radius of

$$r(L) = \sqrt{\frac{(2N+1)V_N}{\pi L}} \tag{57}$$

which is a function of the constrained volume and the exponent N. Thus, for given volume the base radius and, hence, the body fineness will vary with N. A typical example of a one-dimensional optimization calculation on the parameter N is presented in figure 30; some typical pressure signatures are presented in figure 31 with corresponding body shapes in figure 32. The results presented in figure 30 are for the same Mach number (1.68) and distance (h/ℓ = 100) as for the base area and length volume constrained solution of figure 21. It can be seen that the volume constrained minimum overpressure solution lies in a somewhat less steep sided valley than the base area constrained solution of figure 21. To the left of the minimum overpressure point, bodies of increasing bluntness would have more volume for a given base area. Conversely, bodies of fixed volume have a higher fineness ratio, L/r_B, and thus tend to have a smaller maximum overpressure than that of a fixed base area body.

In volume constrained solutions it has proven convenient to employ a non-dimensional volume measure. Volumes are based on a non-dimensional volume coefficient, V_F, which relates the desired volume to that of a reference cone having the same length as the body under study and a base radius r_m. When V_F = 1.0, the bodies studied will all have a volume $\pi r_m{}^2 L/3.0$; in general

$$V = V_F \cdot (\pi r^2{}_m L/3.0) \tag{58}$$

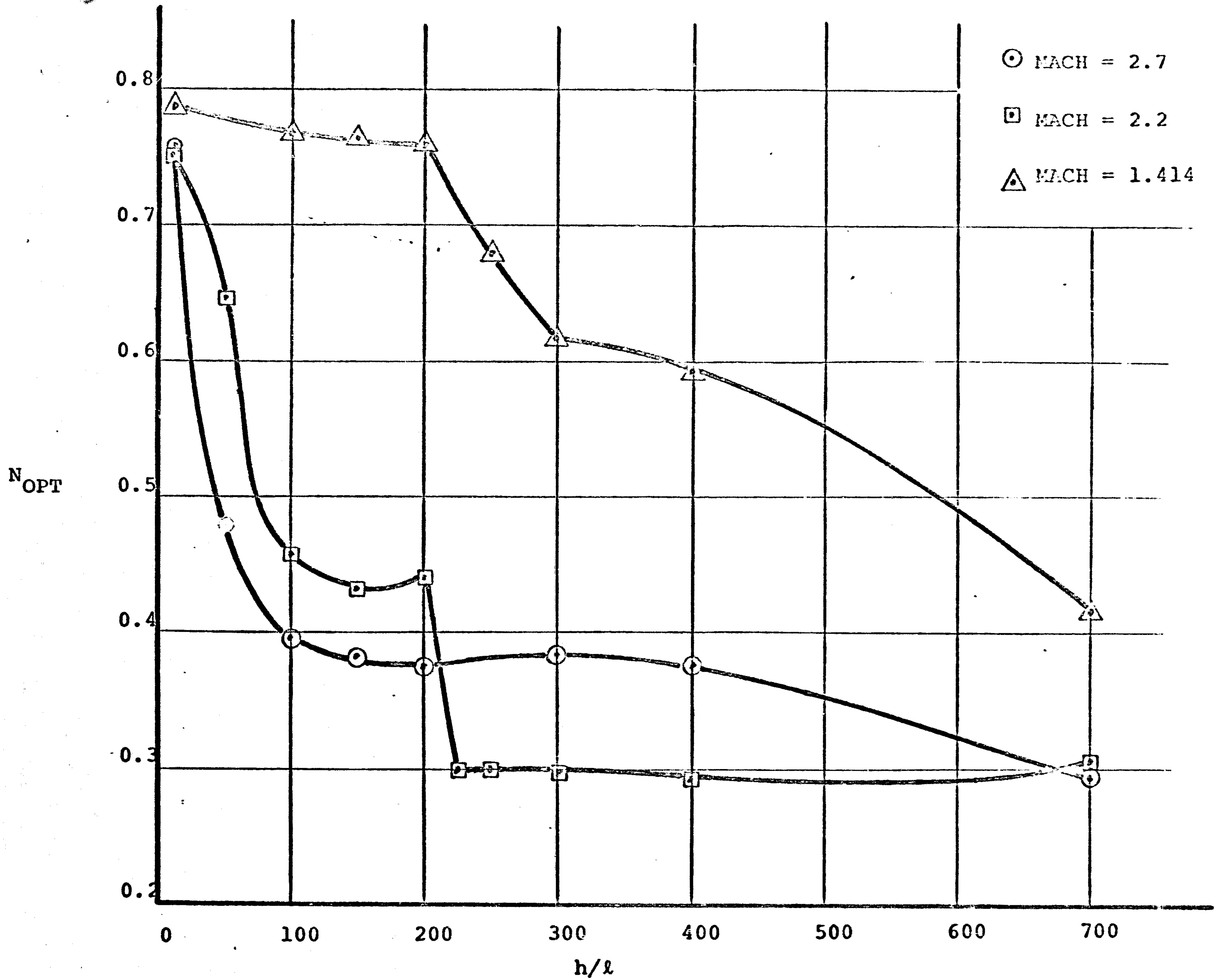

Figure 28.—Variation of Optimum Exponent, N*, with Mach h/ℓ, Base and Length Constrained

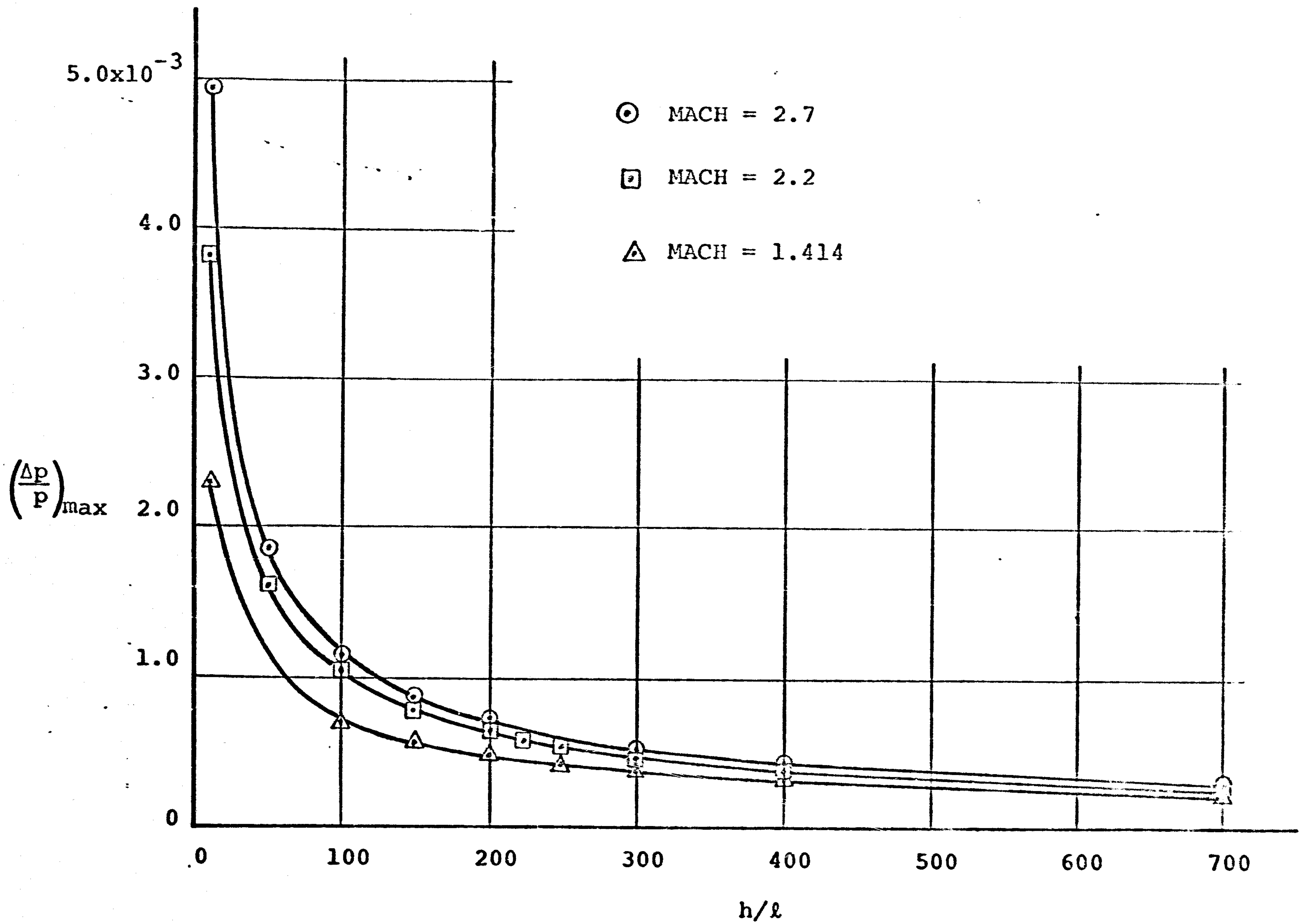

Figure 29.—Variation of Maximum Overpressure with Distance, Single Arc Base Constrained Power Bodies

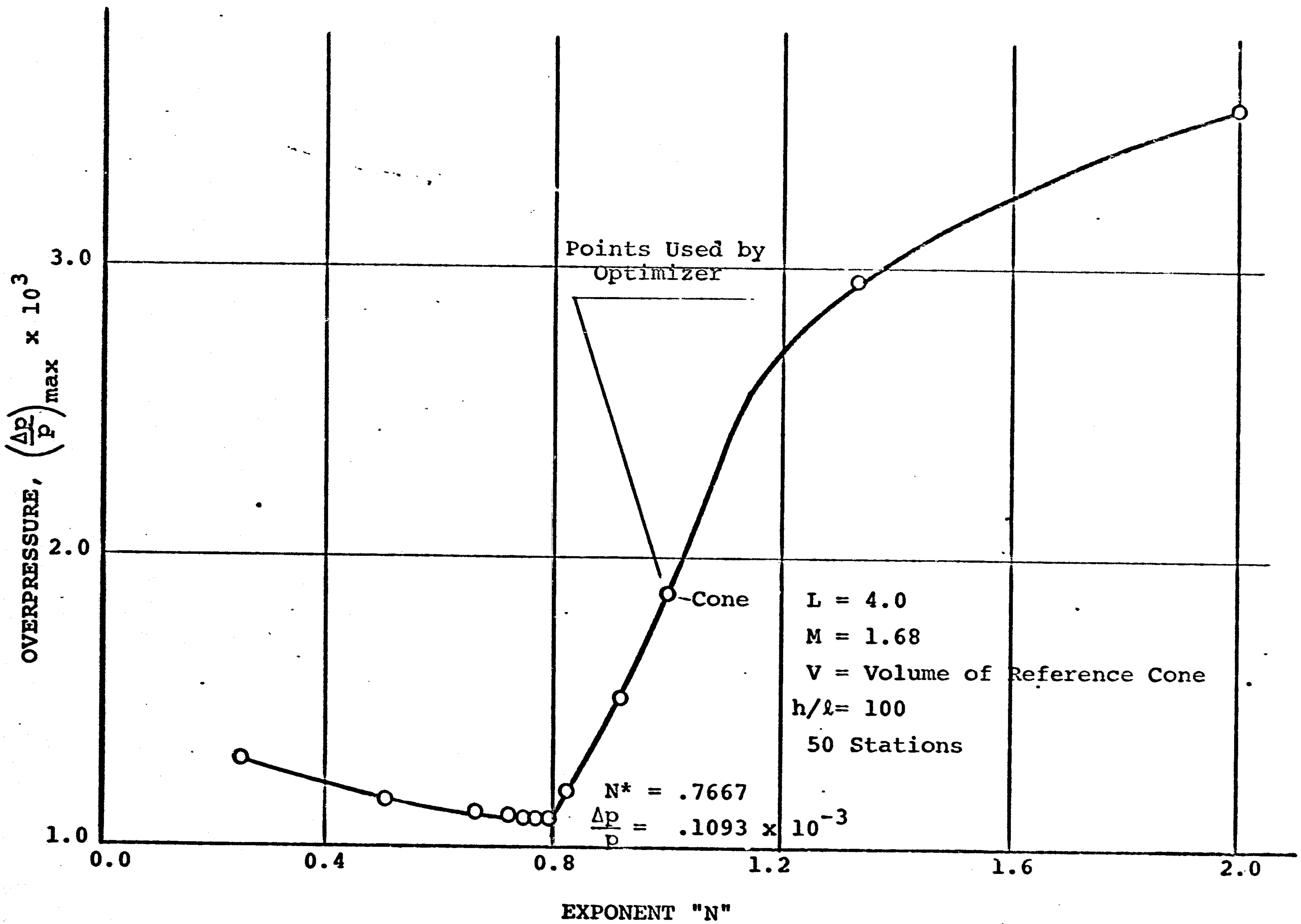

FIGURE 30—VARIATION OF MAXIMUM OVERPRESSURE WITH POWER BODY EXPONENT, CONSTRAINED V AND L

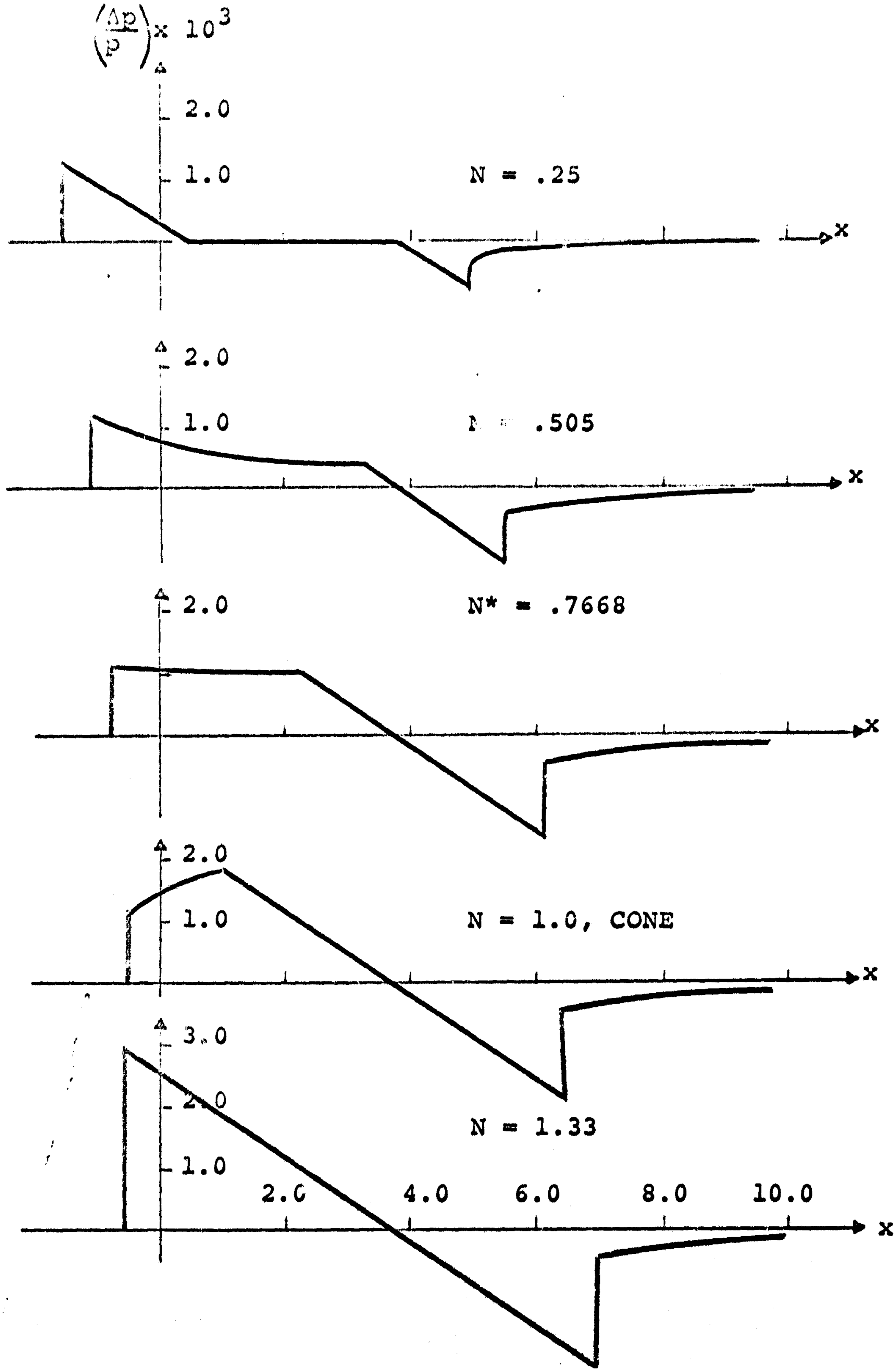

FIGURE 31—SELECTED SINGLE-ARC POWER BODY SIGNATURES; V AND L CONSTRAINED

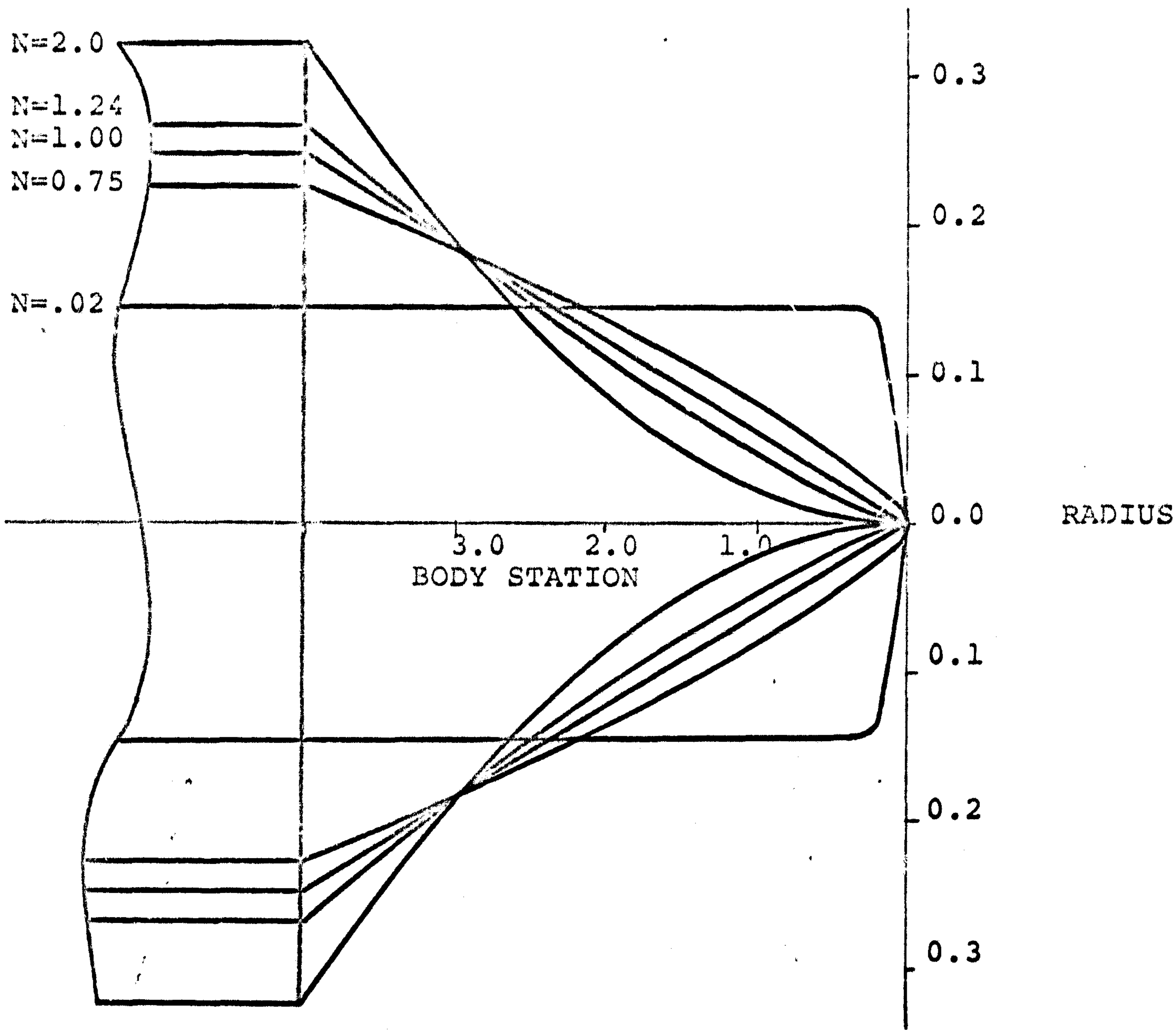

Figure 32.—Family of Bodies with Equal Nose Volume

A sequence of solutions for $M = 2.7$, $V_F = 1.0$ are presented in figure 33. It can be seen that the variation of overpressure with N and h/ℓ is quite similar to that obtained with base area and length constrained. The optimum value of N for a given h/ℓ is generally somewhat less that that obtained for base and length constrained solutions, figure 25, achieving a value of .27 within an h/ℓ value of 50.

In figure 34, the effect of varying volume at constant Mach number (2.7) and h/ℓ (100) is presented. It can be seen that as volume increases, the optimum exponent decreases. Again, as in the case of base area and length constrained solutions, it should be noted that the slope constraint of equation (53) is imposed on the body to insure that local slopes do not exceed the Mach angle. Imposition of the slope constraint may reduce the body volume. When this occurs the overpressure is factored according to the expression

$$\left(\frac{\Delta p}{p}\right) = \left(\frac{\Delta p}{p}\right)_{computed} \times \frac{\text{Volume Required}}{\text{Actual Volume}} \tag{59}$$

The effect of varying Mach number at constant volume is illustrated in figure 35. Here, as Mach number increases, the optimal exponent decreases. This is in general agreement with the volume effect of figure 34; for both increasing volume and Mach number effectively increase the body bluntness.

Two Arc Bodies

A restricted class of bodies consisting of two consecutive arcs have been investigated. This class of body is illustrated in figure 36. In the investigation the nose length, X_2, and base radius, R_2, were constrained. The parameters X_1, R_1, N_1, and N_2 were free for optimization. It follows immediately from figure 36 that

$$C_1 = \frac{R_1}{X_1^{N_1}} \tag{60}$$

and

$$C_2 = \frac{(R_2-R_1)}{(X_2-X_1)^{N_2}} \tag{61}$$

hence,

$$r(x) = \frac{R_1}{X_1^{N_1}} \cdot x^{N_1};\ 0 \leq x < X_1 \tag{62}$$

and

$$r(x) = R_1 + \frac{(R_2-R_1)(x-X_1)^{N_2}}{(X_2-X_1)^{N_2}};\ X_1 \leq x \leq X_2 \tag{63}$$

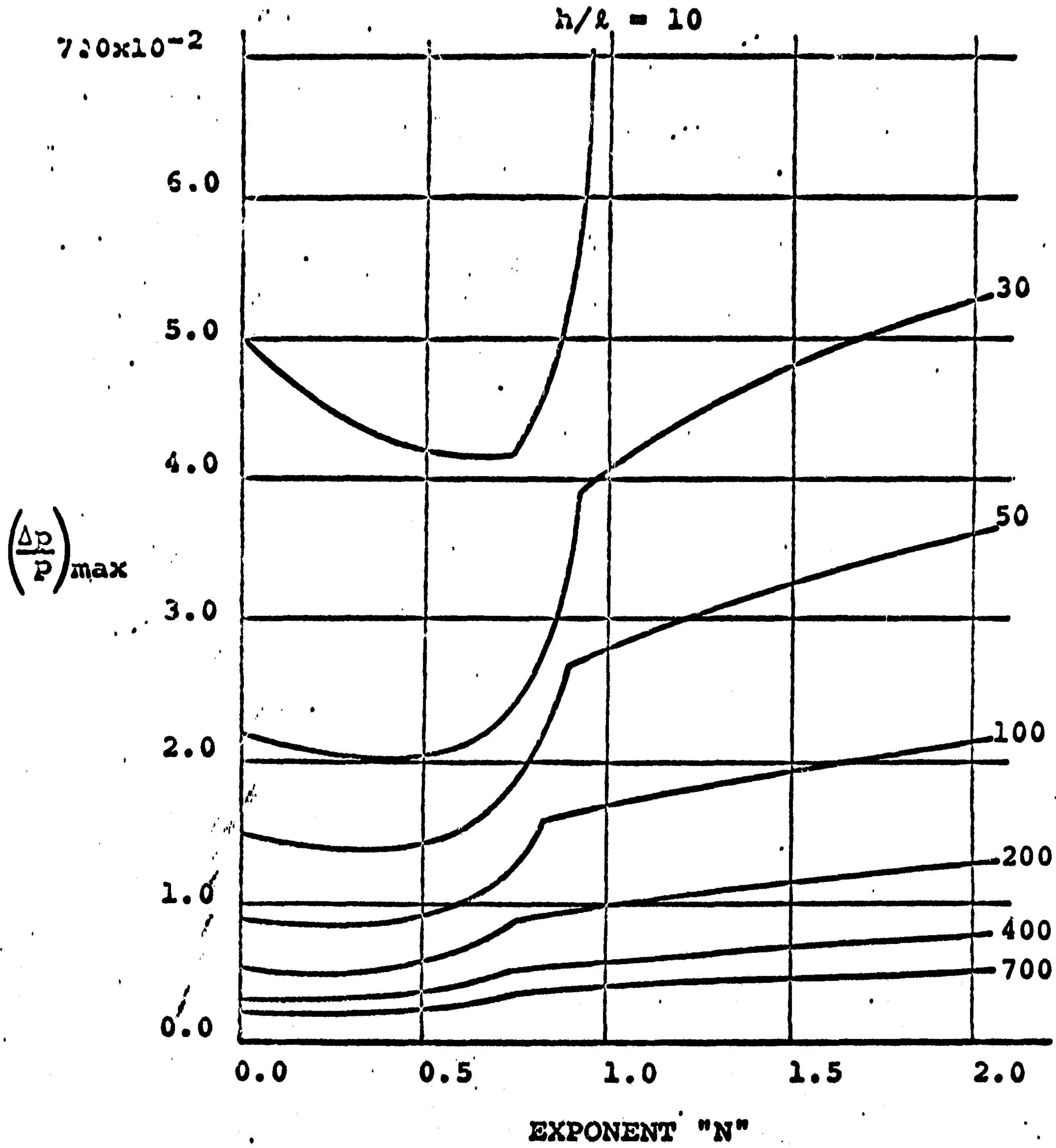

Figure 33—Volume Constrained Single Power Arc Solutions, Effect of Distance, $M = 2.7$, $V_F = 1.0$

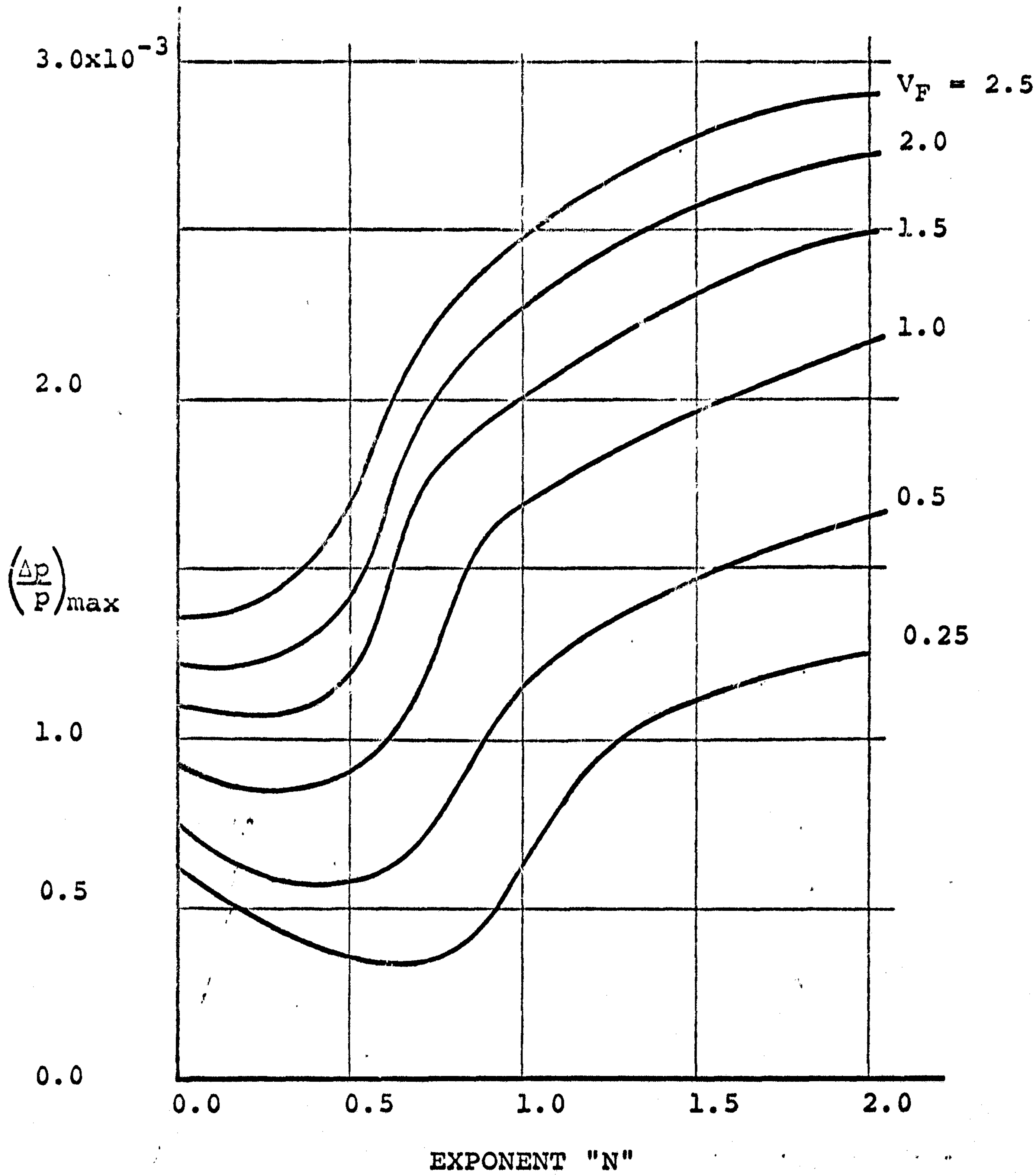

Figure 34.—Volume Constrained Single Power Arc Solutions, Effect of Volume, $M = 2.7$, $h/\ell = 100$

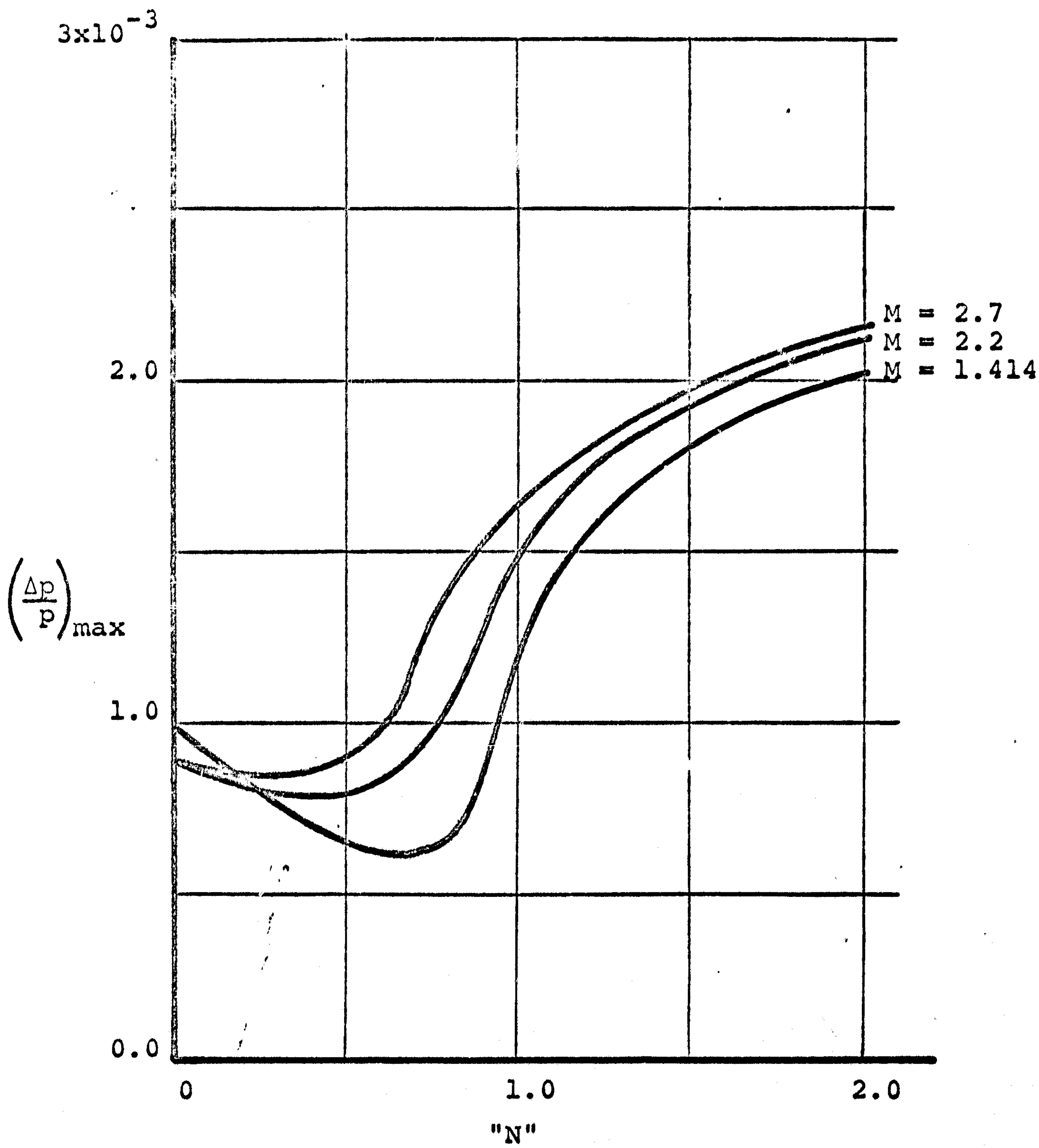

Figure 35.—Effect of Mach Number on Single Power Arc Volume Constrained Bodies, $V_F = 1.0$, $h/\ell = 100$

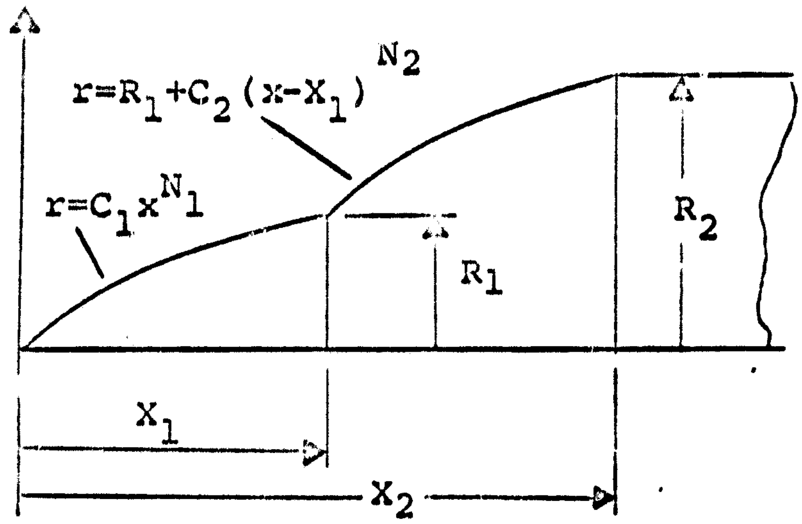

Figure 36.—Two-Arc Power Body

A minimum overpressure solution was sought using the free parameter vector

$$\lfloor \alpha \rfloor = \lfloor R_1, X_1, N_1, N_2 \rfloor \qquad (64)$$

The Mach number was 1.68 and $h/\ell = 100$. Nominal values employed for the computation were

$$\lfloor \alpha \rfloor = \lfloor .14734, 1.99, .75, .75 \rfloor \qquad (65)$$

The point (X_1,R_1) lay on the corresponding optimum single power body with constrained base radius. The signature obtained for this nominal body is presented in figure 37a. The best body shape obtained for this class of body is presented in figure 37b. Parameters for this final body were

$$\lfloor \alpha^* \rfloor = \lfloor .15320, 1.99, .47163, .9854 \rfloor \qquad (66)$$

with corresponding maximum overpressure of

$$\frac{\Delta p}{p} = 1.2516 \times 10^{-3} \qquad (67)$$

It should be noted that the upper limit employed on α_2 was 1.99; thus, the final shoulder line position at $X_1 = 1.99$ indicates that this constraint should be relaxed. The shoulder line should be permitted to move in a rearward direction. The final pressure signature is compared to the nominal signature in figure 37a Nominal and final body shapes are given in figure 37b.

Calculations were performed using stations at .2 intervals along the body axis, $(\Delta x = .2)$. With this spacing a three-quarter power body of the same base radius would have a maximum overpressure of $\Delta p/p = 1.276 \times 10^{-3}$. The final two-arc pressure signature is compared to that of a three-quarter power body of the same base radius in figure 38a. It can be seen that while the two maximum overpressures are practically the same, the total impulse

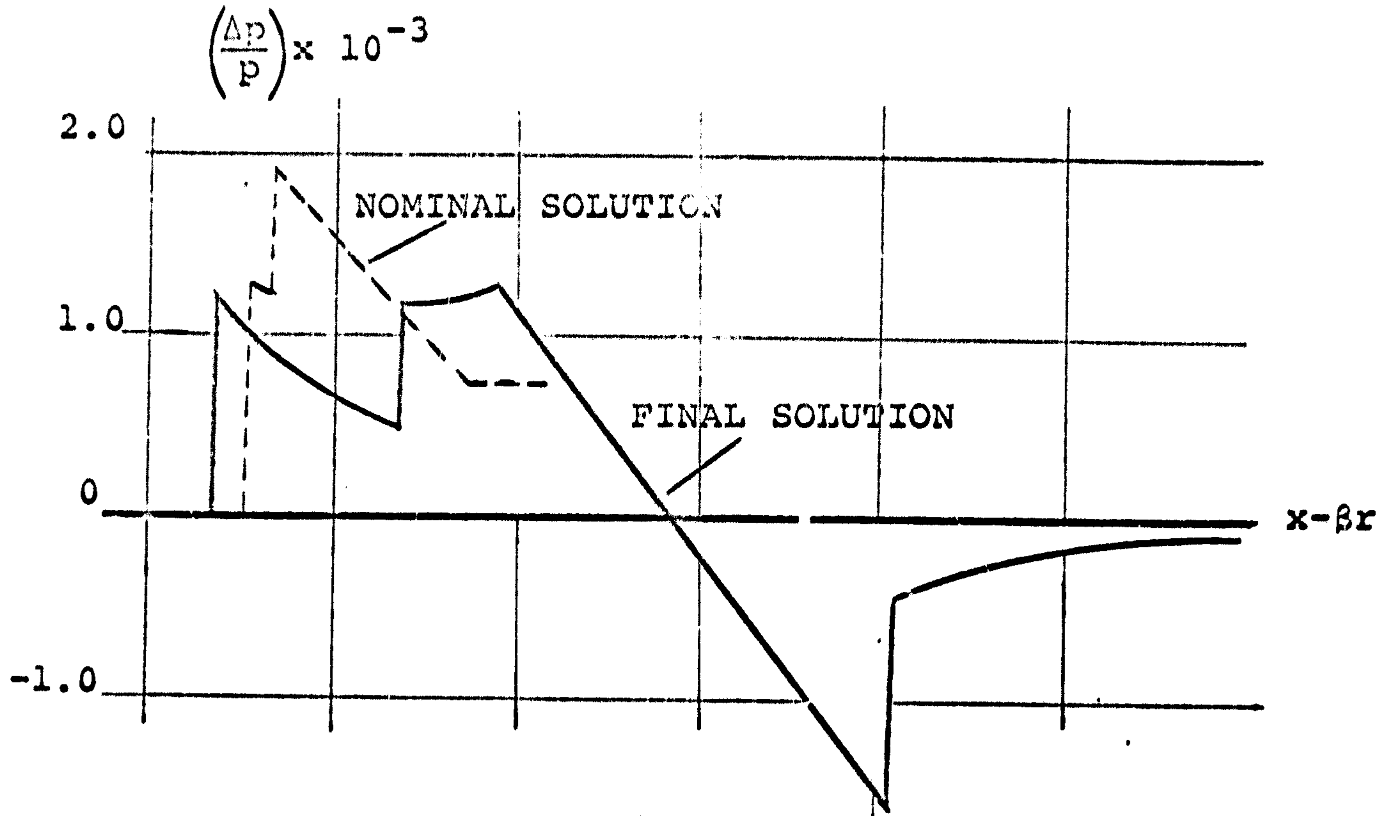

FIGURE 37a.— TWO-ARC SIGNATURES

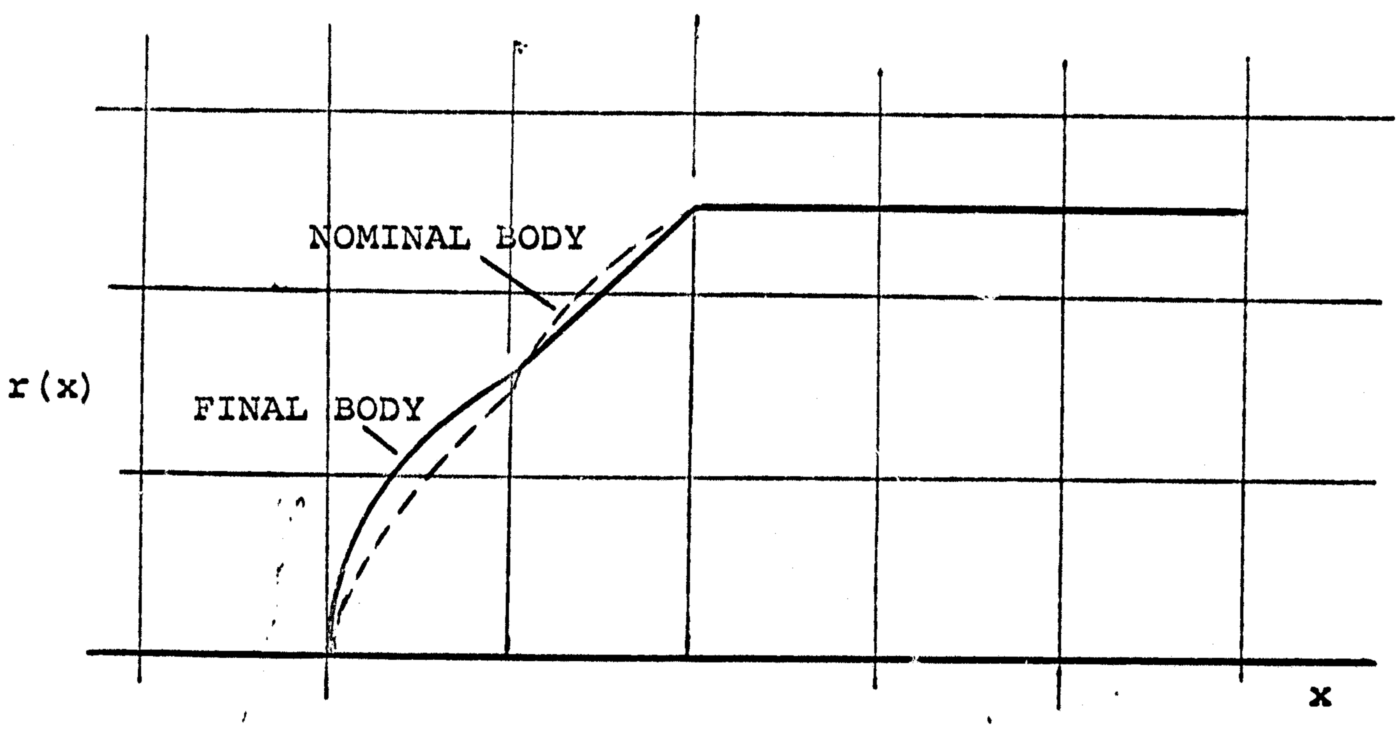

FIGURE 37b.—TWO-ARC BODY PROFILES

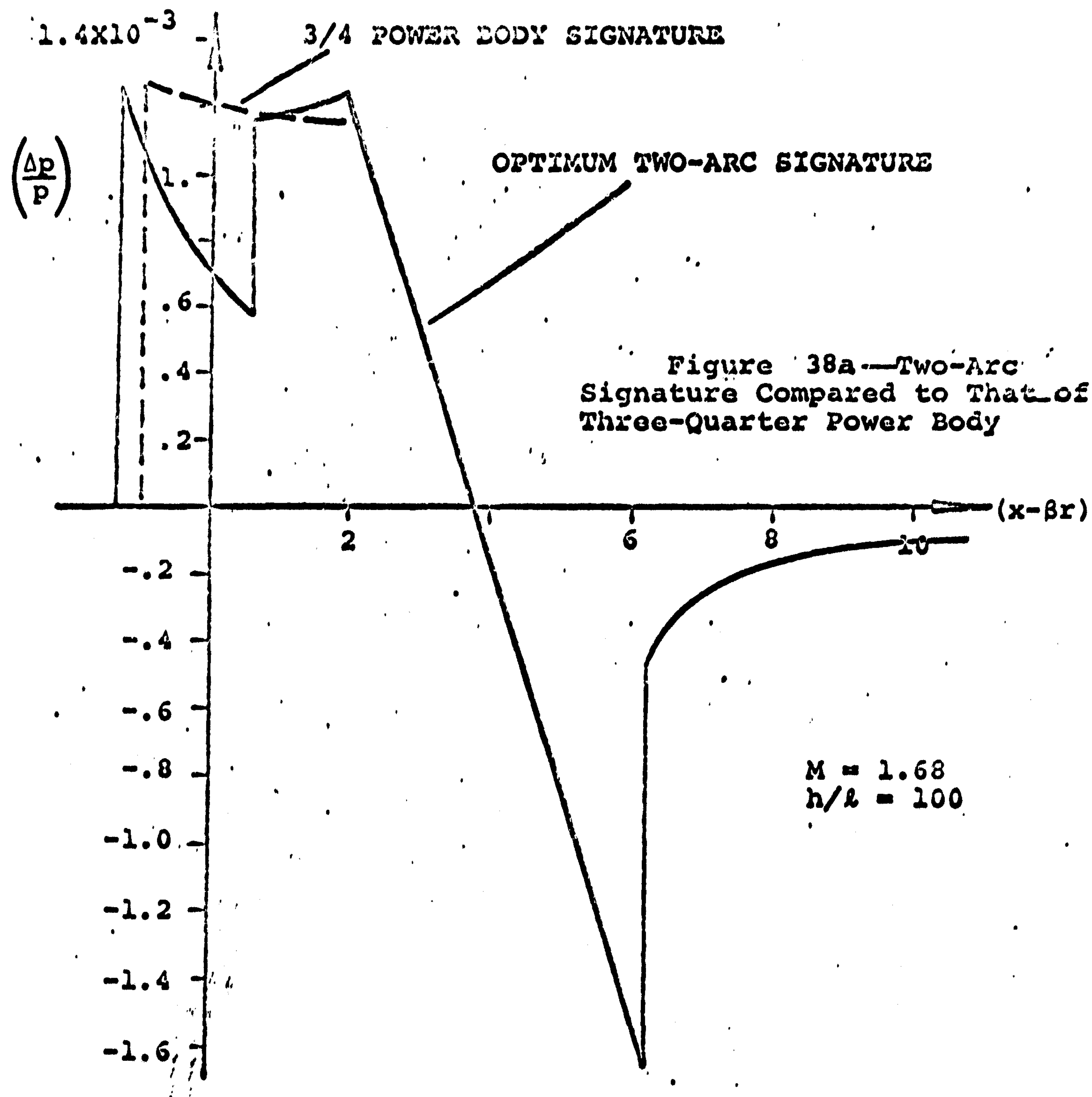

Figure 38a—Two-Arc Signature Compared to That of a Three-Quarter Power Body

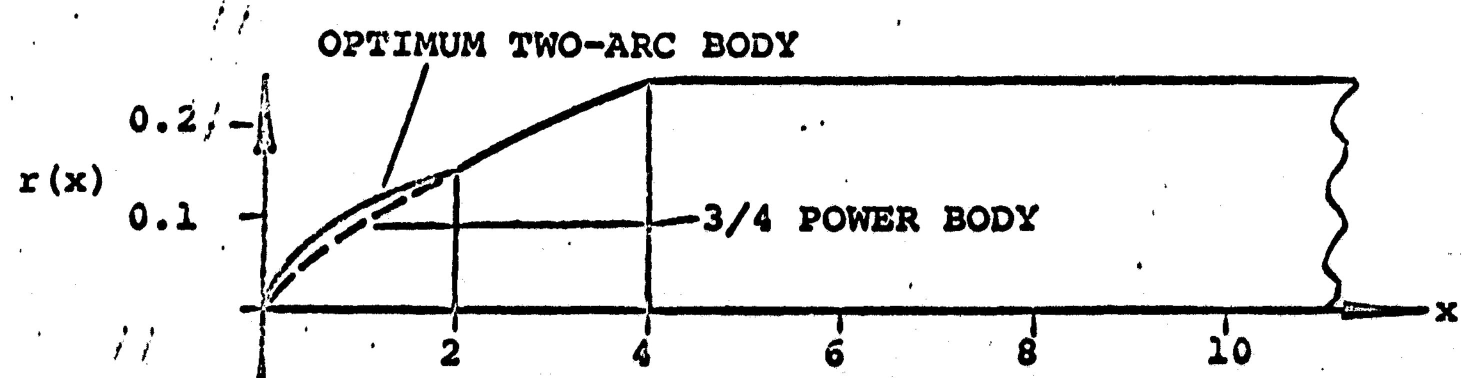

Figure 38b.—Two-Arc Body Shape Compared to That of a Three-Quarter Power Body.

of the two-arc solution is less than that of the three-quarter power body. While the front shock structure differs between the two bodies, the rear shocks are indistinguishable from each other. The optimal two-arc body shape is compared to the three-quarter power body in figure 38b. It can be seen from the figure that the two-arc body has more forebody bluntness than the three-quarter power body. The rear of the two forebodies are practically identical in shape, however. This probably accounts for the similar rear shock strengths and locations.

A second representative two-arc solution is presented in figure 39. The solution is obtained at a Mach number of 2.7 and $h/\ell = 30$. The nominal control vector for this solution is $\lfloor \alpha_0 \rfloor = \lfloor .0833, 1.333, 1.0, 1.0 \rfloor$, which generates a conical body. Maximum overpressure on the nominal, a well-developed N wave, is $(\Delta p/p) = 4.18 \times 10^{-3}$. A selected sequence of signatures developed by the optimization algorithm employed (adaptive creeping, pattern, random ray) are presented in figure 40. A convergence plot showing the successive reduction in maximum overpressure as a function of the number of evaluations is presented in figure 41.

Three-Arc Power Bodies

The multiple-arc model can readily be estended to include three arcs. Body geometry for such a model is presented in figure 42. The free parameters employed are seven in number:

$$\alpha_1 = X_1 \tag{68}$$

$$\alpha_2 = K, \text{ where } X_2 = X_1 + K(X_3 - X_1) \tag{69}$$

$$\alpha_3 = R_1 \tag{70}$$

$$\alpha_4 = R_2 \tag{71}$$

$$\alpha_5 = N_1 \tag{72}$$

$$\alpha_6 = N_2 \tag{73}$$

$$\alpha_7 = N_3 \tag{74}$$

Figure 43 illustrates a typical optimal body shape defined by application of multivariable search techniques to the model of Figure 42. The calculation was performed at $M = 1.68$, $h/\ell = h/(2X_3) = 50$. Base radius, $R = .25$, and nose length, $X_3 = 4.0$, were constrained. Again, as in previous studies, the quantity minimized was maximum positive overpressure.

The final parameter vector obtained by optimization studies was

$$\lfloor \alpha^* \rfloor = \lfloor 3.6755, .52003, .18203, .09259, .82574, 2.2741, .1 \rfloor \tag{75}$$

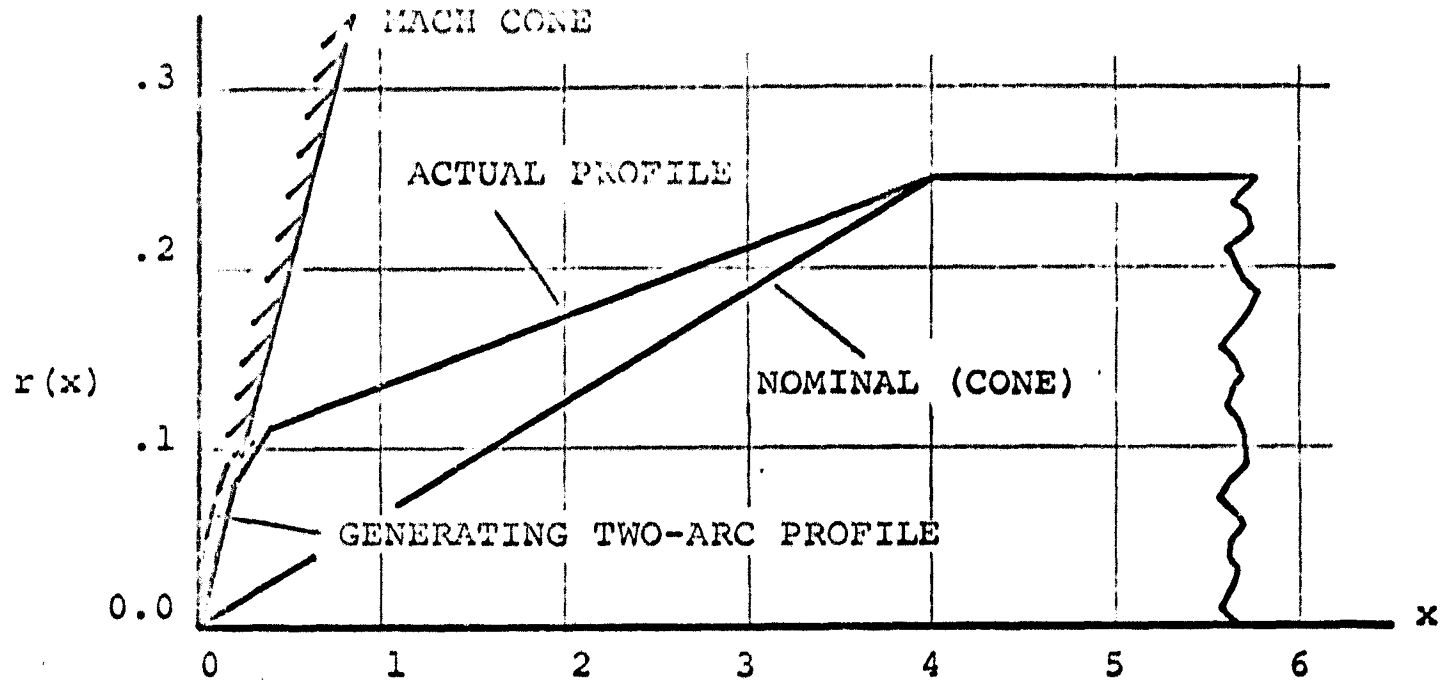

Figure 39.—Optimal Two Arc Body, M=2.7, h/ℓ=30

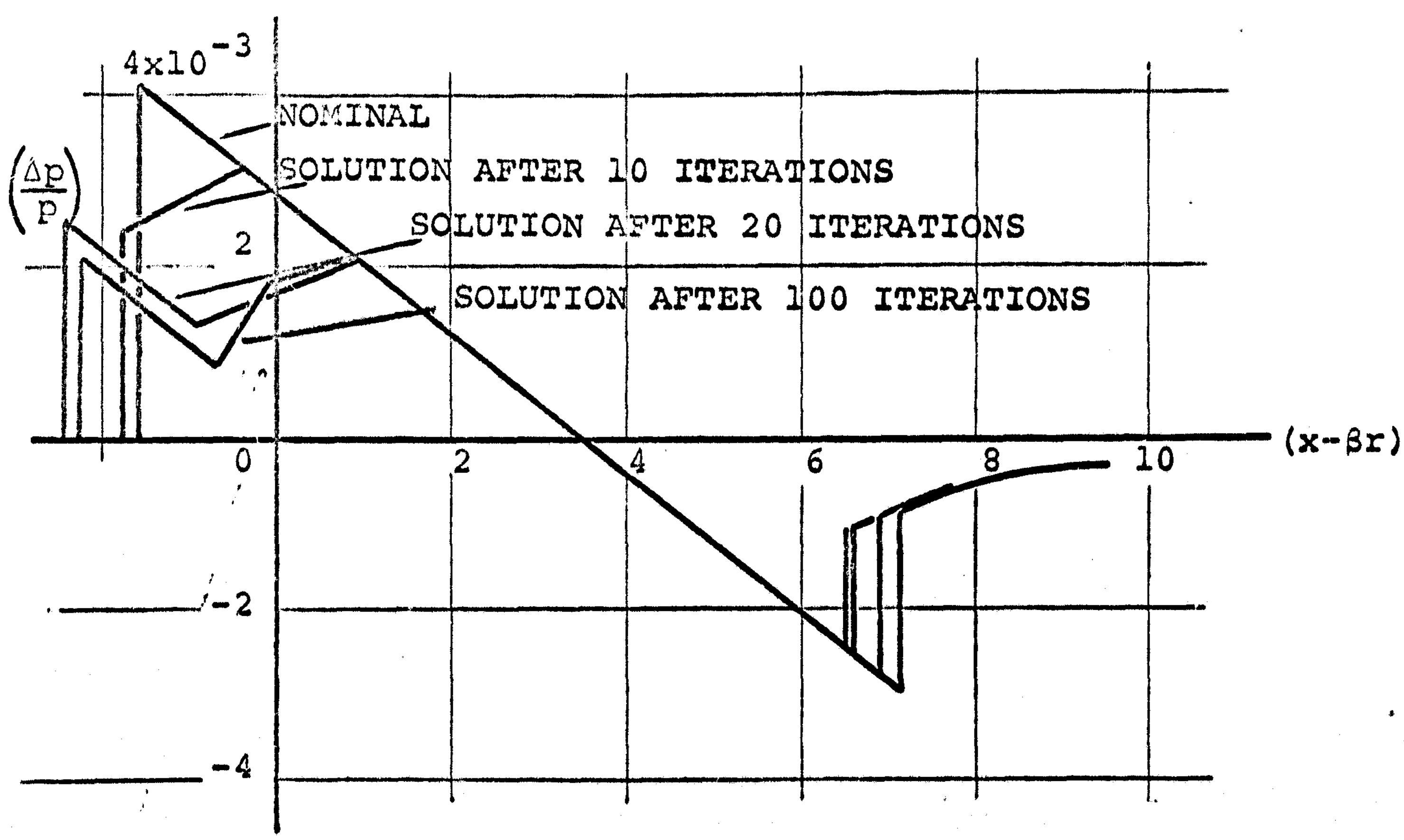

Figure 40.—Typical Signatures, Two-Arc Solution

M = 2.7, h/ℓ = 30

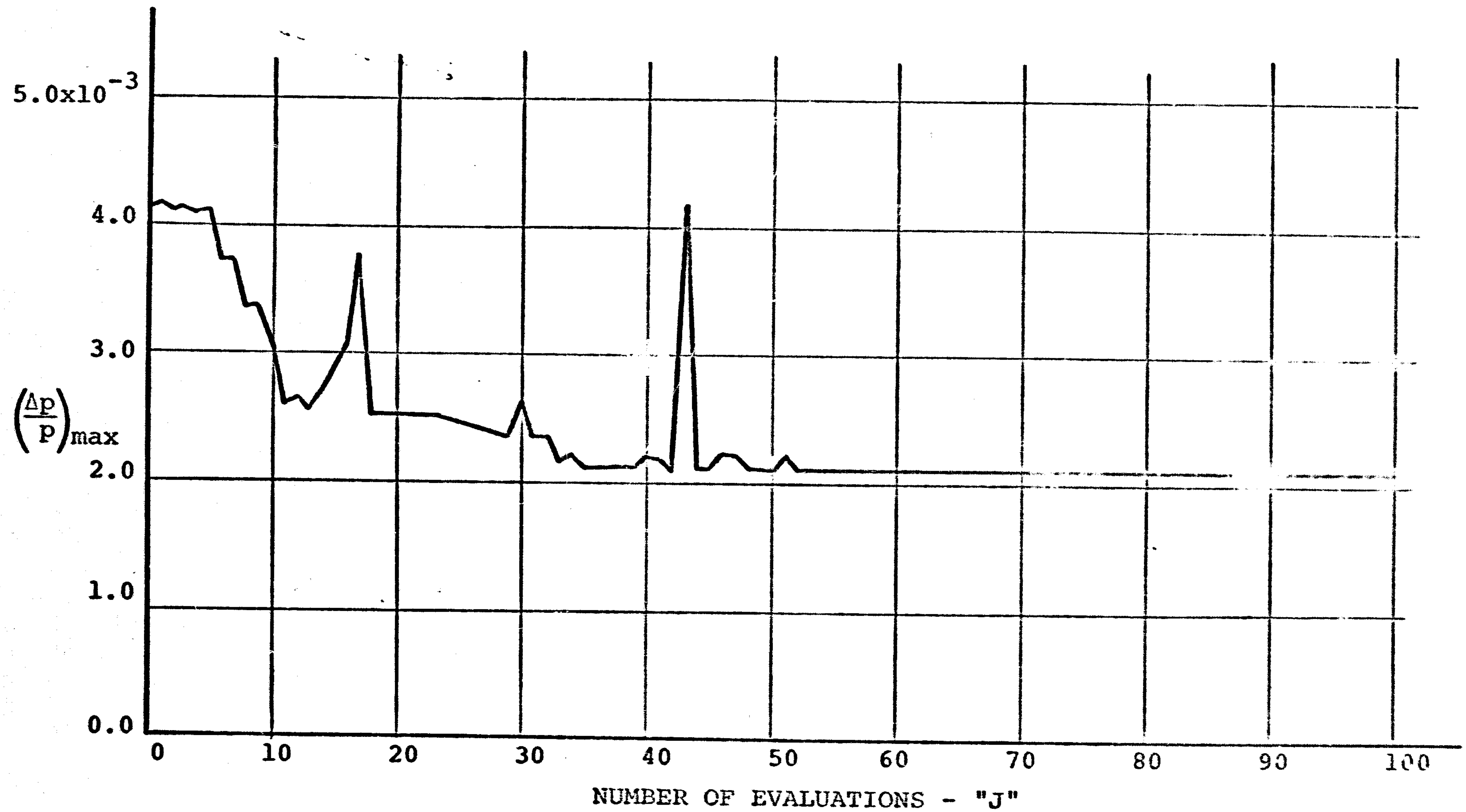

Figure 41.—Convergence Plot, Two-Arc Solution; M=2.7, h/ℓ=30, Cone Nominal

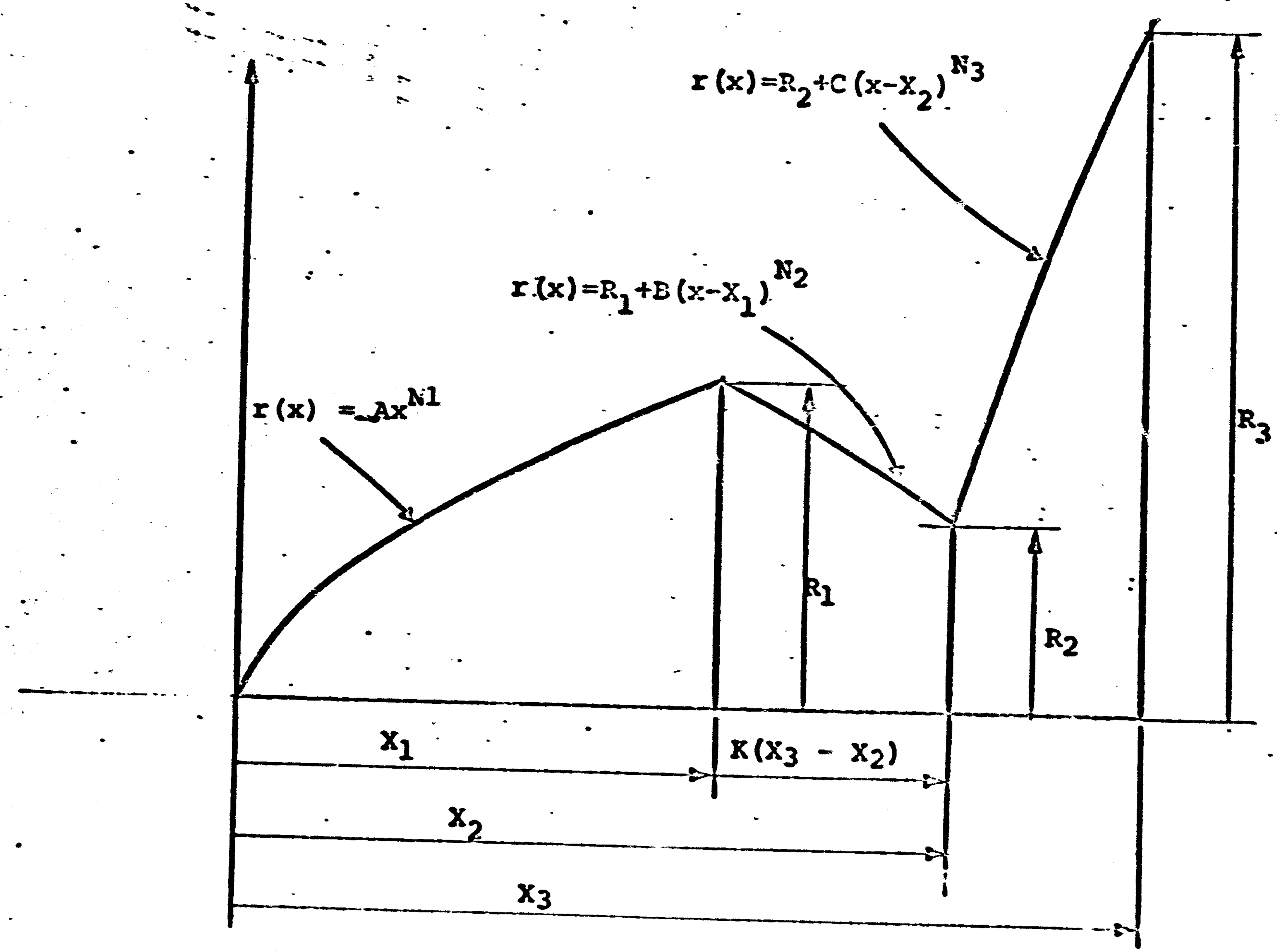

FIGURE 42 — THREE-ARC BODY PARAMETERS

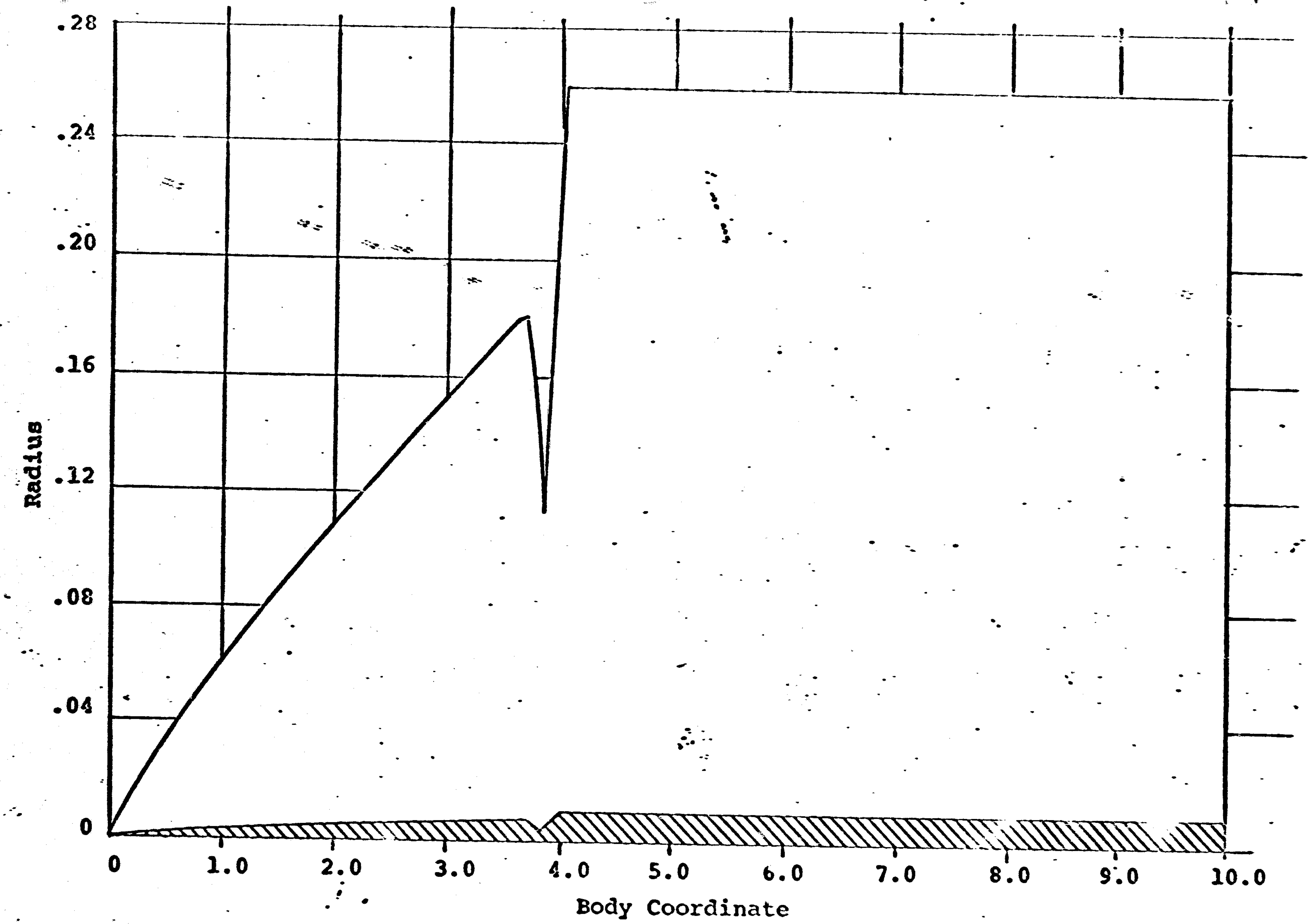

FIGURE 43—OPTIMAL THREE-ARC BODY

Maximum signature overpressure obtained with this model was 7.99×10^{-4}. For comparison purposes the three-quarter power body satisfying the same nose length and base radius constraints has a maximum overpressure of 1.25×10^{-3}. The computed three-arc maximum overpressure is, therefore, 64 per cent of the corresponding three-quarter power body, the optimal single-power arc solution for the specified conditions. Final body shape is drawn full scale in Figure 43 together with the associated area distribution. The computed pressure signature, including shock location, is given in Figure 44. It should be noted that although the class of shapes considered is a quite restrictive set of three-arc bodies, the result indicates that previously defined single-arc minimum overpressure body shapes obtained by the variational calculus may not be true minimum boom shapes.

A second example illustrating the three-arc power body solution was computed at $M = 2.7$, $h/\ell = 50$. Constraints were base radius = .25 and $X_3 = 4.0$ as before. Again, as in the previous three-arc solution, a notched three-arc body was obtained. Body shape parameters were

$$\lfloor \alpha^* \rfloor = \lfloor 3.6816, .51169, .17550, .089945, .76278, .19181, .07543 \rfloor \tag{76}$$

Maximum overpressure obtained was

$$\frac{\Delta p}{p} = 1.237 \times 10^{-3} \tag{77}$$

approximately sixty-six per cent of the corresponding single arc overpressure, Figure 25. This result confirms that multiple arc solutions can reduce the maximum overpressure over a wide range of Mach numbers.

The mechanism of overpressure reduction is apparent from Figures 43 and 44. The first arc occupying most of the active body length employs a conventional single arc minimum overpressure shape to a reduced radius R_1 at X_1. The body then waists inwards rapidly creating a strong negative pressure wave. This arc is followed by a third rapidly increasing radius arc which attains the desired base radius. The strong positive wave emanating from the third arc interacts with the strong negative wave emanating from the second arc, and a pressure cancellation results. Whenever this effect is possible, the maximum overpressure occurs in the portion of the pressure signature created by the first arc of reduced base radius. A direct consequence of the reduced base radius is reduced maximum overpressure. It should be noted that in both three-arc solutions computed above, the second and third arcs are practically sonic.

<u>Solution Convergence and Numerical Accuracy</u>.—The first three-arc solution was subjected to detailed numerical investigation. It was found that an initial optimal shape obtained

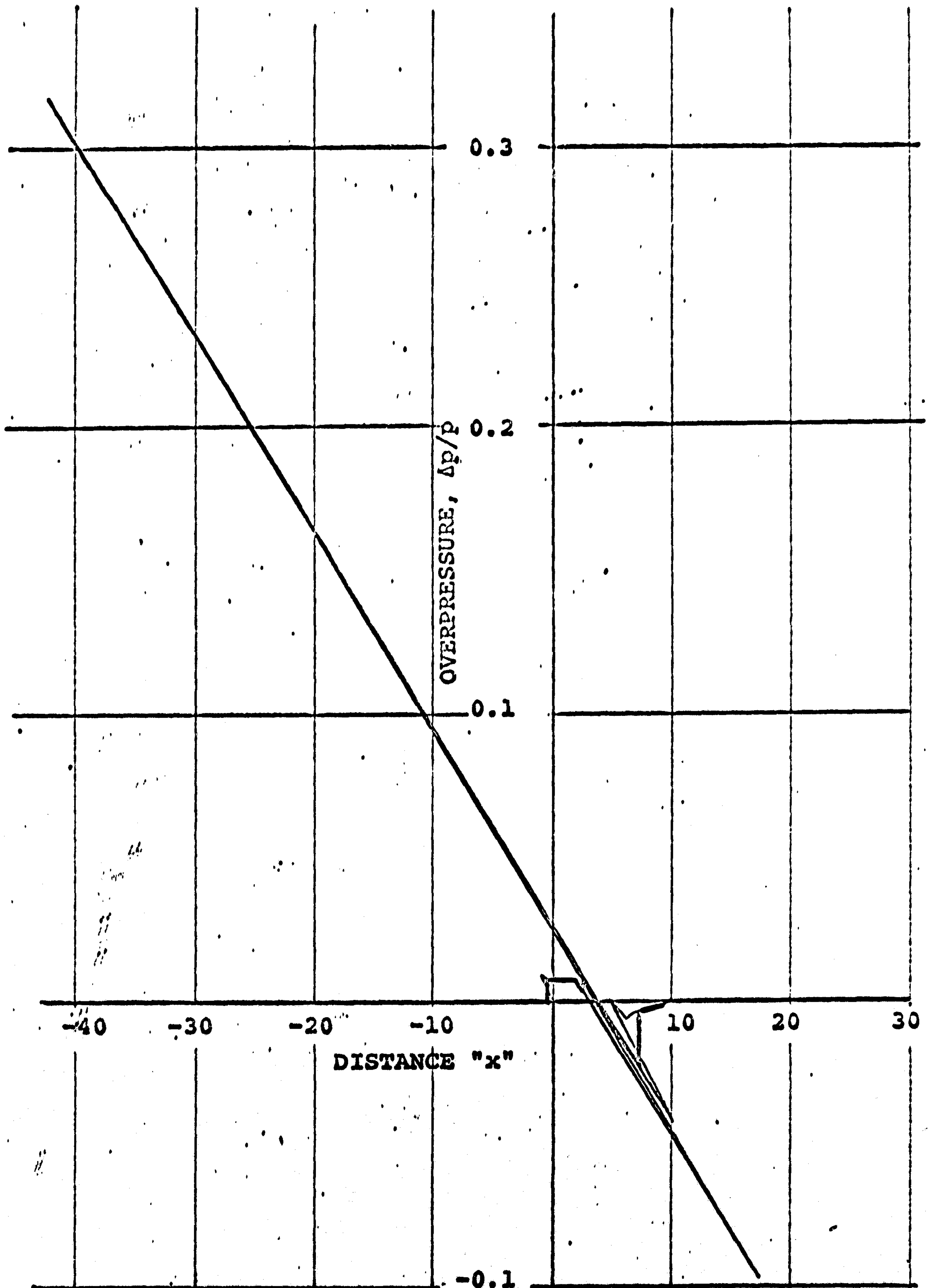

FIGURE 44.—PRESSURE SIGNATURE, THREE-ARC BODY

by the use of fifty body stations failed to reproduce the low boom characteristic when the analysis was repeated using 100 stations. However, on "reoptimization" of the 100 station shape, a low boom body was rapidly developed. This 100 station shape was similar in physical appearance to the original 50 station shape. On increasing the number of body stations to 200, the 100 station body shape failed to achieve a low boom; however, on reoptimization using 200 body stations a low boom body profile was rapidly attained. On increasing the number of body stations to 300, this shape again lost the low boom property and needed to be reoptimized.

The optimal 300 body station shape was then analyzed using 400 and 500 body stations. The solution was stable, and the maximum boom overpressure was independent of the number of body stations. These results are given in Table I.

TABLE I.—VARIATION OF MAXIMUM BOOM OVERPRESSURE WITH NUMBER OF BODY STATIONS

N	Δx	$\Delta p/p$
50	.20	7.77×10^{-4}
300	.033	7.99×10^{-4}
400	.025	7.98×10^{-4}
500	.020	7.97×10^{-4}

It was concluded from the results discussed above that the stable 300 body station solution represents an optimal body shape. It is the lowest front shock overpressure body shape at $h/\ell = 50$, $M = 1.68$ ($\ell = 8.0$ and base radius $R_B = .25$) which consists of no more than three distinct arcs.

The ability to determine an approximate optimal shape using a relatively small number of body stations has a significant effect on computer time requirement for solution of the sonic boom minimization problem. Optimization requires repetitive evaluation of the body shock structure. With 100 stations a typical point evaluation of the shock structure about a body requires two seconds on the CDC 6600 computer. With 200 stations the time rises to approximately five seconds per evaluation. At 300 stations a typical point calculation requires eight seconds. With the repetitive evaluation required for optimization, the use of a large number of stations can rapidly lead to quite large computer time requirements.

A Note on Variational Optimization.—It should be noted that previous variational solutions presented in the literature assume no slope discontinuities; they are single-arc solutions. Extension of the variational calculus to the multiple-arc formulation is possible but unwieldy. Analytically, variational multiple-arc solutions require the use of Denbow's method (University of Chicago, Ph.D. thesis). Numerically, multiple-arc variational solutions may be obtained by the method of reference 5 or 6. Both variational multiple-arc methods have seen only limited application to-date.

It is assumed that failure of variational solutions to achieve the boom level obtained by multivariable search may be due to this assumption of a single-arc solution, thereby omitting the corner possibility.

Sensitivity Studies.— A series of trade curves presenting maximum overpressure sensitivity as a function of the seven body profile generating parameters, $\alpha_i, i=1,2 \ldots, 7$, are presented in Figures 45(a) to 45(f). The study is carried out on the M = 1.68 solution. It can be seen that

(a) Coordinate of First and Second Arc: Small errors in this parameter, α_1, would not result in a significant increase in maximum overpressure.

(b) Coordinate of Corner of Second and Third Arcs: The maximum overpressure is completely insensitive to small errors in the position of this corner point. It should be noted that the parameter, α_2, is a non-dimensional measure of the corner point location.

(c) Radius at Corner of First and Second Arcs: It is apparent that this parameter, α_3, is not quite optimized. A smaller value of $R_1 = .177$ would be slightly superior to the value of $R_1 = .18203$ quoted in Equation (75).

(d) Radius at Corner of Second and Third Arcs: Maximum overpressure is insensitive to this parameter, α_4, about the quoted value.

(e) Exponent of First Arc: This is a very sensitive parameter; the forebody shape should be maintained within strict limits. Errors in the effective forebody exponent could rapidly destroy the body's low boom property. It should be noted that the trade curve of Figure 45(e) is similar in nature to Figure 21 as might be anticipated.

(f, g) Exponent of Second and Third Arcs: The maximum overpressure is insensitive to these parameters.

It should be noted that when perturbation of a body parameter would cause a local body slope to exceed the Mach angle, the program modifies the body shape generated. The modification consists of checking body shape from front to rear for violations of the local slope constraint. Where a slope constraint is violated, the body radius is decreased (or increased in the case of a negative slope violation), to maintain the local slope constraint. This geometrical effect is present in all the trade curves of Figure 45.

Effect of Body Slope Limitation.—A sequence of optimization calculations were performed to assess the effect of limiting maximum (and minimum) body slopes, dr/dx. In these studies the three-arc body shape of minimum-maximum overpressure (mini-max overpressure) was determined subject to the constraints $r_B = .25$, $X_3 = 4.0$, and maximum body slope was limited to a given percentage of the slope providing sonic conditions. Computations were made at $M = 2.7$ and $h/\ell = h/(2X_3) = 100$. One hundred stations were employed to define the body shape.

It was found, as could be anticipated, that as the maximum permissible body slope decreases, the mini-max overpressure increases. Figure 46 presents the variation of mini-max overpressure with slope limitation. At a slope limitation equal to eighty per cent of the sonic slope, the three-arc bodies approach the single-arc mini-max overpressure. However, the three-arc body shape retains the characteristic form of Figure 43 which indicates the possibility of more than one extremal solution in parameter space. For small slope limitation changes about the one hundred per cent (sonic) slope condition, approximately down to ninety-five slope, increasing the severity of the slope limitation has little effect on the mini-max overpressure. Thus, the low boom three-arc solutions are not overly sensitive to the sonic notch condition. This is reassuring; a shape which was sensitive to a sonic condition would naturally be suspect for it might result from exploitation of a weakness in the aerodynamic model employed in the analysis.

Effect of Increasing Notch Width.—A single optimization calculation was performed to assess the effect of constraining the notch width. This constraint can readily be imposed in the form

$$X_1 < \bar{X} \qquad (78)$$

where the notch width is $X_3 - \bar{X}$.

Physical and body shape conditions employed in the calculation are the same as those employed in the preceding slope limitation effect study, $M = 2.7$, $h/\ell = 100$, $R_3 = .25$, $X_3 = 4.0$, 100 body stations. The maximum body slope, dr/dx, was limited at the sonic condition. The notch width was constrained to occupy at least 20 per cent of the nose length by setting $\alpha_{H_1} = 3.2$, equations (68) and (78). Final mini-max overpressure obtained in the computation was

$$\left(\frac{\Delta p}{p}\right) = 8.121 \times 10^{-4} \qquad (79)$$

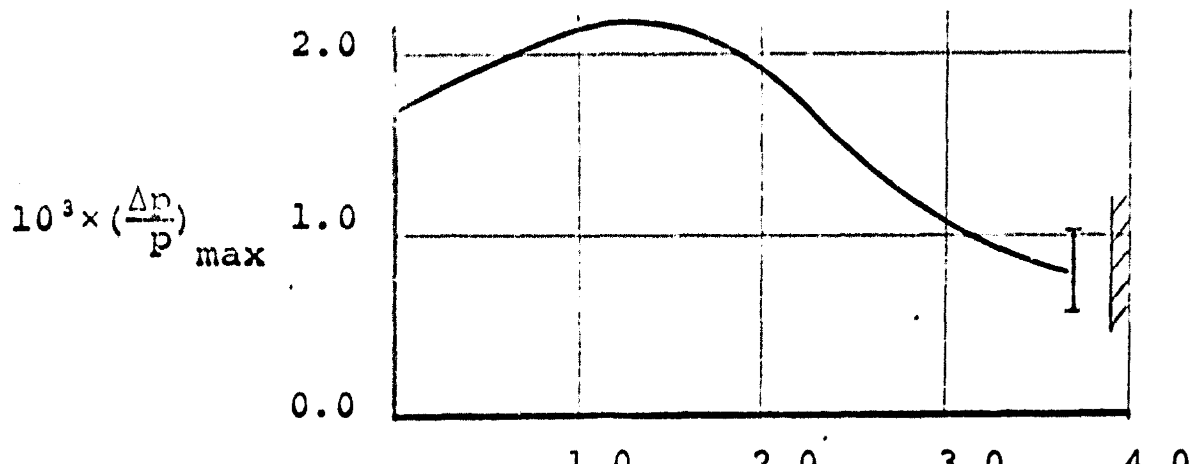

Coordinate of Corner of First and Second Arcs, α_1

Figure 45(a)

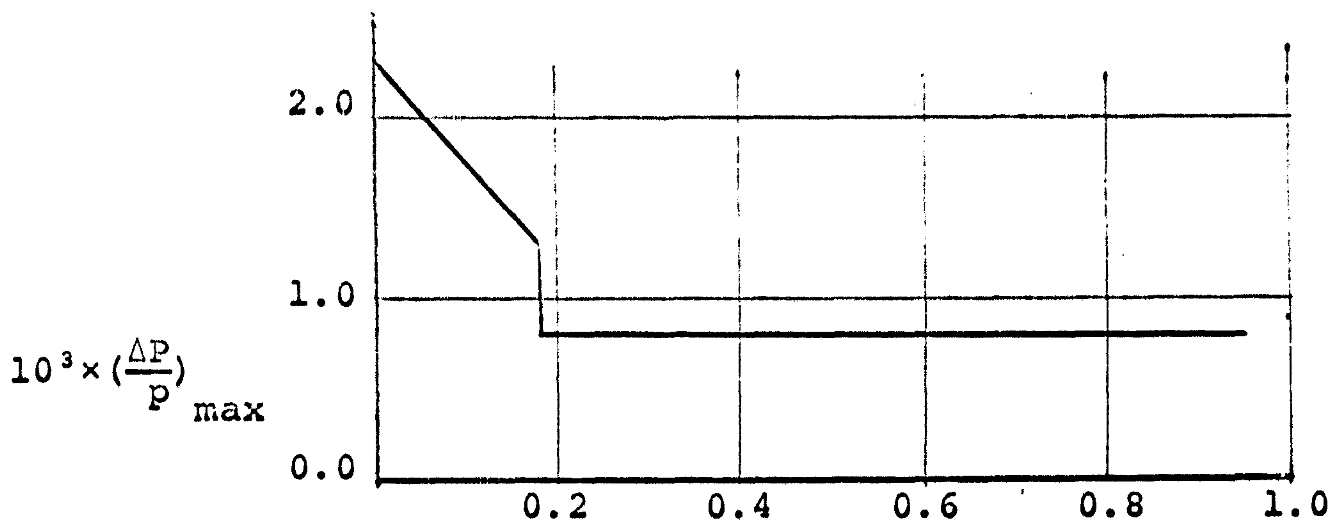

Coordinate of Corner of Second and Third Arcs, α_2

Figure 45(b)

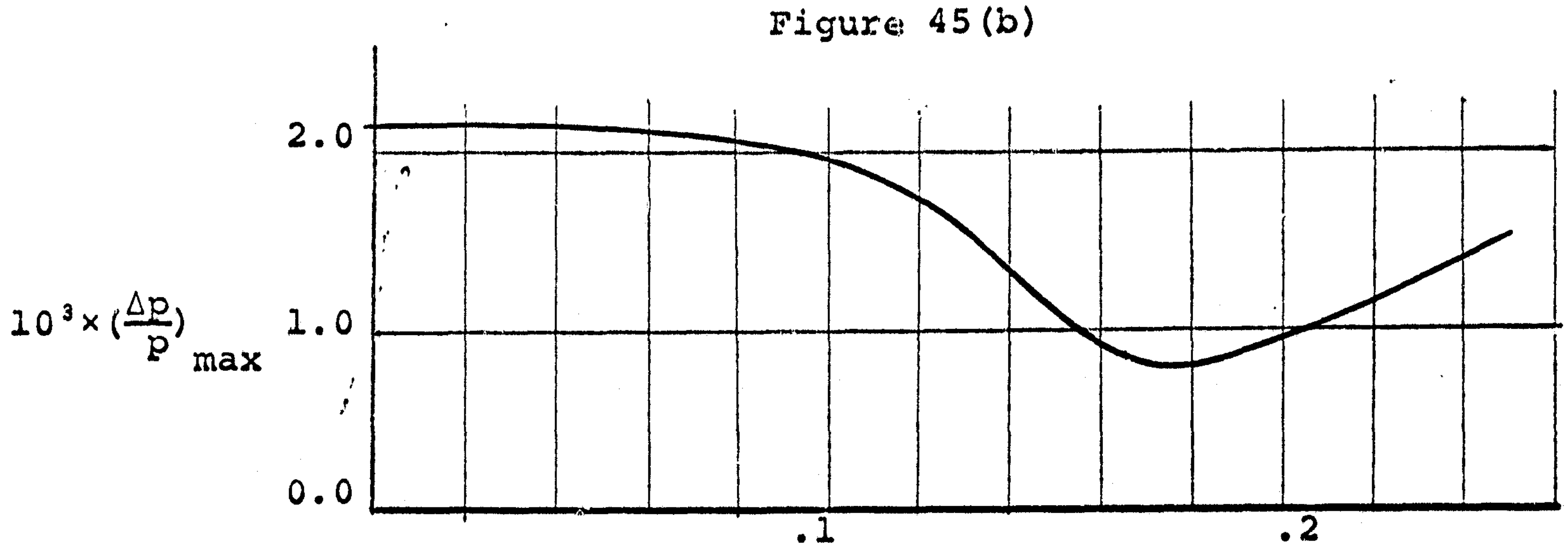

Radius at Corner of First and Second Arcs, α_3

Figure 45(c)

Figure 45—Trade Curves for Three-Arc Body

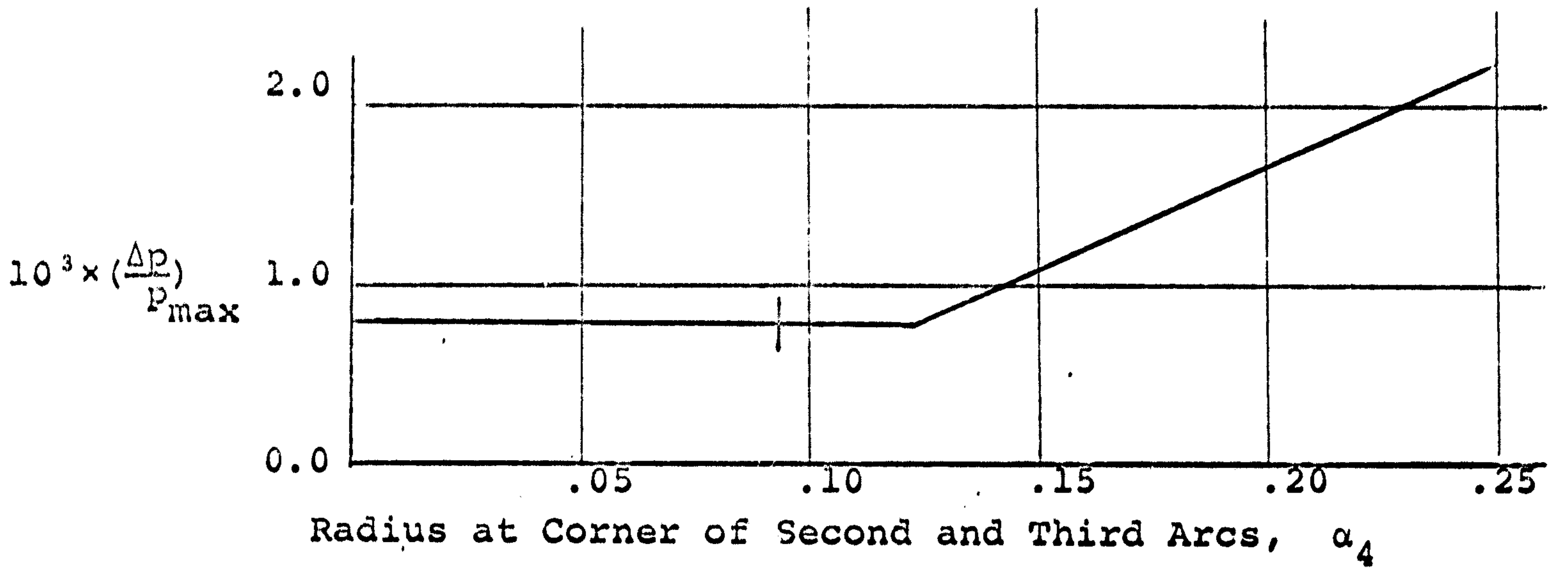

Figure 45(d)

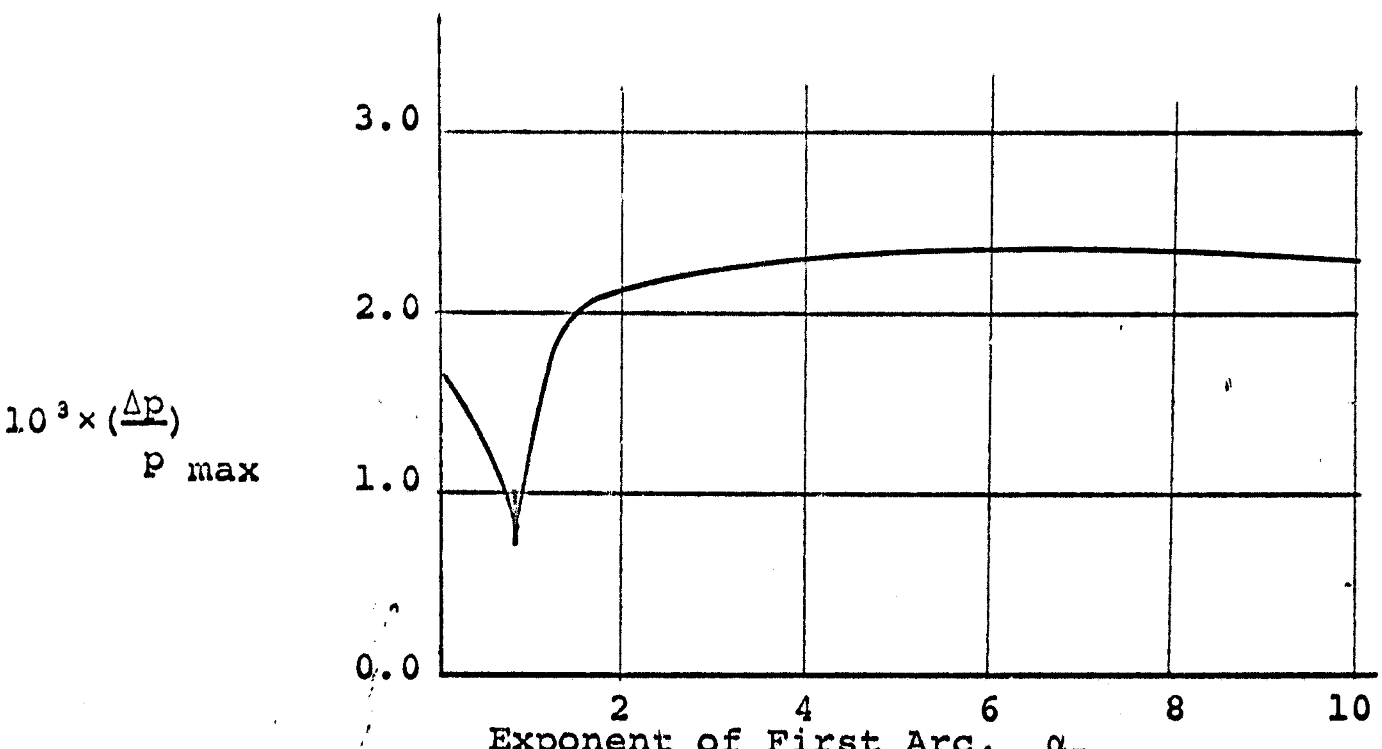

Figure 45(e)

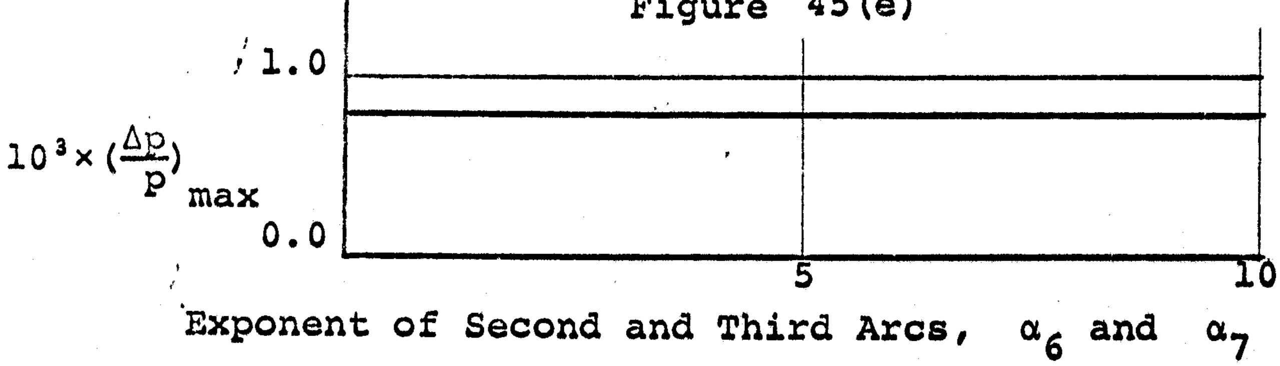

Figure 45(f)

Figure 45 —(Continued)

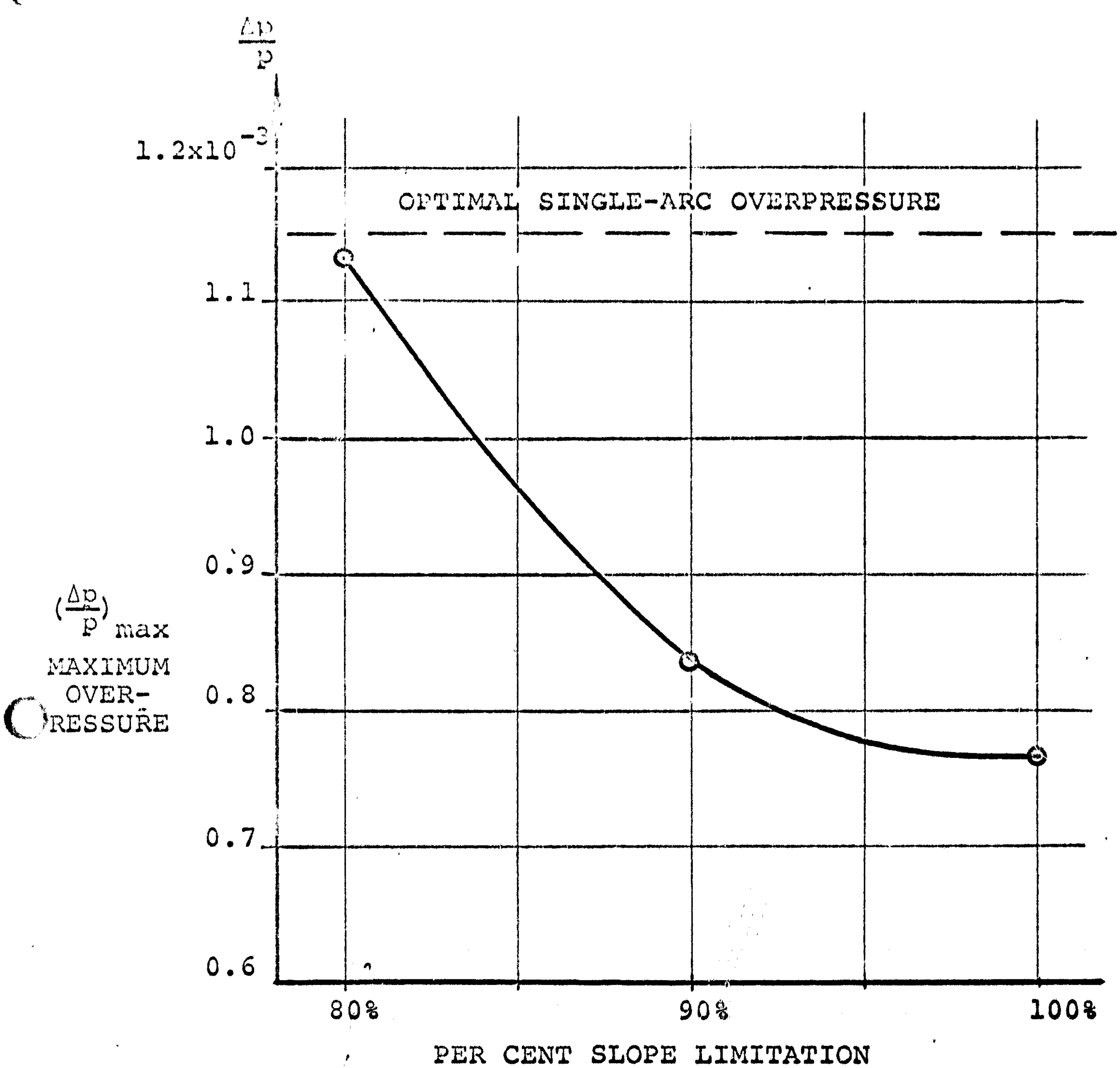

Figure 46.—Effect of Maximum Body Slope Limitation

with the corresponding control parameter vector

$$\lfloor \alpha^* \rfloor = \lfloor 3.2, .50623, .16709, .0810, .7590, .15836, .08808 \rfloor \tag{80}$$

The resulting body shape and signature are presented in Figures (47) and (48), respectively. Forcing a solution with a wider notch has lead the optimization algorithm seeking to define a body shape employing a deeper notch. The overpressure rise associated with the wider, deeper notch is approximately six per cent.

Bodies of Arbitrary Radius Distribution

The option to consider body shapes in the form of an arbitrary radius distribution, R_C, is available within the sonic boom optimization program. Free parameters for the optimization parameters are

$$R_i = \alpha_i; \; \alpha_1 = 1, \ldots, N \quad N < 100 \tag{81}$$

In the i^{th} interval

$$r(x) = R_i + \frac{(R_{i+1} - R_i)}{(X_{i+1} - X_i)} (x - X_i) \tag{82}$$

The body shape is thus approximated by a series of truncated cones in the manner successfully employed in reference

Two solutions have been obtained with this technique. The solutions consider the same optimization problem: maximum overpressure, minimization with constrained body length and radius at $x = \ell/2$. Body length is unity, $r(\ell/2) = .05$, Mach number is $\sqrt{2}$, and the signature is computed at ten body lengths from the axis.

The solutions each commence from a different nominal starting shape. Nominal I is a parabolic body; nominal II is a cusped body. Nominal and final shapes obtained are presented in Figures 49 and 50. It can be seen that two different irregular shaped bodies result. The final minimum overpressure of the two bodies is similar, however. Convergence behavior is presented in Figure 51.

Interpretation of the results obtained from the arbitrary body method is difficult. It is apparent from Figure 51 that both solutions should be pursued further. It is also apparent from Figures 49 and 50 that the optimization algorithm is seeking to minimize the maximum overpressure by creating a sequence of interacting arcs in a manner suggesting the two and three-arc solutions reported above. It may be that some form of smoothing criteria will have to be created in order to consider acceptable arbitrary body shaping for sonic boom overpressure minimization. Such a smoothing criteria could involve specification of additional constrained radii at selected points along the body axis or a direct limitation on the body slopes.

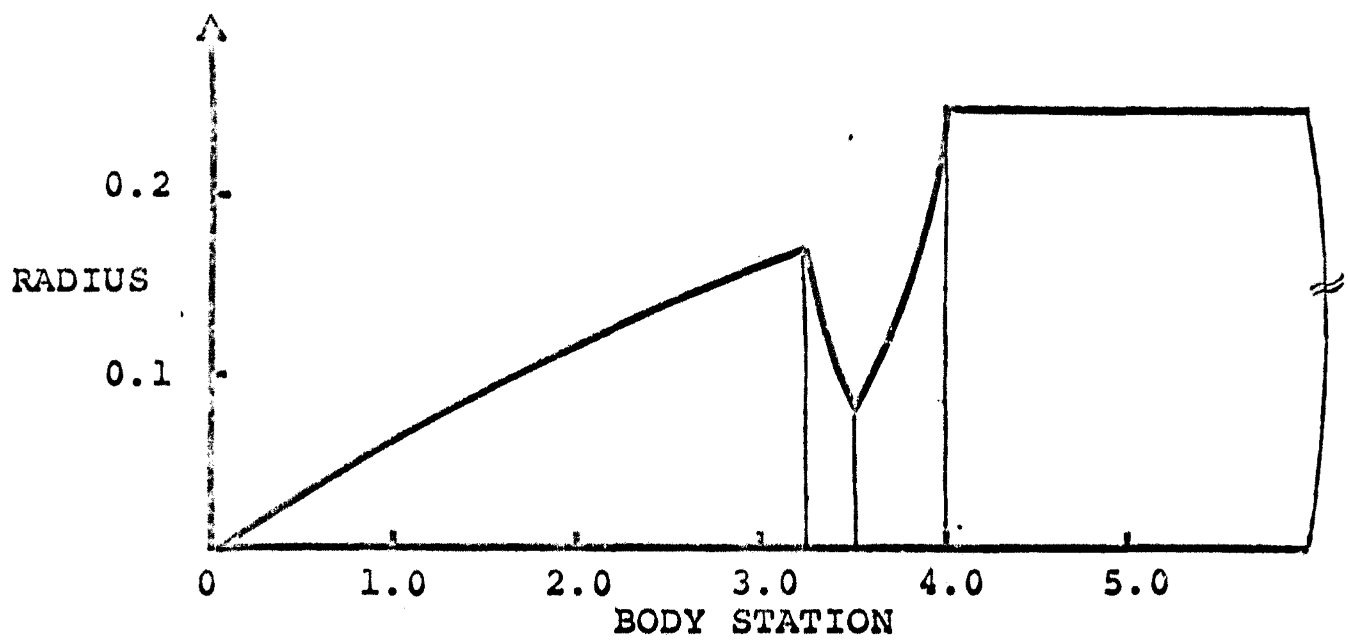

Figure 47. Wide Notch Solution-Body Shape

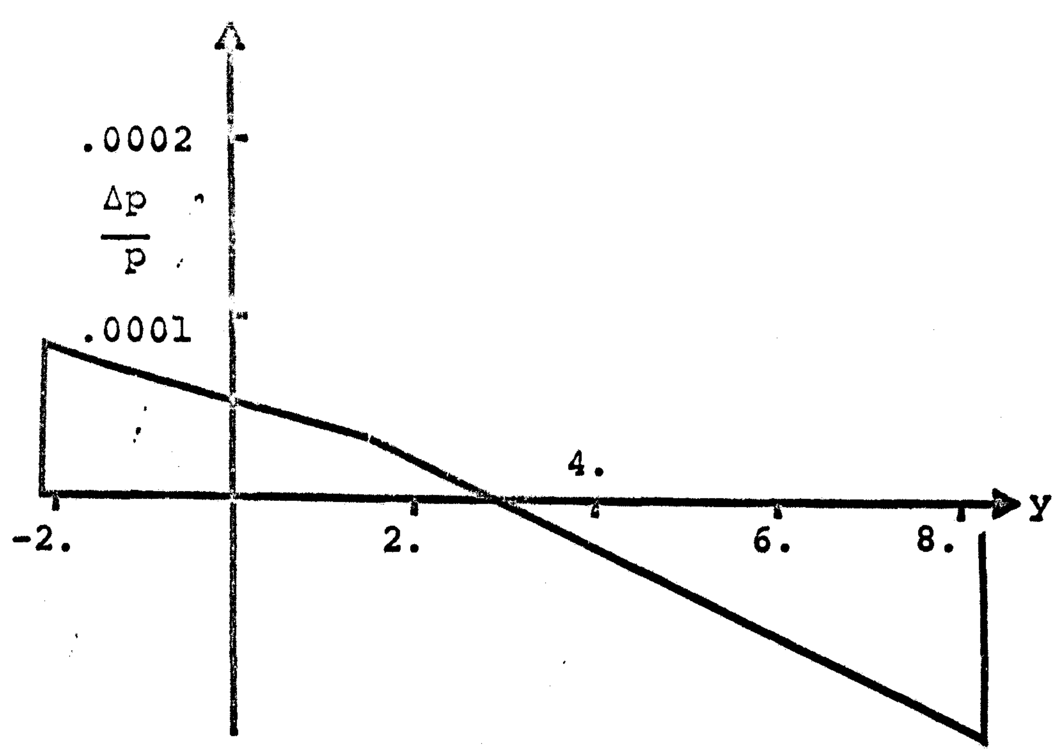

Figure 48. Wide Notch Solution
-Pressure Signature

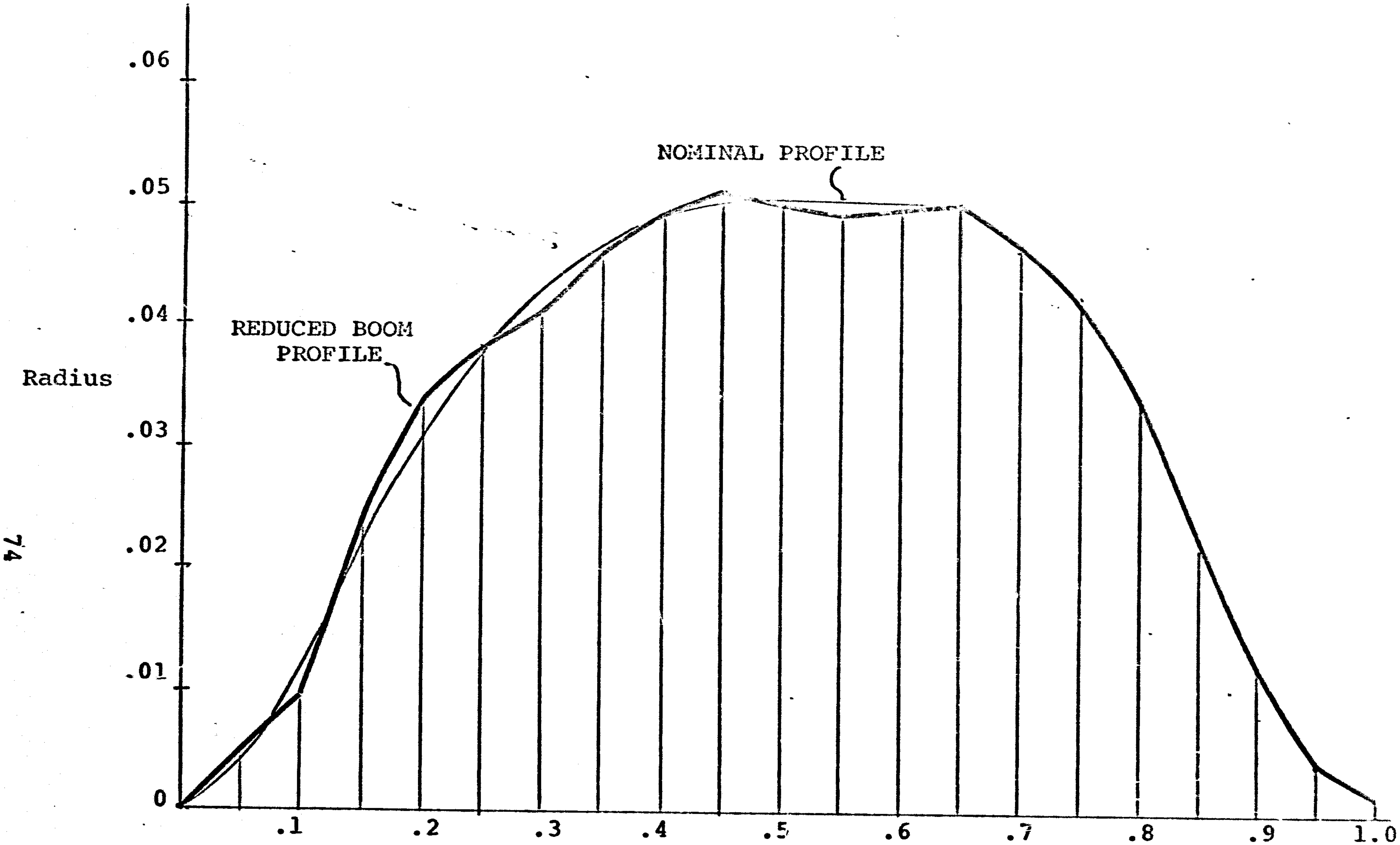

Figure 49.—Solution Developing From Cusped Body

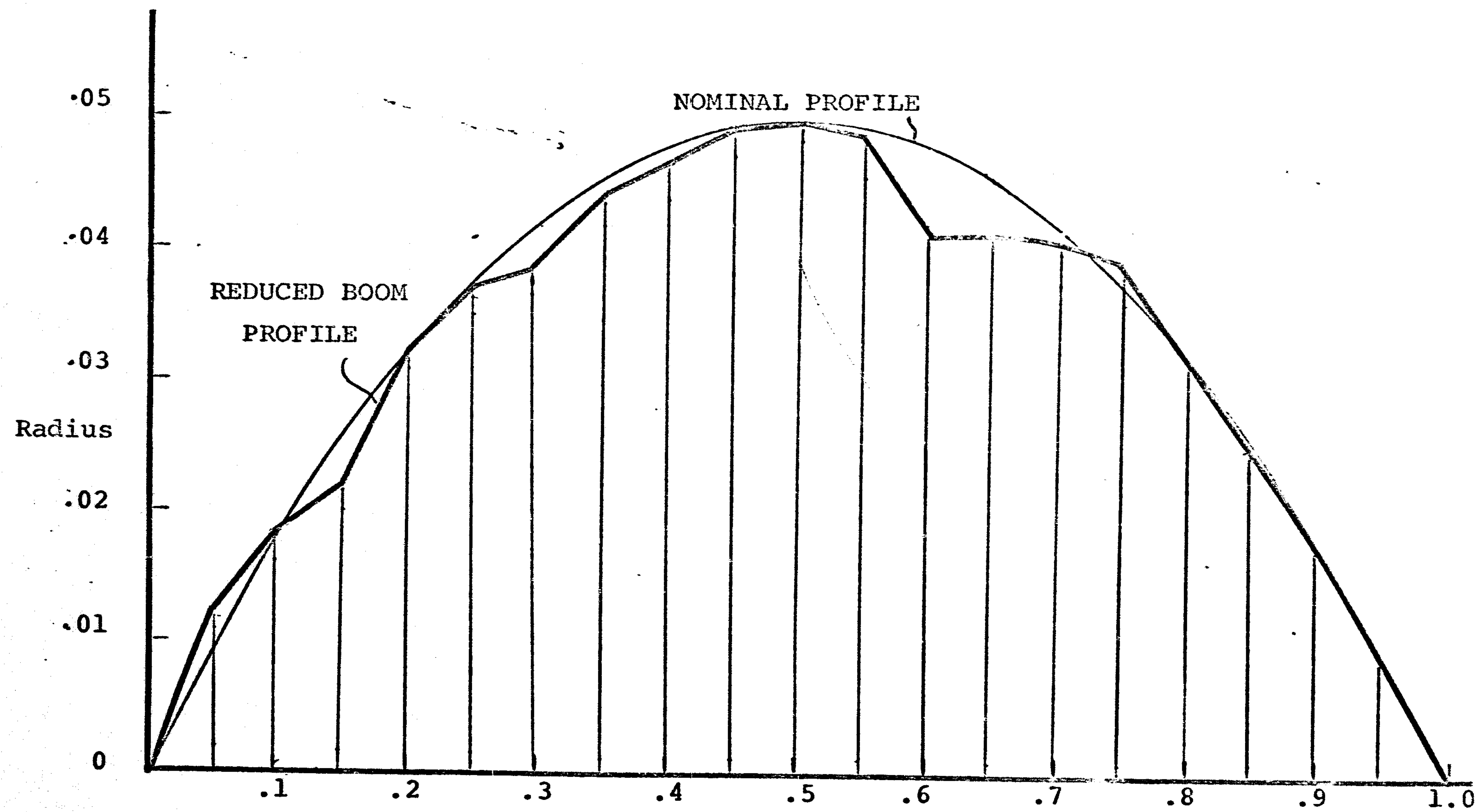

Figure 50—Solution Developing From Parabolic Body

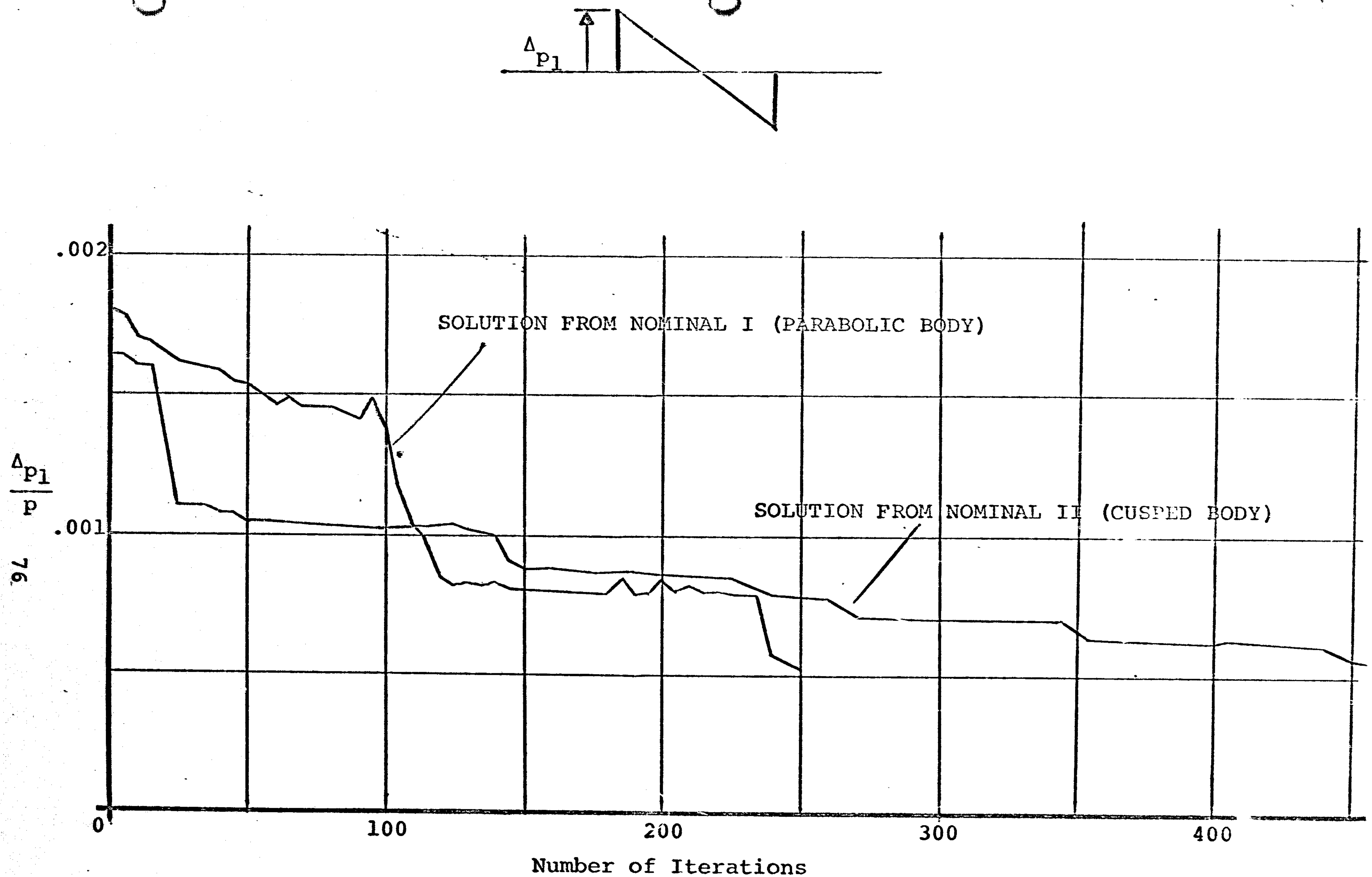

Figure 51—Conversion of Two Test Problems

CONCLUSION

A variety of sonic boom minimization problems have been investigated by multivariable search techniques. The most elementary problems studied are those involving a single-power arc. In these problems geometric constraints can be applied to reduce the optimization to one involving a single parameter. Such problems are readily solved by the sectioning algorithm. The problem simplicity permits the construction of charts illustrating the variation of sonic boom overpressure over a wide range of Mach numbers and distances from the body axes. The charts and optimization studies reveal that close to the body a three-quarter power shape will provide the lowest overpressure. Deviations from this exponent result in rapid increase in overpressure. As distance from the body axis increases, an insensitive extremal shape appears at gradually decreasing values of the power body exponent. With this class of bodies an increase in Mach number, base radius or volume, all tend to drive the solution toward the more sensitive higher power-arc solution.

Next in order of complexity above the single-power arc solutions are those involving two-power arcs with a slope discontinuity at the junction between the two arcs. Geometric constraints immediately reduce the two-arc shape optimization problem to one involving four free parameters. An extensive range of solutions cannot be obtained over a range of Mach number and h/ℓ; instead, each case must be examined as it arises. In general, the two-arc solutions obtained fail to produce a minimum-maximum overpressure significantly below that of the single-power arc body subject to the same physical conditions and geometric constraints. The total impulse of the pressure signature is well below that of the corresponding single-power solution, however.

Next in order of complexity are the three-power arc bodies involving seven free parameters. Body shapes of this type produce a significant reduction in minimum-maximum overpressure when compared to the corresponding single-arc solution. In all cases considered the overpressure is reduced by approximately one third. The sonic boom overpressure is obtained by the device of a conventional forebody of reduced base area followed by a notch creating strong self-cancelling positive and negative pressure waves. The notch walls are ideally sonic; however, it is shown that a moderate reduction in slope is possible without significant increase in overpressure. The notch ideally occupies a small portion of the body length. Again, it is shown that the notch width can be increased for a small increase in overpressure. When the body shape is viewed as an equivalent body of revolution, it is apparent that the first two arcs would physically represent body volume, and the third arc would physically represent wing lift. Such a configuration would imply a relatively unswept canard configuration.

The most general optimization problem considered in the investigation was that of shaping an arbitrary body of revolution. While the resulting shapes possess low sonic boom overpressure, their irregularity appears to prohibit their use in an aircraft configuration unless the low boom property can be maintained while imposing some reasonable smoothness criteria. This was not achieved within the study.

It is recommended that further work in this area concentrate on

1. Use of the alternative small perturbation theory aerodynamics to confirm the low boom properties of the body shapes developed.

2. Experimental verification of the low boom shapes. (This may be difficult with a simple body of revolution due to flow separation effects).

3. Further development of multiple-arc approximations to the body shaping problem including mathematical models permitting a reduction in both forward and rear shocks.

4. Further development of the arbitrary body mathematical model.

5. The extension and application of multivariable search techniques to the general three-dimensional shaping problem.

6. Introduction of real atmosphere effects into the optimization process.

REFERENCES

1. Whitham, G.B.: The Flow Pattern of a Supersonic Projectile. Commun. Pure and Appl. Math., Vol. V, No. 3, August 1952, pp. 301-348.

2. Lighthill, M.J.: Higher Approximations in Aerodynamic Theory. Princeton Aeronautical Paperbacks, 1960.

3. Woodward, F.A.: Analysis and Design of Wing-Body Combinations at Subsonic and Supersonic Speeds. Journal of Aircraft, Vol. V, No. 6, November-December 1968.

4. Bryson, A.E. and Denham, W.F.: A Steepest-Ascent Method for Solving Optimum Programming Problems. Raytheon Report BR1303.

5. Hague, D.S.: Three-Degree-of-Freedom Problem Optimization Formulation - Analytical Development. Part I, Vol. 3, FDL-TDR-64-1 (Prepared under USAF Contract AF33(657)-8829 by McDonnell-Douglas Corporation), October 1964.

6. Hague, D.S.: The Optimization of Multiple-Arc Trajectories by the Steepest-Descent Method. Recent Advances in Optimization Techniques, Edited by Lavi and Vogl, John Wiley: 1966, pp. 489-517.

7. Hague, D.S.: Atmospheric and Near Planet Trajectory Optimization by the Variational Steepest-Descent Method. NASA CR-73365, 1969.

8. Wilde, D.J.: Optimal Seeking Methods. Prentice-Hall, Inc. 1964.

9. Hague, D.S. and Glatt, C.R.: An Introduction to Multivariable Search Techniques for Parameter Optimization. NASA CR-73200, April 1968.

10. Hague, D.S. and Glatt, C.R.: A Guide to the Automated Engineering and Scientific Optimization Program, AESOP. NASA CR-73201, April 1968.

11. Hague, D.S. and Glatt, C.R.: Application of Multivariable Search Techniques to the Optimal Design of a Hypersonic Cruise Vehicle. NASA CR-73202, April 1968.

12. Sandrin, W.A., Glatt, C.R., and Hague, D.S.: Design of Arrays with Unequal Spacing and Partially Uniform Amplitude Taper. IEEE Transaction on Antennas and Propagation, September 1969.

13. Hague, D.S., Rozendaal, H.L., and Woodward, F.A.: Application of Multivariable Search Techniques to Optimal Aerodynamic Shaping Problems. Journal of Astronautical Sciences, Vol. 15, No. 6, November-December 1968, pp. 283-296.

APPENDIX A

MAIN PROGRAM AND PROGRAM STRUCTURE

The main program controls both shock computations through subprograms LIGHT and MIDDLE and optimization computations through subprogram AESOP, references 1 through 4. Communication between the shock computation subroutines is primarily carried out through two labelled COMMON blocks, SHOCK1 and SHOCK2. The shock program contains a detailed computation print option controlled by data input (IPDBUG=1) to aid in program debugging.

Communication between subroutines of the optimization subprogram AESOP and with the MAIN program are carried out exclusively through the AESOP data base labelled COMMON-AESOPD. Figure A1 illustrates the program function in schematic form. Problem type is selected from the following options:

1. Volume Constrained, Single-Arc

2. Base Constrained, Two-Arc

3. Base Constrained, Three-Arc

4. Base Constrained, Single-Arc

5. Arbitrary Radius Distribution

Following problem selection the appropriate data for the problem and the optimization data is read to permit problem initialization. Total data input is contained in three NAMELIST inputs: IPGM, SHOCKS, and IAESOP, figure A2. The function of these three data input blocks is as follows:

1. Problem Selection Data

2. Shock Computation Data

3. Optimization Data

The data read and subsequent program initialization are followed by a translation of the optimizer parameters, α_i, into the body defining parameters and body radius distribution. Subprogram LIGHT then computes the body F function, reference 5, which is passed on to the shock location subroutines called from subprogram MIDDLE. Each of these major subprograms employs a chain of subroutines to complete the shock calculation. The complete subroutine structure is defined in figure A.3. Following shock location and computation of the final pressure signature, typical functions such as maximum overpressure are translated into the optimization functions F_i of references 1 to 3. Subprogram AESOP examines the pressure signature functions and defines a new set of optimization parameters, α_i, for the next body shape to be analyzed.

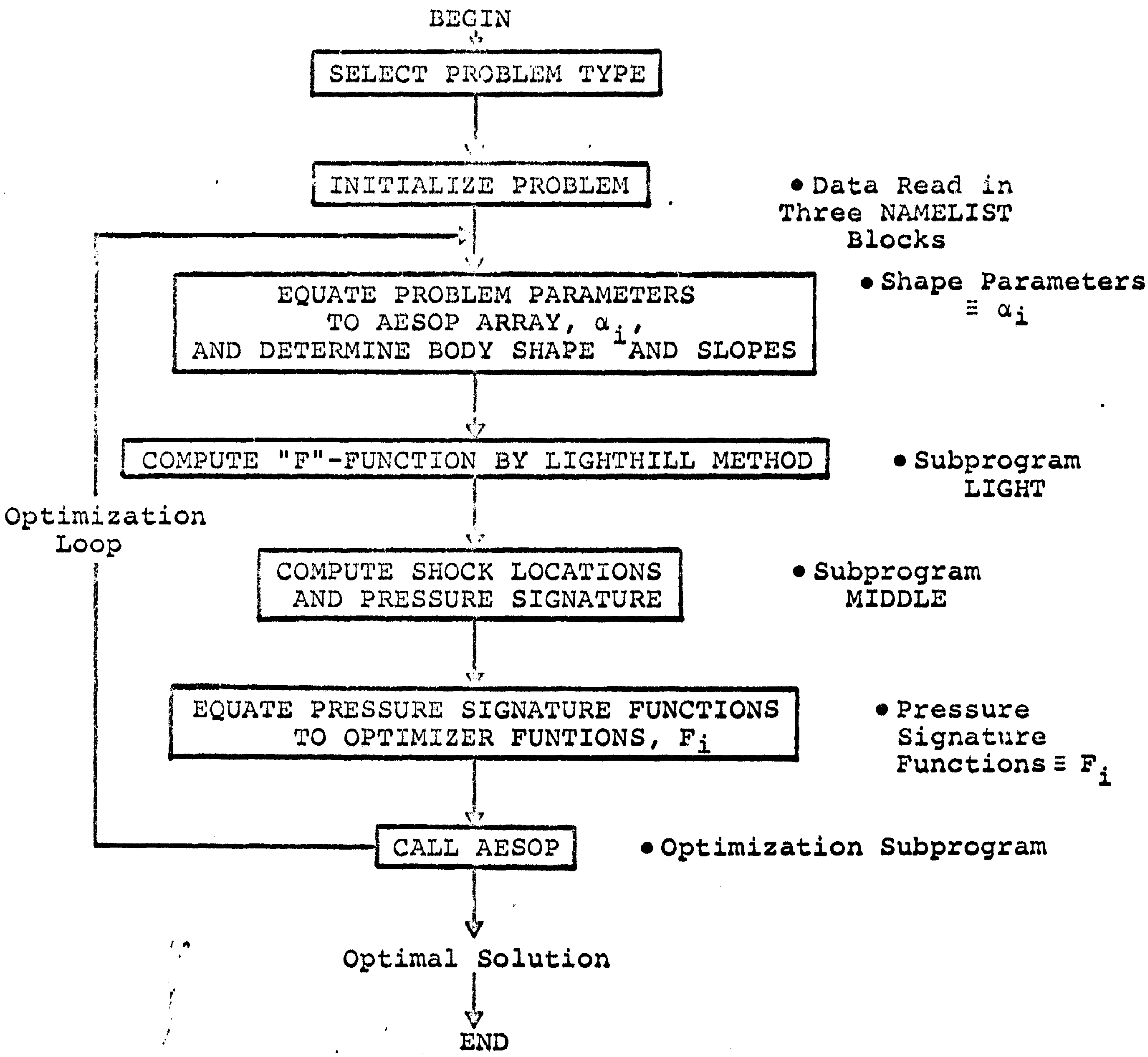

Figure A1.—Function of Main Program

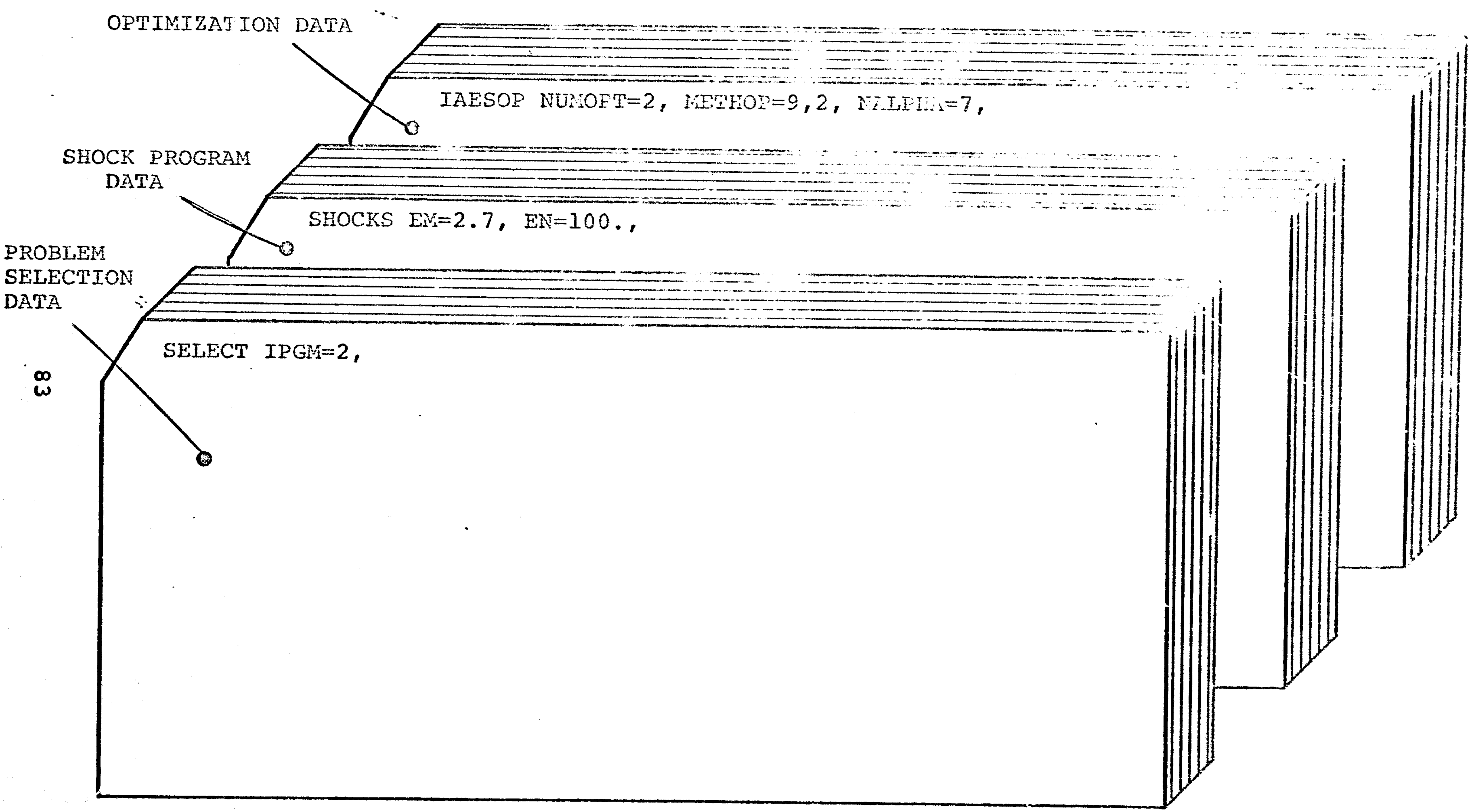

Figure A2—Typical Data Set-Up

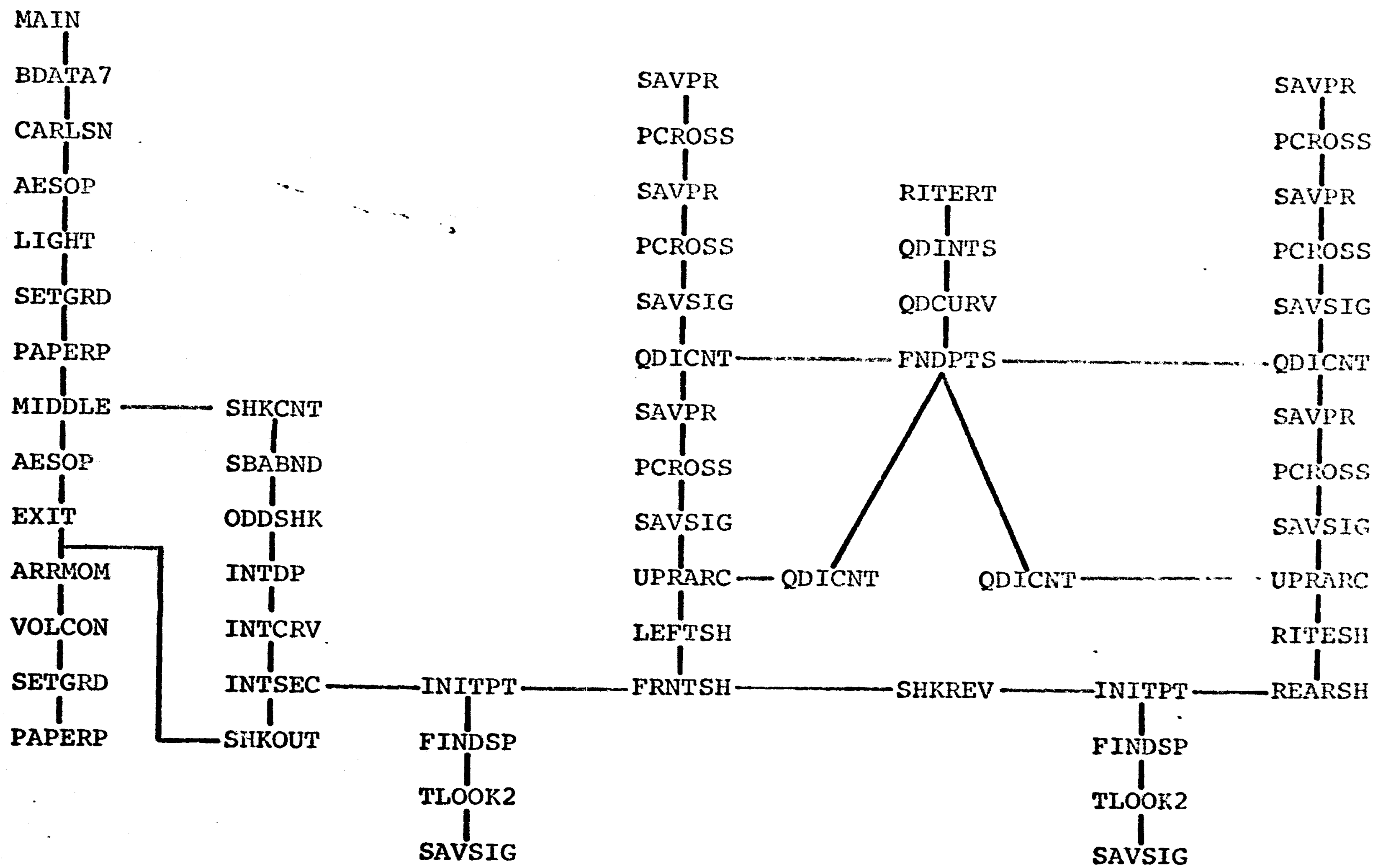

Figure A3.—Subroutine Structure

The process then repeats as indicated in figure A1 with AESOP defining a succession of body shapes which lead to minimization of a selected pressure signature function. A schematic of the program structure is presented in figure A.4.

DATA INPUT

All data to the sonic boom overpressure optimization program is entered in the three NAMELIST data blocks described previously. Each data block content is described in this section. All data in the three blocks is nominally established within the program; therefore, only data which differs from the nominal values need be read into the program.

NAMELIST Data Block "SELECT"

This data block is defined and read by the MAIN program. Data block SELECT contains one input, IPGM. The function of this input is selection of the problem type to be solved. Input must satisfy

$$1 < IPGM < 5$$

Specific options are

IPGM=1, Select single-arc volume constrained solution

=2, Select two-arc base constrained solution

=3, Select three-arc base constrained solution

=4, Select single-arc base constrained solution

=5, Select arbitrary radius distribution

The main distinction between these cases lies in the manner in which body gross physical characteristics are transformed into an appropriate body radius distribution, R_i, where R_i is the body radius at point $x = X_i$. It should be noted that program options can readily be extended to additional problem options by incorporating new radius distribution definitions in the MAIN program.

NAMELIST Data Block "SHOCKS"

This data block is defined and read in the MAIN program. It contains all input data for the computation of the F function and pressure signature of the five problems classes embodied in the program. Input data is described in Table I.

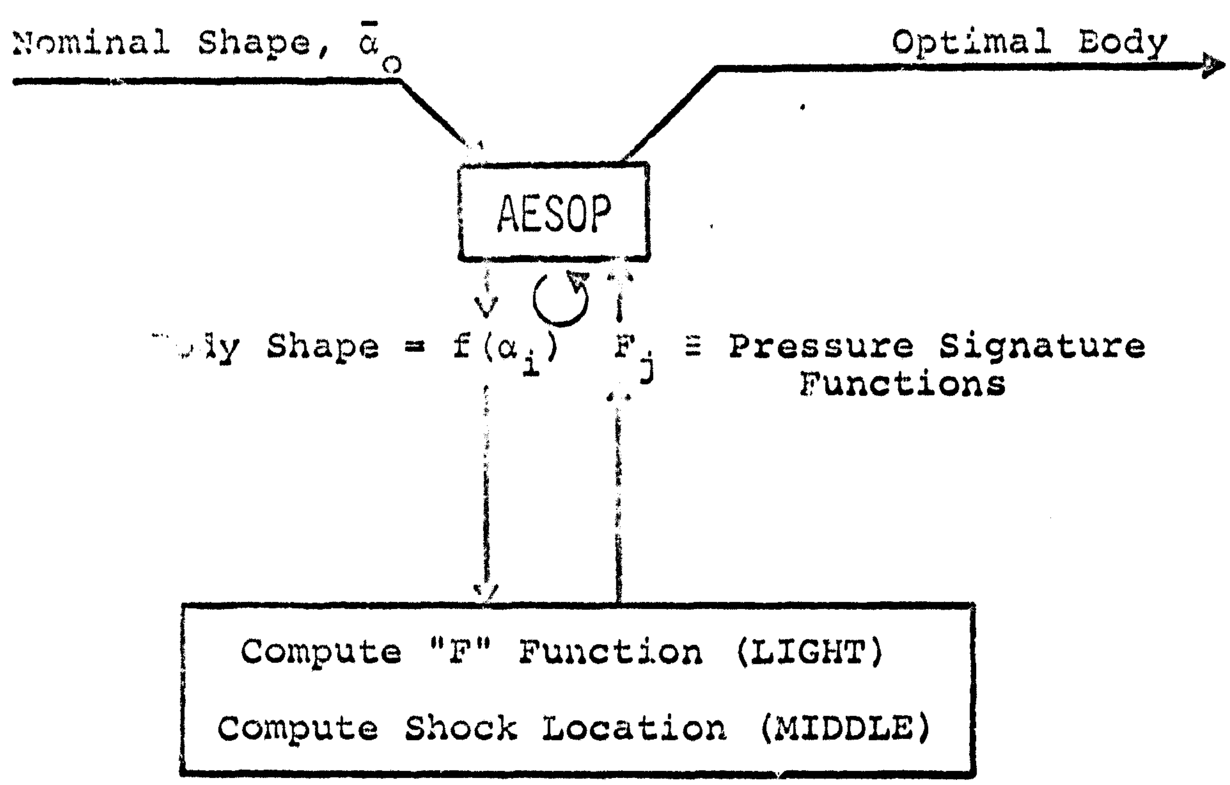

Figure A4.—Schematic of Optimization Procedure

TABLE I.—DATA BLOCK "SHOCKS"

MNEMONIC	NOMINAL VALUES	DESCRIPTION
ALT	100.	Non-dimensional body height above ground, h/(EL).
BUGOFF	0.	Turns debug print off at iteration BUGOFF
CMODE	0.0	=0.0, perform normal optimization calculation =1.0, Read in auxiliary data block, YFUNCT, and compute one signature directly from the Y function.
DELX	0.1	Spacing of body stations, X_i.
EL	8.0	Body reference length
EM	1.414	Free stream Mach number
EN	100.	Number of body stations, X_i, i=1, 2,. . ., EN
EXPORD	2.0	The signature moment order.
IFIN	0.	Program terminates when IFIN=1.
IPANYW	10	A detailed running print is obtained every (IPANYW)th iteration.
IPDBUG	0.	=1, Provides detailed program debug information.
IPLINT	0.	=1, Plots the integral arc curves on printer.
IPLSHK	0.	=1, Plots the F function on printer.
JJDBUG	0.	The iteration at which a debug print will commence.
MAXPT		
MINPT		
MODEL	0.	=I, Uses MODEL I of NASA TN D-3106 as nominal.

MNEMONIC	NOMINAL VALUES	DESCRIPTION
NON-DIM	0.	=1, Plot signature in non-dimensional form.
NPTS	20	Number of points on each enriched integral arc.
PLIMIT	0.0	Signature moment is computed for regions where $\Delta p/p$ > PLIMIT.
POWRN1	1.0	First body arc exponent.
POWRN2	1.0	Second body arc exponent.
POWRN3	1.0	Third body arc exponent.
RMAX	.25	Maximum body radius.
R1	.08333	Body radius at first corner.
R2	.16667	Body radius at second corner.
R3	.25	Body radius at third corner.
SLPCHK	0.0	-1.0, Perform body slope limit test from front to rear and rear to front. 0.0, Omit body slope check. 1.0, Perform body slope check.
SLPLIM	1.0	Body slope limit, $\|dr/dx\|$.
VFACTR	1.0	Non-dimensional body volume.
X1	1.3333	Location of first body corner.
X2	2.6667	Location of second body corner.
X3	4.0	Location of third body corner.
XK	0.5	Non-dimensional location of second body corner; three arc bodies only.

NAMELIST Data Block "IAESOP"

This data block is read and defined in the optimization subprogram by subroutine BAESOP. All nominal data values are established by the optimization subroutine BDATA7. Data block IAESOP primarily defines which combination of the nine optimization search algorithms of the optimization subprogram are to be employed, how they are to be employed, and how many times the optimization cycle is to be repeated.

The nine search algorithms available are described in reference 5 or reference 1; these are listed below.

1. Sectioning
2. Pattern
3. Magnification
4. Steepest-Descent
5. Adaptive Creeping
6. Quadratic
7. Davidon
8. Random Point
9. Random Ray

A complete list of optimization data is presented in Tables II and III. Table II contains the basic optimization control data. Table III contains the specialized print control data. It should be emphasized that all items in Tables II and III are read by the single NAMELIST input block IAESOP.

AESOP Print Control

AESOP has a flexible print output capability. Varying levels of printout are available at user option as follows:

Summary of function and control parameter values at the beginning and end of the optimization process;

Summary of function and control parameters values at the end of each cycle;

Summary of function and control parameter values at the end of each evaluation;

Detailed printout of individual search parameters.

The convention adapted for print indicator is a six-letter mnemonic as described below.

NOTE: In all cases print is given when the indicator is non-zero and omitted when it is zero.

EXAMPLES: 1) IPACRP=1, Print control vector following creeping search

2) IPDPEN=1, Supply detailed print output from subroutine PENALTY

<u>IP</u> <u>X</u> <u>XXX</u>

<u>Subroutine Reference</u>

CRP - CREEPR

CYC = MAINOP (End of Cycle)

DVD - DAVIDN

MAG - MAGIFY

PAT - PATERN

PEN - PENLTY

QUA - QUADRA

RPT - RPOINT

RRS - RANRAY

SEC - SECTON

STD - STDESC

<u>Type of Print</u>

A - Control Vector - ALPHA

D - Detailed Print

F - Function Array - FUNCTN

Means PRINT INDICATOR

An alphabetical list of print control indicators follows in Table III; relevant search is identified for each input in the same way described earlier for the optimization data.

TABLE II.—BASIC OPTIMIZATION DATA

MNEMONIC	RELEVANT SEARCH									NOMINAL VALUES	DESCRIPTION
	1	2	3	4	5	6	7	8	9		
$ALFSIN_i$					X					100*1.	Determines first perturbation directions in creeping search.
$ALPHA_i$	X	X	X	X	X	X	X	X	X	100*1.	Nominal values of control parameters.
$ALPHI_i$	X	X	X	X	X	X	X	X	X	100*1.	Upper control parameter search limits.
$ALPLO_i$	X	X	X	X	X	X	X	X	X	100*1.	Lower control parameter search limits.
$CREPMN_i$					X					100* .0000001	Minimum perturbations to be employed in creeping search.
$DCREEP_i$					X					100*.001	Starting perturbations for creeping search.
FACTHI	X			X		X	X			.001	Initial termination tolerance on Golden Section.
FACTLO	X			X		X	X			.00001	Final termination tolerance on Golden Section
$FTOL_i$*	X	X	X	X	X	X	X	X	X	20*1.	Final desired constraint tolerances.
INDWMA				X						1	Steepest-descent weighting matrix indicator. 0 - Unit matrix 1 - Empirical matrix 2 - Alternates between unit and empirical matrix
IRANDM	X				X					0	Selects the order in which the control variables are perturbed and sectioning searches. 0 - Uniformly random 1 - Natural order 2 - Reverse natural order

* Used only in constraint logic

MNEMONIC	RELEVANT SEARCH 1	2	3	4	5	6	7	8	9	NOMINAL VALUES	DESCRIPTION
IREPET	X	X	X	X	X	X	X	X	X	10	Number of optimization cycles to be completed.
ISECOF										1000	Cycle number at which sectioning search is terminated.
ISIDE	X			X		X			X	0	Selects extreme of the search interval to be used when performance is constant on search ray. 0 - Lower limit 1 - Upper limit
IWARP	X	X	X	X	X	X	X	X	X	0	Controls multiple extremal option. 0 - Performance response surface unaltered 1 - Performance response surface is warped
LIMIT	X									2	Number of sectioning searches.
MAXCRP					X					5	Number of complete creeping searches to be performed when search is called.
MAXDVD							X			10	The number of Davidon searches carried out when this method is selected.
MAXJJJ	X	X	X	X	X	X	X	X	X	200	The maximum number of performance evaluations.
MAXMAG			X							99	Maximum number of magnification searches in an optimization calculation.
MAXRPT								X		10	Number of random point evaluations.
MAXRRS									X	100	Number of random rays to be employed.

MNEMONIC	RELEVANT SEARCH									NOMINAL VALUES	DESCRIPTION
	1	2	3	4	5	6	7	8	9		
$METHOP_i$	X	X	X	X	X	X	X	X	X	1,2,3,4,5	The sequence of searches to be employed. 1 - Sectioning 2 - Pattern 3 - Magnify 4 - Steepest-Descent 5 - Creeping 6 - Quadratic 7 - Davidon 8 - Random Point 9 - Random Ray
NALPHA	X	X	X	X	X	X	X	X	X	3	Number of control parameters to be employed.
NFUNC	X	X	X	X	X	X	X	X	X	1	Number of functions to be considered.
NMAXLO	X			X		X			X	10	Initial maximum number of evaluations in Golden Section.
NMAXUP	X	X		X		X			X	20	Final maximum number of evaluations in Golden Section and to limit the number of evaluations in pattern.
NPHIAC	X	X	X	X	X	X	X	X	X	1	Function number of the performance criteria.
$NPSI_i$*	X	X	X	X	X	X	X	X	X	0	The number of constraints.
NUMSTD				X						2	Number of steepest-descent searches.
PHIEPS	X			X		X			X	0.0	Performance values within PHIEPS of the minimum value yet attained are treated as being equal in Golden Section.
$PSIWT_i$*	X	X	X	X	X	X	X	X	X	20*. .0001	Initial constraint error weights.

* Used only in constraint logic

MNEMONIC	RELEVANT SEARCH 1	2	3	4	5	6	7	8	9	NOMINAL VALUES	DESCRIPTION
QFACTR						X				1.0	Quadratic perturbation factor.
$QPERT_i$						X				20*.005	Initial control parameter perturbations for quadratic and Davidon searches.
RANGEN								X	X	1.0	Random number generator trigger (1.0 means uniform distribution), (-1.0 means normal distribution).
RUFHI									X	.01	Maximum nondimensional random ray perturbation size on any component. Value of 1.0 gives maximum perturbation equal to search range.
RUFLO									X	.00001	Minimum nondimensional random ray perturbation size on any component.
$SIBAR_i$*	X	X	X	X	X	X	X	X	X	20*0.0	Desired constraint values.
$TOLFAC_i$*	X	X	X	X	X	X	X	X	X	20*0.5	Constraint tolerance reduction factor.
$TTOL_i$*	X	X	X	X	X	X	X	X	X	20*100.	Initial constraint tolerances.
$WITER_i$*	X	X	X	X	X	X	X	X	X	100*1.0	Starting values for iterative component of steepest-descent weighting matrix.
$WTDOWN_i$*	X	X	X	X	X	X	X	X	X	20*0.5	Constraint weight decrease factor.
$WTUP_i$*	X	X	X	X	X	X	X	X	X	20*2.0	Constraint weight increase factor.
$XTENHI_i$	X			X		X			X	100*0.0	Used to extend upper search limit in Golden Section if performance is constant in feasible origin.

* Used only in constraint logic

MNEMONIC	RELEVANT SEARCH 1	2	3	4	5	6	7	8	9	NOMINAL VALUES	DESCRIPTION
$XTENLO_i$	X			X		X			X	100*0.0	Used to extend lower search limit in Golden Section if performance is constant in feasible region.
$WARPAL_i$	X	X	X	X	X	X	X	X	X	100*0.0	The warping origin in the control parameter space for multiple extremal feature.
WARPN	X	X	X	X	X	X	X	X	X	2.0	The exponent of the warping transformation.

* Used only in constraint logic

TABLE III.—OPTIMIZATION PRINT CONTROL DATA

MNEMONIC	RELEVANT SEARCH 1	2	3	4	5	6	7	8	9	NOMINAL VALUES	DESCRIPTION
IPACRP					X					0	Creeping control parameter print indicator.
IPACYC	X	X	X	X	X	X	X	X	X	0	Cycle control parameter print indicator.
IPADVD							X			0	Davidon control parameter print indicator.
IPAMAG			X							0	Magnification control parameter print indicator.
IPAPAT		X								0	Pattern control parameter print indicator.
IPAPEN*	X	X	X	X	X	X	X	X	X	0	Constraint penalty control parameter print indicator.
IPAQUA						X				0	Quadratic control parameter print indicator.
IPARPT								X		0	Random point control parameter print indicator.
IPARRS									X	0	Random ray control parameter print indicator.
IPASEC	X									0	Sectioning control parameter print indicator.
IPASTD				X						0	Steepest-descent control parameter print indicator.
IPDCRP					X					0	Detailed creeping print indicator.
IPDDVD						X				0	Detailed Davidon print indicator.

MNEMONIC	RELEVANT SEARCH 1	2	3	4	5	6	7	8	9	NOMINAL VALUES	DESCRIPTION
IPDMAG			X							0	Detailed magnification print indicator.
IPDPAT		X								0	Detailed pattern print indicator.
IPDQUA						X				0	Detailed quadratic print indicator.
IPDRIV				X		X				0	Detailed derivatives print indicator.
IPDRPT								X		0	Detailed random point print indicator.
IPDRRS									X	0	Detailed random ray print indicator.
IPDSEC	X									0	Detailed sectioning print indicator.
IPDSTD				X							Detailed steepest-descent print indicator.
IPFCRP					X					0	Creeping function print indicator.
IPFCYC	X	X	X	X	X	X	X	X	X	0	Optimal function print indicator at the end of each cycle.
IPFDVD							X			0	Davidon function print indicator.
IPFMAG			X							0	Magnification function print indicator.
IPFPAT		X								0	Pattern function print indicator.
IPFQUA						X				0	Quadratic function print indicator.
IPFRPT								X		0	Random point function print indicator.

MNEMONIC	RELEVANT SEARCH 1	2	3	4	5	6	7	8	9	NOMINAL VALUES	DESCRIPTION
IPFRRS									X	0	Random ray function print indicator.
IPFSEC	X									0	Sectioning function print indicator.
IPFSTD				X						0	Steepest-descent function print indicator.
IPGAIN	X	X	X	X	X	X	X	X	X	1	Print every iteration which will improve the performance.
IRLIST	X	X	X	X	X	X	X	X	X	0	Namelist output control = 0, omit print = 1, print namelist data

AESOP Data Listings

Program AESOP data can be conveniently grouped according to search and function. The user employing a particular search can independently specify the characteristics of that search and may not be concerned with input relevant to the other searches. Hence, a data grouping by search and by function is presented below for user convenience. It should be noted that certain inputs are common to more than one search; where this occurs, the input is repetitively defined in each search.

Search Selection and Control.—

NUMOPT - The number of optimization techniques to be employed. Each individual search request in a sequence of requests adds to this input (e.g., the search pattern 4,2,4,2 requires NUMOPT = 4). Maximum number of searches employed must satisfy NUMOPT $\leq$ 20.

$METHOP_i$ - The search sequence by numeric identification. For example, the input METHOP(1) = 1,2,3,4,5,6,7,8,9 signifies the following search sequence:

1 - Sectioning
2 - Pattern
3 - Magnification
4 - Steepest-Descent
5 - Adaptive Creeping
6 - Quadratic
7 - Davidon (Fletcher-Powell)
8 - Random Point (Monte-Carlo)
9 - Random Ray (random evolution)

The complete search sequence will be referred to as an optimization cycle.

MAXJJJ - The maximum number of system evaluations. A direct iteration number limit.

IREPET - The maximum number of times the search sequence (optimization cycle) defined in $METHOP_i$ will be utilized

Parameter Selection.—

NALPHA - The number of parameters available for optimization. No more than one hundred parameters may be employed.

$ALPLO_i$ - Lower bounds on each parameter search range

$ALPHI_i$ - Upper bounds on each parameter search range

$ALPHA_i$ - The nominal parameter values. Note that $ALPLO_i \leqslant ALPHA_i \leqslant ALPHI_i$ must be satisfied. If a particular parameter, say $ALPHA_j$, is to be fixed in value in a particular computation, then set $ALPLO_j = ALPHA_j = ALPHI_j$. This effectively reduces the parameter space dimension by one for each such parameter.

Multiple Extremal Option.—

IWARP - Controls multiple extremal option
IWARP = 1, automatically warp the response surface
IWARP = 0, leaves the response surface unmodified

$WARPAL_i$ - The point at which the warping transformation is centered, i.e., the location of a known extremal point.

WARPN - The degree of the warping transformation. The greater WARPN, the greater the response surface distortion.

Optimization Function Selection.—

$FUNCTN_i$	- AN INTERNAL ARRAY CONTAINING ALL COMPUTED OPTIMIZATION FUNCTIONS

NFUNC - The total number of functions ($FUNCTN_i$) being computed in the system model (sonic boom model) NOTE: NFUNC $\leqslant$ 100.

NPHIAC - The function to be minimized. AESOP always searches for a minimum;to maximize $FUNCTN_m$ define $FUNCTN_n = -FUNCTN_m$ and minimize $FUNCTN_n$.

NUMPSI - The total number of functions being constrained. NOTE: NUMPSI $\leqslant$ 20.

$NPSI_i$ - The functions to be constrained, e.g., NPSI(1) = 3, 5, 1, 7 indicates that $FUNCTN_3$, $FUNCTN_5$, $FUNCTN_1$, and $FUNCTN_7$ are to be constrained.

$SIBAR_i$ - The desired values of the constraint functions defined by $NPSI_i$

FTOL$_i$ - The acceptable tolerances on the constraint function values, SIBAR$_i$.

TTOL$_i$ - Initial acceptable tolerances on the constraint function values, (should be approximately 100 times greater than the corresponding FTOL$_i$).

PSIWT$_i$ - Initial constraint error weighting factors in the augmented performance function, ϕ^*, where

$$\phi^* = \phi + \sum_i W_i (\psi_i - \bar{\psi}_i)^2 \tag{23}$$

Here

$$W_i \equiv PSIWT_i$$

WTUP$_i$ - Incremental multiplicative constants used to increase the W_i on constraints which prove difficult to satisfy. The nominal values of WTUP$_i$ = 2.0 should be acceptable; hence, this input can normally be omitted.

WTDOWN$_i$ - Decremental multiplicative constants used to decrease the W_i when a constraint is easily satisfied. The nominal values of WTDOWN$_i$ = 0.5 should be acceptable; hence, this input can normally be omitted.

Sectioning Search Data (METHOP$_i$ = 1).—

LIMIT - The number of times each parameter will be sectioned during a single sectioning search

NMAXLO Maximum number of point evaluations employed in a single parameter's sectioning at search commencement (first optimization cycle). In successive cycles, the maximum number of points employed is increased by one.

NMAXUP An upper bound on the maximum number of point evaluations employed in sectioning a particular parameter.

ISIDE - Indicator specifying selection of left or right boundary for a parameter that does not appear to affect the system performance

ISIDE = 0, Select lower limits
ISIDE = 1, Select upper limits

$XTENHI_i$ - Extension of higher search limits ($ALPHI_i$) for a parameter that does not appear to affect performance

$XTENLO_i$ - Extension of lower search limits for a parameter that does not appear to affect performance

IRANDM - Controls the order in which the parameters are sectioned

IRANDM = 0, Random order selected
IRANDM = 1, Natural Order selected
IRANDM = 2, Reverse natural order selected

FACTHI - Section termination criteria. If three successive performance function values are within FACTHI of each other during sectioning of a given parameter on the first optimization cycle, the section search of that parameter will cease. The termination criteria is internally reduced with each optimization cycle.

FACTLO - The lower limit on the termination criteria in any optimization cycle.

ITRADE - Optimization/trade study indicator

ITRADE = 0, Carry out a normal optimization search
ITRADE = 1, Determine performance function sensitivity to each parameter by sectioning each parameter in turn about a given fixed point in parameter space.

IPASEC, IPDSEC, IPFSEC - Print indicators (See Table III, Page 97) for section search

Pattern Search Data ($METHOP_i$ = 2).—

IPAPAT, IPDPAT, IPFPAT - Pattern Search print indicators (See Table III, Page 97).

Magnification Search Data ($METHOP_i$ = 3).—

MAXMAG - Maximum number of point evaluations performed during a single magnification search

DELMAG - The magnification perturbation size, nominally set to 1% of distance to origin. Not no-mally modified from nominal value

IPAMAG, IPDMAG, IPFMAG - Magnification search print indicators, (See Table III, Page 97)

Steepest-Descent Search Data ($METHOP_i = 4$).—

NUMSTD - Number of gradient evaluations and one-dimensional searches performed each time that a steepest-descent search is requested during the optimization cycle.

INDWMA - Steepest-descent weighting matrix indicator
INDWMA = 0., Unit matrix
INDWMA = 1., Empirical matrix
INDWMA = 2., Alternate on each cycle between unit and empirical matrices

$WITER_i$ - Learning factors for steepest-descent weighting matrix

NMAXLO - Maximum number of point evaluations employed in the steepest-descent one-dimensional ray search at search commencement (first optimization cycle). In successive cycles, the maximum number of point evaluations permitted is increased by one.

NMAXUP - Upper bound on the number of point evaluations along a steepest-descent one-dimensional ray in *any* optimization cycle.

FACTHI - One-dimensional steepest-descent ray search termination criteria during first cycle. The termination criteria is reduced in each successive optimization cycle.

FACTLO - Lower limit on one-dimensional steepest-descent ray search termination criteria, in *any* optimization cycle.

IPASTD, IPDSTD, IPFSTD - Steepest-descent search print control indicators, (see Table III, Pate 97).

Adaptive Creeping Search Data ($METHOP_i = 5$).—

MAXCRP - Number of creeping search perturbations introduced into each parameter by a single adaptive creeping search in the optimization cycle.

IRANDM - Controls the order in which parameters are perturbed
IRANDM = 0 , Random order
IRANDM = 1 , Natural order
IRANDM = 2 , Reverse natural order

$DCREEP_i$ - The initial perturbations to each parameter

$CREPMN_i$ - Minimum perturbations for each parameter

$CREPMX_i$ - Maximum perturbations for each parameter

$ALFSIN_i$ - Direction of perturbation for each parameter ($ALFSIN_j = \pm 1.0$)

IPACRP, IPDCRP, IPFCRP - Adaptive creeping search print indicators (see Table III, Page 97).

Quadratic Search Data ($METHOP_i = 6$).—

$QPERT_i$ - Parameter perturbation magnitudes employed in computation of numerical partial derivative matrices $\frac{\partial^2 \phi}{\partial \alpha_i \partial \alpha_j}$ and $\frac{\partial \phi}{\partial \alpha_i}$

QFACTR - Scaling factor on the $QPERT_i$

NMAXLO - Maximum number of point evaluations employed in the quadratic one-dimensional ray search at search commencement (first optimization cycle). In successive optimization cycles, the number of point evaluations permitted increases by one.

NMAXUP - Upper bound on the number of point evaluations along a quadratic one-dimensional ray search, in *any* cycle.

FACTHI - One-dimensional quadratic ray search termination criteria during first cycle. The termination criteria is decreased in each successive optimization cycle.

FACTLO - Lower limit on one-dimensional quadratic ray search termination criteria, in *any* optimization cycle.

IPAQUA, IPDQUA, IPFQUA - Quadratic search print indicators (see Table III, Page 97).

Davidon Search Data ($METHOP_j = 7$).—

MAXDVD - Number of Davidon (Fletcher-Powell) gradient evaluations and one-dimensional searches performed each time that a Davidon search is requested in the optimization cycle

$QPERT_i$ - Parameter perturbation magnitudes employed in computation of numerical partial derivatives,

$$\frac{\partial \phi}{\partial \alpha_j}$$

NMAXLO - Maximum number of point evaluations employed in the Davidon one-dimensional ray search at search commencement (first optimization cycle). In successive optimization cycles, the number of point evaluations permitted is increased by one.

NMAXUP - Upper bound on the number of point evaluations along a Davidon search one-dimensional ray in any cycle

FACTHI - One-dimensional Davidon ray search termination criteria during first optimization cycle. The termination criteria is decreased in each successive optimization cycle.

FACTLO - Lower limit on one-dimensional Davidon ray search termination criteria, in *any* optimization cycle

IPADVD, IPDDVD, IPFDVD - Davidon print control indicators, (see Page 97, Table III).

Random Point Search ($METHOP_j = 8$).—

MAXRPT - The maximum number of random points to be employed in the first request for a random point search within the optimization cycle. In successive requests, MAXRPT is set to zero,and no evaluations result.

IPARPT, IPDRPT, IPFRPT - Random point search print control indicators (see Table III, Page 97).

Random Ray Search (METHOD = 9).—

MAXRRS - The maximum number of random rays, one or two-sided, investigated each time the optimization cycle requests a random ray search.

RUFHI - The initial maximum non-dimension perturbation measure for each parameter. This is reduced each time random ray search consistently fails to improve performance.

RUFLO - Minimum-maximum non-dimensional perturbation measure for each parameter.

IPARRS, PIDRRS, IPFRRS - Random ray search print control indicators (see Table III, Page 97).

Subroutine Function

A brief description of each subroutine follows. Subroutines are discussed in the approximate order encountered within the program, Figure A.3.

MAIN - The main program for the combined AESOP/SHOCK program. Controls all shock computation options.

BDATA7 - Block data routine; sets nominal values in the AESOP data base.

CARLSN - Sets up geometry for a set of test cases defined in NASA TN D-3106, at user's option.

AESOP - The control program for all optimization calculations.

LIGHT - Computes F-function by Lighthill method.

SETGRD - Sets the grid size for plots produced on the computer print output.

PAPERP - Plots output on the printer

MIDDLE - Computes pressures from F function and calls the shock calculations

SHKCNT - Control program for shock calculations

SBABND - Determines number of sub-arcs in F function

ODDSHK - Enriches the F function curve by definition of "NPTS" Equi-spaced points in each arc

INTDP - Integrates the enriched F function

INTCRV - Adds forward and rearward reaching boundary arcs and prints the enriched arc data on request (IPDBUG = 1)

INTSEC - Control program for computation of integral-arc intersections

INITPT - Computes upper-arc at y = 0

FINDSP - Finds the tabulated integral arc point to the left of a given point

TLOOK2 - Interpolates in a tabulated integral-arc to determine arc value at a specified point

SAVSIG - Saves points lying on the F function integral

FRNTSH - Controls computation of the signature forward of the point y = 0

LEFTSH - Determines the point immediately to the left of a specified point for all integral arcs during computation of signature to left of y = 0

UPRARC - Controls computation of upper integral arc at a specified point

QDICNT - Controls quadratic intersection calculation

FNDPTS - Finds the three points to be employed in the local quadratic representation of each integral arc

QDCURV - Fits a local quadratic representation to each integral arc

QDINTS - Determines the two intersections of two quadratic arcs

RITERT - Determines the desired intersection from the two quadratic intersection points

PCROSS - Computes the pressure on the i^{th} arc at a given point using linear interpolation

SAVPR - Saves points along the pressure signature

SHKREV - Reverses the points which lie on the signature forward of y = 0. (The points are initially computed from y = 0 in a forward direction).

REARSH - Control program for computation of signature for y > 0.

SHKOUT - Prints and plots the final pressure signature

ARRMOM - Computes the signature moment

VOLCON - Computes the body volume

EXIT - System EXIT routine

AESOP Function List for Shock Program

FUNCTN(1)-Initial signature overpressure

FUNCTN(2)-Signature N^{th} moment

FUNCTN(3)-Total body volume

FUNCTN(4)-Maximum signature overpressure

FUNCTN(5)-Drag, D/q

FUNCTN(6)-Last radius, R(NR)

FUNCTN(7)-Maximum radius, R(NR)

FUNCTN(8)-Computer time used

FUNCTN(9)-Nose volume